

STUDIES OF CERTAIN NUCLEAR PROCESSES IN STARS

Part I: Neutron Capture Chains in Heavy Element Synthesis

Part II: A Search for Excited States in  $N^{14}$  Pertaining to  
the Synthesis of  $C^{13}$

Thesis by

Donald D. Clayton

In Partial Fulfillment of the Requirements

for the Degree of

Doctor of Philosophy

California Institute of Technology

Pasadena, California

1962

## ABSTRACT

### I.

A. An analysis of the abundance distributions resulting from a chain of successive neutron captures is presented in considerable generality. The solutions are applied to the stellar problem of neutron capture at a rate slow compared to beta-decay, the so-called s-process. Theoretically allowable abundance distributions are correlated with present knowledge of element and isotope abundances in order to draw inferences about the "history" of stellar neutron capture. A semiempirical analysis of isotopic neutron capture cross sections is appended. This work was carried out in conjunction with W. A. Fowler, T. E. Hull, and B. A. Zimmerman. The presentation is in the form of a reprint of an article from the Annals of Physics by the same authors.

B. The studies described in Section A have been independently extended in this thesis. A theoretical table of solar abundances is presented for the stable heavy nuclei whose formation is attributable to the operation of the r- and s-processes. The importance of the normalization of these two theories to certain key abundance determinations is emphasized. The table facilitates a comparison of these theories of nucleosynthesis with current observations on the abundances of the elements and their isotopes.

## II.

Experimental nuclear studies relevant to astrophysical situations constitute the second part of this thesis research. Alpha particle groups from the reactions  $N^{15}(\text{He}^3, \alpha) N^{14}$  and  $N^{14}(\text{He}^3, \alpha) N^{13}$  leading to states in the 7-8 Mev excitation range of the two nitrogen isotopes are reported. States were observed in  $N^{14}$  at excitations of 8.06, 7.97, and  $7.034 \pm .008$  Mev and in  $N^{13}$  at excitations of  $7.388 \pm .008$  and  $7.166 \pm .008$  Mev. Differential cross sections are evaluated for these reactions at laboratory angles of  $90^\circ$  and  $150^\circ$  and a bombarding energy of 2.76 Mev. No other states in this range of excitation were observed. In particular, a state does not appear near 7.6 Mev excitation in  $N^{14}$ , indicating that the reaction  $C^{13}(p, \gamma) N^{14}$  in the CNO-cycle at stellar temperatures is nonresonant.

## ACKNOWLEDGMENTS

The author is indebted to Professor William A. Fowler for suggesting the problems examined in this thesis and for his constant supervision and encouragement. It is a pleasure also to acknowledge the mathematical analysis of neutron capture chains provided by Professor Thomas E. Hull and the many hours of calculations performed by Barbara A. Zimmerman. Helpful suggestions on experimental technique were provided by many of the personnel of the Kellogg Radiation Laboratory.

The author is grateful to Dr. D. F. Hebbard for providing the nitrogen targets and to Lionel Senhouse for preparing the solid-state particle detector.

Finally, the author would like to express his appreciation for the financial support of Institute tuition scholarships from the beginning of the work. The research was supported in part by the joint program of the Office of Naval Research and the U. S. Atomic Energy Commission.

## TABLE OF CONTENTS

<u>PART</u>	<u>TITLE</u>	<u>PAGE</u>
I.	NEUTRON CAPTURE CHAINS IN HEAVY ELEMENT	
	SYNTHESIS . . . . .	1
	A. "Neutron Capture Chains in Heavy Element	
	Synthesis," by D. D. Clayton, W. A. Fowler,	
	T. E. Hull, and B. A. Zimmerman . . . . .	1
	1. Introduction . . . . .	2
	2. The Empirical Correlation of Cross	
	Sections and Abundances . . . . .	6
	3. The Problem . . . . .	11
	4. The Search for a Solution . . . . .	15
	5. An Approximate Solution of High	
	Reliability . . . . .	21
	6. Application to Problem with Experimental	
	Cross Sections . . . . .	27
	7. The Branch at Atomic Weight 64 . . . . .	30
	8. Termination of the $s$ -Process . . . . .	32
	9. Neutron Requirements for the Abundance	
	Distributions . . . . .	35
	10. Applications to the Observed $\sigma_N$ Curve .	42
	11. Neutron Economy . . . . .	47
	12. New and Revised Abundances . . . . .	49
	13. Lead and Bismuth Abundances . . . . .	52
	14. Appendix A: The Neutron Capture Cross	
	Sections . . . . .	58

TABLE OF CONTENTS (Continued)

<u>PART</u>	<u>TITLE</u>	<u>PAGE</u>
	15. Appendix B: Neutron Capture at High Energy . . . . .	74
	16. Appendix C: Relative Sources of Element Abundances . . . . .	75
	B. Calculated Abundances of the Heavy Nuclei .	80
II.	A SEARCH FOR EXCITED STATES OF $N^{14}$ PERTAINING TO THE SYNTHESIS OF $C^{13}$ IN THE CNO-CYCLE IN STARS . . . . .	106
	A. General Nuclear and Astrophysical Considerations . . . . .	106
	1. Summary of $C^{12}/C^{13}$ Abundance Evidence and the CNO-cycle . . . . .	106
	2. Possibility of Stellar Resonances in $C^{13}$ (p, $\gamma$ ) . . . . .	110
	B. Excited States of $N^{14}$ from $N^{15}$ ( $He^3, \alpha$ ) $N^{14*}$	114
	1. Suitability of This Reaction . . . . .	114
	2. General Experimental Arrangement . . . . .	117
	a. Equipment . . . . .	117
	b. Targets . . . . .	120
	c. Calibrations and Errors . . . . .	121
	3. Results . . . . .	124
	4. Comparison of $N^{13}$ and $C^{13}$ Energy Level Diagrams . . . . .	132

I. NEUTRON CAPTURE CHAINS IN  
HEAVY ELEMENT SYNTHESIS

- A. "Neutron Capture Chains in Heavy Element Synthesis"  
by D. D. Clayton, W. A. Fowler, T. E. Hull, and  
B. A. Zimmerman. Reprinted from Annals of Physics,  
12, 331 (1961).

## Neutron Capture Chains in Heavy Element Synthesis\*

The Universe, too, loves to create  
whatsoever is destined to be made.  
—Marcus Aurelius, *Meditations IX*.

D. D. CLAYTON, W. A. FOWLER, T. E. HULL,† AND B. A. ZIMMERMAN

*Kellogg Radiation Laboratory, California Institute of Technology, Pasadena, California*

This paper is concerned with stellar neutron capture processes which occur at a rate slow compared to the intervening beta decays, the so-called *s*-process in the synthesis of the elements. An approximate method of high reliability has been devised to solve for the abundance distributions resulting from the exposure of seed nuclei, such as Fe<sup>56</sup>, to a weak neutron flux in stars. The capture chain differential equations are solved by approximately matching the Laplace transforms of the exact solutions to the Laplace transform of an easily calculable function. From the sequence of abundance distributions generated in this manner for specified numbers of neutrons per initial seed nucleus, one can estimate the superpositions of neutron exposures required to reproduce the experimentally observed abundance distribution for the *s*-process isotopes of the elements. Not only can the validity of the *s*-process model of heavy element synthesis in stellar interiors be demonstrated in this way, but certain inferences about the "history" of stellar neutron processes also appear. Special attention is paid in this regard to the "terminal" exposures which have synthesized lead and bismuth at the end of the line in the *s*-process. An analysis is appended of neutron capture cross sections near 25 keV for the *s*-process nuclei, including interpolations based upon empirical cross sections guided where necessary by isotopic and elemental abundances. A complete correlation between neutron capture cross sections and *s*-process abundances cannot be made at the present stage of knowledge, but the methods described will lead to an eventual solution as more empirical information becomes available.

### I. INTRODUCTION

Burbidge *et al.* (1)<sup>1</sup> (hereafter designated as B<sup>2</sup>FH) showed that neutron capture processes have played the primary role in the synthesis in stars of the

\* Supported in part by the joint program of the Office of Naval Research and the U. S. Atomic Energy Commission.

† Now at the University of British Columbia, Vancouver, British Columbia, Canada.

<sup>1</sup> We refer to the synthesis of the heavy elements in the so-called "universal" or "cosmic" abundance distribution of the elements. Greenstein (1) first suggested the C<sup>13</sup> ( $\alpha, n$ ) reaction in stars as a source of neutrons which, on capture, could lead to anomalous abun-

heavy elements beyond the iron group. Because of repulsive Coulomb forces, charged particle reactions have been rather ineffective at the temperatures ( $10^8$  to  $10^9$  degrees) at which the main line of heavy element synthesis has apparently occurred. The small relative abundance (0.1 to 1 per cent) of the lightest, "charge rich" isotopes of the heavy elements attests to the infrequent operation of charged particle reactions in the synthesis of these elements. On the other hand, neutrons interact rapidly with heavy nuclei at the "low" energies ( $kT \sim 10$  to  $100$  kev) corresponding to the temperatures just cited. In fact, neutron reaction cross sections vary roughly as  $1/v \sim 1/E^{1/2}$  where  $v$  is the neutron velocity and  $E$  the energy. Furthermore, at low energies the only reaction other than elastic scattering which is allowed energetically in most cases is the capture of the neutron. This leads to an increase in atomic weight by one unit, a slow but sure mechanism for the synthesis of heavier and heavier nuclei. Eventually, of course, neutron induced fission becomes possible in the very heaviest nuclei at low energies. This process or alpha particle decay, or even spontaneous fission, depending on circumstances, terminates the synthesis.

Gamow (2) and his collaborators, Alpher and Herman (3), suggested neutron capture as the mechanism of synthesis of all the elements starting with neutron decay in an early, highly condensed, high-temperature stage of the expanding universe. The density was taken to be  $\rho \sim 10^{-7}$  grams/cm<sup>3</sup> and the temperature to be  $T \sim 10^{10}$  degrees ( $kT \sim 1$  Mev). The measurements of Hughes (4) and his collaborators on the capture cross sections of nuclei for fission spectrum neutrons in the Mev energy range indicated an inverse relationship between these cross sections ( $\sigma$ ) and isotopic abundances ( $N$ ) such that  $N \sim 1/\sigma$ . This was to be expected in general from the point of view of synthesis in a chain of successive neutron captures. Nuclei with small cross sections would be expected to build up to large abundances in the chain and vice versa so that the number of captures per unit time would be uniform over contiguous sections of the chain. However, in recent years it has become clear from nuclear and astrophysical evidence that charged particle reactions must have played a considerable role in the synthesis of the *light* elements. Gamow (5) has emphasized one critical aspect of the problem as follows: "However, since the absence of any stable nucleus of atomic weight 5 makes it improbable that the heavier elements could

---

dances of the heavy elements in stars. Cameron (1) treated the  $C^{13}(\alpha, n)$  reaction and the build-up of the anomalous abundances quantitatively. Fowler *et al.* (1) pointed out other  $(\alpha, n)$ -reactions such as  $Ne^{21}(\alpha, n)$  and proposed neutron capture processes in stars as the mechanism of production of the "universal" heavy element abundances. They took the iron-group nuclei as the initial "seeds" for the capture process. Element synthesis up to iron and nickel and the general idea of element synthesis in stars had been discussed by Hoyle (1). Fowler and Greenstein (1) discussed the experimental and observational aspects of element building in stars.

have been produced in the first half hour (of the universal expansion) in the abundances now observed, I would agree that the lion's share of the heavy elements may well have been formed later in the hot interior of stars." The absence of a stable nucleus at mass 8 accentuates this difficulty. In addition, other complications and difficulties have arisen in the abundance peak in the iron group elements which do not have anomalously low capture cross sections.

B<sup>2</sup>FH borrowed Gamow's basic idea of neutron capture in their treatment of element synthesis in stars, but avoided the difficulties just mentioned by using charged particle reactions during various stages of stellar evolution to synthesize the elements up to and including the iron group (titanium through iron to nickel). Neutron production and capture then serves in the intermediate and terminal stages of stellar evolution as the main line of element synthesis beyond iron. In fact a small fraction, slightly over one tenth of one per cent, of the abundant iron group nuclei are used as the "seed" nuclei at the start of the chain of captures. Mass spectroscopy has shown that the chain is unbroken in atomic mass in this region. (The chain is indeed unbroken beyond  $A = 8$ .)

It has been suggested by Suess and Urey (6) and Coryell (7), and shown in detail by B<sup>2</sup>FH that two quite different and independent neutron capture processes have been necessary to synthesize the abundant isotopes of the heavy elements. In one of these processes, called the *s*-process, the neutron captures occur at a *slow* (*s*) rate compared to the intervening beta decays. Thus, the synthesis path lies along the bottom of the valley of mass stability and in general bypasses both the proton rich, lightest isotopes and the neutron rich, heaviest isotopes of the elements involved. On the other hand, in the second neutron process, called the *r*-process, the neutron captures occur at a *rapid* (*r*) rate compared to beta decay. The captures lead rapidly from stable seed nuclei, predominantly Fe<sup>56</sup>, to the very neutron rich side of the mass valley and are stopped only by photo ejection of the weakly bound neutrons by the ambient gamma-ray flux associated with the high temperature necessary for the production of the neutrons. Equilibrium between (*n*,  $\gamma$ ) and ( $\gamma$ , *n*) reactions is established and progress along the synthesis path occurs only through electron-antineutrino ejection or beta decay which permits further neutron capture. On termination of the synthesizing neutron flux the neutron rich isobars at each atomic mass beta decay to the first stable isobar which then "shields" from *r*-process production those remaining isobars, if any, having fewer neutrons and more protons. The *s*-process and the *r*-process account in these ways for the synthesis of *all* the relatively abundant isotopes of the heavy elements. An exposure of a small fraction of the *s*- and *r*-process material to a hot proton flux or an intense photon flux will account for the production of the relatively rare, proton rich, lighter isotopes of the heavy elements. This infrequent mechanism has been termed the *p*-process by B<sup>2</sup>FH. It may have occurred in the solar nebula during the forma-

tion of the solar system, just as did the formation of the rare light nuclei,  $H^2$ ,  $Li^6$ ,  $Li^7$ ,  $Be^9$ ,  $B^{10}$ , and  $B^{11}$ .

It follows from the evidence for two different neutron capture processes which occur at quite different rates, that two separate and distinct stages of stellar evolution are demanded. B<sup>2</sup>FH assign the *s*-process to the red giant stage of stars which were formed from galactic material containing light elements, particularly He, C, O, Ne, and Mg and the intermediate iron group elements. These elements had been previously synthesized in other stars and ejected into the interstellar medium, mostly primordial hydrogen, of the Galaxy. The He, C, O, Ne, and Mg were required for the production of neutrons by  $\alpha, n$ -reactions on  $C^{13}$ ,  $O^{17}$ ,  $Ne^{21}$ ,  $Ne^{22}$ ,  $Mg^{25}$ , and  $Mg^{26}$  during the relatively slow helium burning in the red giant, with lifetimes  $10^6$  to  $10^8$  years. In private conversation, A. G. W. Cameron has pointed out that  $Ne^{22}(\alpha, n)$  is only slightly endoergic ( $Q = -0.48$  Mev) and thus will proceed under thermal excitation in giant stars along with the other exoergic reactions.

The *r*-process is thought of as taking place in the exploding envelopes or cores of supernova outbursts. In this case the energy producing and neutron producing processes occur in the short interval of the supernova explosion, 1 to 100 seconds, and the neutron captures accordingly occur at a rapid rate.

B<sup>2</sup>FH have delineated in detail the manner in which the isotopes of the elements, in so far as their production is concerned, may be assigned to one or the other of the *p*, *s*, and *r*-processes. This will not be elaborated here. Suffice it to repeat at this point that in general the light, proton rich isotopes of a given element are produced in the *p*-process, the intermediate in the *s*-process, and the neutron rich in the *r*-process. Some *r*-process nuclei are by-passed in the *s*-process and certain *s*-process nuclei are shielded by more neutron rich stable isobars in the *r*-process decay. In these cases the assignments can be made unambiguously; in others, recourse is made to the relative abundance produced by the three processes in unambiguous cases of approximately the same atomic weight. Nuclear species with no isobars, usually odd atomic weight, can be produced as a result of all three processes and assignments are possible only by reference to nearby species with even atomic weight.

We discuss in this paper the *s*-process. It will accordingly be clear from the above, that a first requirement is a list of nuclear species whose production can be ascribed in full or in part to the operation of this process. Such a list has been abstracted from the Appendix of B<sup>2</sup>FH and is presented as Table I. Unambiguous *s*-process assignments are underlined as indicated and nuclei with closed shells of neutrons are indicated by M for "magic". Cycling in the Pb and Bi isotopes due to the onset of natural radioactivity in Po is indicated by C. Other notations are explained in the caption of the table. Table I contains the

TABLE I  
ISOTOPES PRODUCED BY NEUTRON CAPTURE AT A SLOW RATE IN RED GIANT STARS  
(*s* PROCESS ON Fe<sup>56</sup>)<sup>a</sup>

<i>Z</i>	<i>Z</i>
28. Ni <sup>64</sup>	56. Ba <sup>134</sup> , (135), <u>136</u> , (137), 138M
29. Cu <sup>63</sup> , 65	57. La <sup>139M</sup>
30. Zn <sup>64</sup> , 66, 67, 68	58. Ce <sup>140M</sup>
31. Ga <sup>69</sup> , 71	59. Pr <sup>141M</sup>
32. Ge <sup>70</sup> , 72, 73, 74	60. Nd <sup>142M</sup> , 143, 144, 145, 146
33. As <sup>(75)</sup>	62. Sm <sup>148</sup> , 150
34. Se <sup>76</sup>	64. Gd <sup>154</sup>
36. Kr <sup>80</sup> , 82	66. Dy <sup>160</sup>
38. Sr <sup>86</sup> , <u>87</u> , 88M	70. Yb <sup>170</sup> , <u>171</u> , (172), (173), (174)
39. Y <sup>89M</sup>	71. Lu <sup>(175)</sup>
40. Zr <sup>90M</sup> , 91, 92, 94	72. Hf <sup>176</sup> , (177), 178, 179, 180
42. Mo <sup>96</sup> , <u>96</u> , 97, <u>98</u>	73. Ta <sup>181</sup>
44. Ru <sup>(99)</sup> , <u>100</u> , <u>102</u>	74. W <sup>182</sup> , (183), 184
46. Pd <sup>104</sup>	75. Re <sup>185</sup>
48. Cd <sup>110</sup> , <u>111</u> , <u>112</u> , <u>113</u> , <u>114</u>	76. Os <sup>186</sup> , <u>187</u>
49. In <sup>115</sup>	78. Pt <sup>192</sup>
50. Sn <sup>116</sup> , 117, 118, 119, 120	80. Hg <sup>198</sup> , 199, (200), <u>201</u> , 202
51. Sb <sup>121</sup>	81. Tl <sup>203</sup> , 205
52. Te <sup>122</sup> , <u>123</u> , <u>124</u>	82. Pb <sup>204</sup> , (206C), (207C), (208CM)
54. Xe <sup>128</sup> , 130	83. Bi <sup>(209CM)</sup>

<sup>a</sup> The code for each isotope number is as follows: underlines, *s* only; no line, *s* >> *r*; parentheses, *s* > *r*; overlined, *s* = *r*; M, magic; C, cyclic. Adapted from B<sup>2</sup>FH and the appendix to this paper.

nuclei whose slow but steady synthesis in countless red giant stars throughout the history of our Galaxy will constitute the burden of what is now to follow.

## II. THE EMPIRICAL CORRELATION OF CROSS SECTIONS AND ABUNDANCES

At our present stage of knowledge, considerable illumination of the subject at hand is obtained by simply correlating empirical capture cross sections ( $\sigma$ ) for *s*-process nuclei with the observed natural abundances ( $N$ ) of these nuclear species. This correlation is made most straightforwardly by forming the product  $N\sigma$  which then ought to be a smoothly varying function of atomic weight ( $A$ ), which is the parameter that determines the sequence in a chain of neutron captures. We will find in subsequent sections of this paper that the function given by  $N\sigma = f(A)$  over a wide range in  $A$  is a measure of the integrated flux-time (or total number of neutron captures) to which lighter seed nuclei, e.g., Fe<sup>56</sup>, have been subjected in red giant stars in the synthesis of the heavier elements.

This integrated flux-time cannot be determined solely from nuclear principles. We require  $f(A)$  as the basic empirical information that theoretical ideas concerning the "history" of element synthesis must attempt to explain. Attempts to determine  $N$  from calculated cross sections using assumed  $f(A)$ , as implied in recent studies by Cameron (8), would seem to overlook the essential nature of the problem involved here. This is not to argue that improvements should not be constantly sought in empirical measures of  $N$ . This, however, is primarily the province of astronomers, geophysicists, and geochemists, and not of the nuclear physicist except through his preoccupation with neutron activation techniques.

The status of the correlation of cross-section values with abundance measurements excluding those made recently by activation techniques is shown in Fig. 1. The abundances are those given by Suess and Urey (6) in their beautiful study of the analytical data on the subject. It would be quite misleading to use Cameron's abundances (8) in this correlation. Abundances determined by neutron

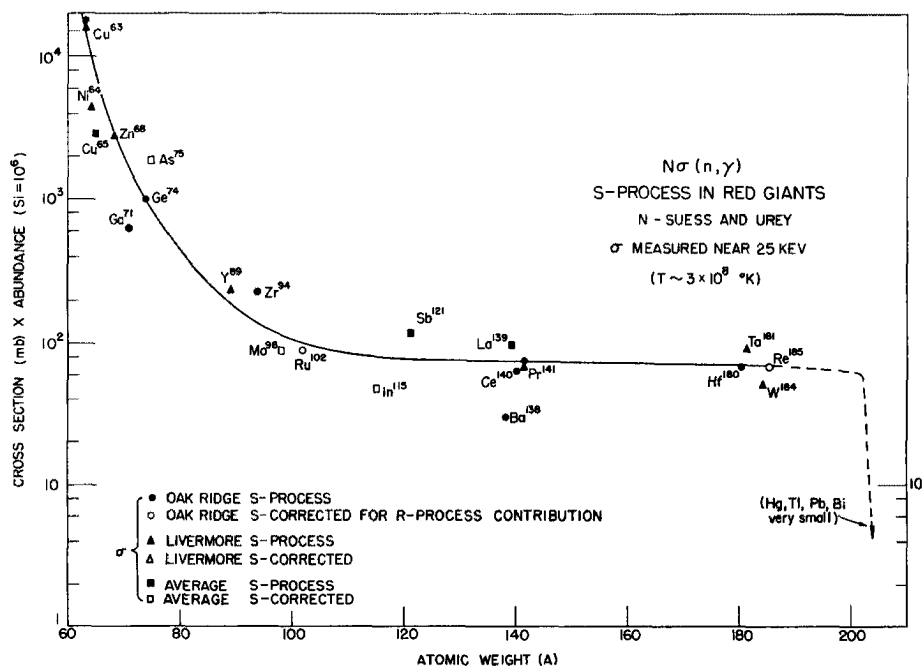


FIG. 1. The product  $\sigma N$  for  $s$ -process nuclei as a function of atomic weight. The cross sections are those measured near 25-keV neutron energies by Macklin *et al.* at Oak Ridge, and by Booth *et al.* at Livermore. The abundances are those given by Suess and Urey. The curve is drawn smoothly for visual aid through the points. The dashed tail represents an uncertain guess as to how a sudden decrease may occur for  $A > 200$ .

activation methods will be discussed later. The cross section measurements are primarily those obtained by Oak Ridge and Livermore groups and are discussed in detail in subsequent sections. Both groups used in part the 25-keV neutrons from an Sb-Be source. This raises a basic problem in regard to the correlation. What neutron energies should be used? Considerations such as those discussed in B<sup>2</sup>FH lead to the expectation that neutrons become available from nuclear processes, such as ( $\alpha, n$ ) reactions in the giant stars, at temperatures of the order of  $10^8$  degrees and somewhat higher. We are thus interested in neutron capture cross sections integrated over Maxwell-Boltzmann distributions in energy with  $kT \sim 10$  keV or perhaps in extreme cases, as high as 100 keV. It may well prove possible, by using the "smoothness" of  $N\sigma(E)$  versus  $A$  for various  $E$  as a criterion, to determine the energy and thus the temperature at which neutron capture processes have taken place in stars. However, this will require very precise measurements both of  $N$  and  $\sigma(E)$ . The possibility of various temperatures being important in different stars or even at different stages of evolution in the same star must not be overlooked. The averaging over the Maxwell-Boltzmann distribution means that high resolution in energy is *not* essential in measurements used in the correlation.

The cross-section measurements, which are available for such correlations as illustrated in Fig. 1, are restricted to the stable isotopes of the elements. The correlation with abundances must only be made for those nuclei which actually take part in the process in which they are produced, namely the *s*-process nuclei. The neutron capture cross sections of stable nuclei produced by beta decay subsequent to the *r*-process should show no correlation with their abundances. This is illustrated in Fig. 2 and leads to some confidence in the "smoothness" of  $N\sigma$  in Fig. 1.

We emphasize at this point that Table I lists the nuclear species on which neutron capture cross sections in the 10- to 100-keV range are most urgently needed for applications in nucleosynthesis in stars. It will be self-evident that isotopic targets and prompt gamma-ray detection techniques will be required in these measurements. The residual nuclei are not always radioactive. It will also be clear that the correlations with the minimum ambiguity can be made for groups of isotopes of the same element. First of all, their abundances have not been subjected to extensive chemical fractionation since their nucleosynthesis in spite of the many vicissitudes in their geological history. Secondly, their relative abundances are determined by accurate mass spectroscopic methods. Thirdly, over the small range in  $A$  covered by the isotopes of a given element, it would not be expected that  $N\sigma$  would vary greatly although this possibility cannot be completely excluded. *In experiments designed to measure isotopic neutron capture cross sections it will be expected that the reaction yield, which will be proportional to  $N\sigma$ , will be approximately equal for *s*-process isotopes in their natural relative*

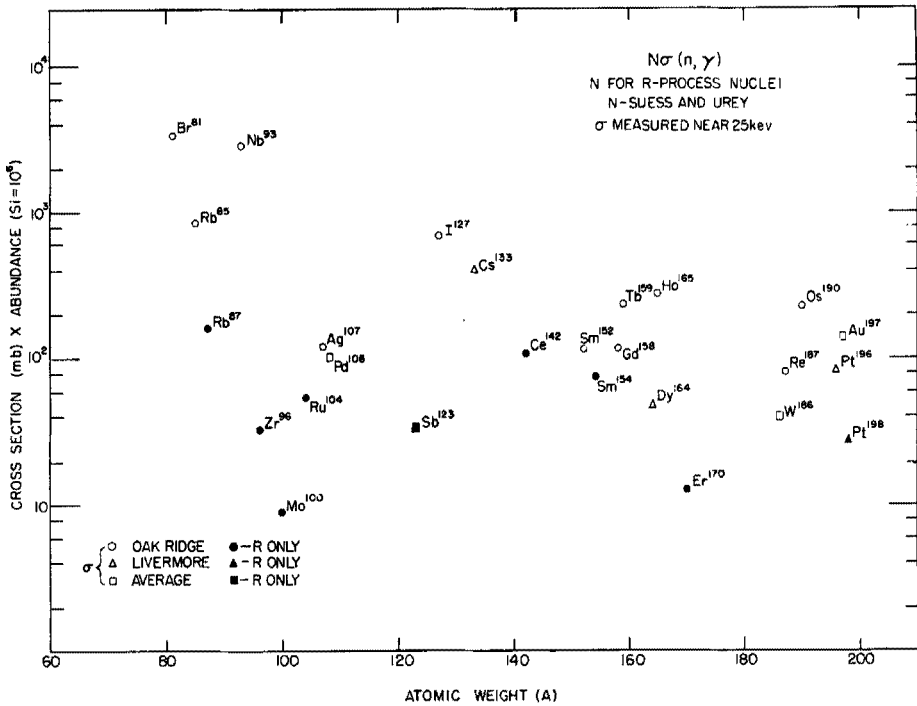


FIG. 2. The product  $\sigma N$  for  $r$ -process nuclei similar to that shown for the  $s$ -process nuclei shown in Fig. 1. The fluctuations in  $\sigma N$  for these nuclei are expected and show that the smooth variation indicated in Fig. 1 is not wholly accidental.

*abundances*. An inspection of Table I shows that the following elements are particularly interesting in regard to isotopic measurements:

Zn, Sr, Zr, Sn, Te, Ba, Nd, Hf, Hg, Tl, and Pb

Because of the cycling mentioned above and because of radiogenic contributions, Pb is a special case in so far as detailed analysis is concerned, but Pb is particularly important in connection with certain aspects of nucleosynthesis such as "age" determinations.

The above comments have been made in the hope that they will prove useful in regard to establishing priorities in neutron capture cross-section measurements and in establishing the urgent need for the production of isotopic targets in substantial amounts. To illustrate the general importance of these considerations in determining isotope abundances, Fig. 3 is appended. This shows the evidence for the operation of the three separate processes,  $p$ ,  $s$ , and  $r$ , in the formation of the stable isotopes of the element tin. By following through the  $s$ -process path shown in Fig. 4 it will be seen that the first three isotopes,  $\text{Sn}^{112}$ ,  $\text{Sn}^{114}$ , and  $\text{Sn}^{115}$ ,

cannot be made in the  $s$  or the  $r$  process. Their low abundances of the order of 1 per cent or less are consistent with their production only in the  $p$  process.

$\text{Sn}^{116}$  is the first isotope which can be made in the  $s$  process and the discontinuity in abundance between  $\text{Sn}^{115}$  and  $\text{Sn}^{116}$  is quite marked. Similarly,  $\text{Sn}^{120}$  is the last isotope which can be made in this process, and again, there is a discontinuity in going to  $\text{Sn}^{122}$  and  $\text{Sn}^{124}$  which can only be made in the  $r$  process.

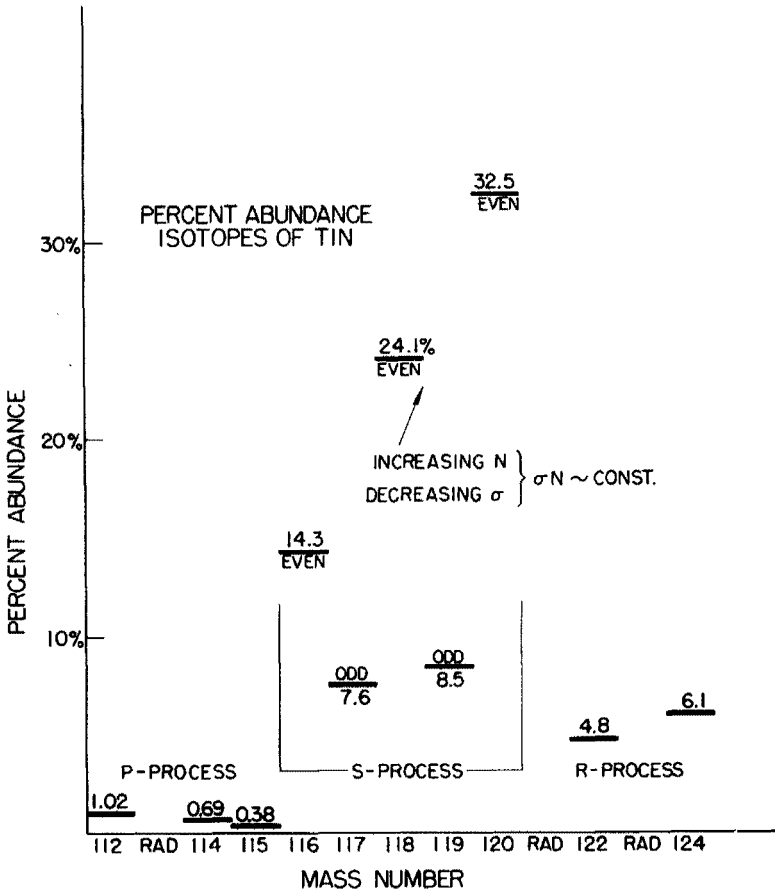


FIG. 3. Abundance evidence for the operation of three separate processes,  $p$ ,  $s$ , and  $r$ , in the formation of the stable isotopes of the element tin. The first three isotopes can only be produced in the relatively rare  $p$ -process involving charged particles (protons) or radiation and their abundances are seen to be quite small. The next five isotopes are produced by neutron capture at a slow rate ( $s$ -process) and exhibit the regularity expected for this process—decreasing capture cross section, hence increasing abundance, with increasing mass number. The last two isotopes are produced only by neutron captures at a rapid rate ( $r$ -process) and the discontinuity between the  $s$ -process and the  $r$ -process is quite apparent.

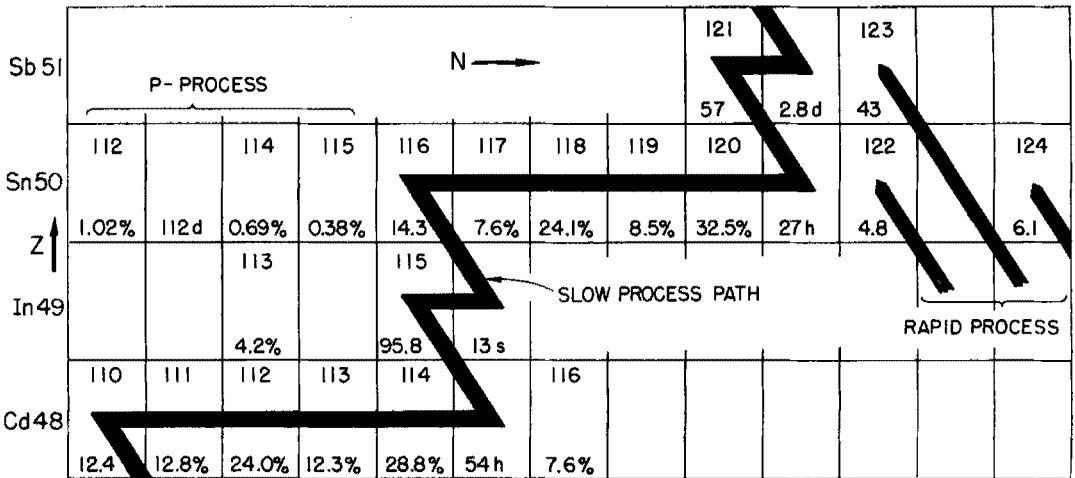


FIG. 4. The  $s$ -process path through the isotopes of tin. The neutron number increases by units of one on a slow time scale until negative beta activity occurs and the path moves to the isobar of higher  $Z$ . This path can be determined from empirical evidence on the beta stability of nuclei. Note that the path bypasses the  $p$ -process and the  $r$ -process nuclei. The  $r$ -process nuclei are the end products of an isobaric beta-decay chain as shown at the far right from neutron-rich progenitors produced in an intense neutron flux. The  $p$ -process nuclei are produced by subjecting a small fraction of  $s$  and  $r$ -process nuclei to an intense proton or photon flux.

The  $r$  process apparently produced somewhat less abundances in this region of atomic weights than the  $s$  process. This is a result of the "history" of the synthesis of the elements of the solar system, not of any fundamental nuclear properties of these isotopes. The rising trend in abundances from Sn<sup>116</sup> to Sn<sup>120</sup> is consistent with  $N\sigma \sim \text{constant}$  if we note that  $\sigma(n, \gamma)$ , in general, decreases as more neutrons are added; and that  $\sigma$ , for odd  $A$  isotopes, is higher than  $\sigma$  for even  $A$  isotopes because of the tendency to pair up the neutrons. It is a quantitative check of these last statements, true or false, which will be supplied by measurements on the capture cross sections of the tin isotopes 116, 117, 118, 119, and 120. At the present stage of knowledge, their relative abundances do seem to depend primarily on their nuclear properties alone.

### III. THE PROBLEM

Since a neutron capture chain occurring at a slow rate would produce  $\sigma N$  values which delineate a smooth curve  $f(A)$  and, alternatively, a smoothly varying  $\sigma N$  would not be expected for other models of heavy element formation, the confirmation experimentally of such a behavior leads to belief in the correctness of the slow capture model. If this is the case, it may be possible to obtain

information concerning the distributions of neutron exposures of seed nuclei from the observed shape of the experimental curve  $f(A) = \sigma N$ . Such information could lead to conclusions regarding the amount of neutron producing nuclei relative to the amount of seed nuclei required in various red giant stars. One may also place limits on the allowable types of  $s$ -process abundance distributions. Such information would have implications on some of the rapid capture abundances in those cases where both the  $r$  and the  $s$  processes contribute to the abundance of an isotope, for the  $s$ -process contribution may then be subtracted to obtain the  $r$ -process contribution for further analysis. With these broad objectives in mind, the mathematical problem of the capture chain will now be investigated.

Assume that a group of heavy elements exists in some interior region of a star. The region chosen will be characterized by a constant temperature  $T$  and a free neutron density  $n_n(t)$  which is uniform over the region but may depend on the time. Let  $N_A(t)$  be the abundance of that nucleus defined by the  $s$ -process path of atomic weight  $A$  contained in the region, and let  $\sigma_A$  be the  $(n, \gamma)$  cross section for that nucleus. The neutron velocity relative to a heavy nucleus is  $v_A$ . Then the differential equation for the local abundance  $N_A$  is

$$\frac{dN_A(t)}{dt} = - \langle v\sigma \rangle_A n_n(t) N_A(t) + \langle v\sigma \rangle_{A-1} n_n(t) N_{A-1}(t). \quad (1)$$

This equation is based on the fundamental assumption of the  $s$ -process that beta decays between isobars are fast compared to the neutron capture rates. The quantity  $\langle v\sigma \rangle$  appearing here is an average necessitated by the fact the relative velocity  $v$  is determined by a Maxwell-Boltzmann distribution and the cross section  $\sigma$  is a function of that  $v$  attending any capture possibility. The nature of this average requires some amplification.

Neutron capture in the heavy elements occurs through many wide overlapping levels of the compound nucleus produced in the capture. Thus, the Maxwell-Boltzmann distribution at temperature  $T$  yields a weighted average of  $v\sigma$  over the contribution of the levels primarily in the vicinity of  $kT$ . Experimentally it is difficult to obtain a neutron energy resolution comparable to the level separation so that the experimental measurements already yield  $\sigma$  or  $v\sigma$  averaged over an energy range such that these quantities vary smoothly with neutron energy. It is found that  $\bar{\sigma}$  (experimental) varies as  $v^{-1}$  at low energies and that this dependence changes over to  $v^{-2}$  in the region of several tens of kilovolts as long as  $s$ -wave neutron capture is alone effective. However, in the heavy elements  $p$ -wave neutron capture, which is proportional to  $v^{+1}$ , begins to contribute just as the  $s$ -wave begins to decrease more rapidly than  $v^{-1}$ . The result is that to a very crude approximation  $v\sigma$  can be taken as a constant and the most reasonable procedure is to evaluate  $v$  and  $\sigma$  at  $kT$ , the most probable Maxwell-Boltzmann

energy. Thus

$$\langle \sigma v \rangle = \sigma_T v_T \quad (2)$$

with  $\sigma_T = \sigma(kT)$  and  $v_T = (2kT/\mu)^{1/2}$ . The reduced mass

$$\mu = M_A M_n / (M_A + M_n) \simeq M_n,$$

where  $M_n$  is the neutron mass. To this last approximation  $v_T \simeq (2kT/M_n)^{1/2}$  is independent of  $A$ . As an indication of the error involved in using  $v_T \sigma_T$  for  $\langle v \sigma \rangle$ , one can show that if  $\sigma \sim v^0$  or  $v^{-2}$ , then  $\langle v \sigma \rangle = (2/\sqrt{\pi}) v_T \sigma_T$ , which is only 13 per cent greater than  $v_T \sigma_T$ . Our choice for  $kT$  will be mentioned later. For the moment we use the fact that  $v_T$  can be factored out on the right side of (1), leaving

$$\frac{dN_A(t)}{dt} = -v_T n_n(t) \sigma_A(kT) N_A(t) + v_T n_n(t) \sigma_{A-1}(kT) N_{A-1}(t) \quad (3)$$

Under these assumptions it is possible to define a new independent variable which will measure the progress of neutron captures uniquely. We define

$$d\tau = n_n v_T dt, \quad \tau = \int n_n(t) v_T dt. \quad (4)$$

Equation (3) becomes

$$\frac{dN_A}{d\tau} = -(\sigma_A N_A - \sigma_{A-1} N_{A-1}). \quad (5)$$

This variable  $\tau$  is the integrated flux-time, a measure of the total accumulated neutron bombardment per unit area. It conveniently resolves variations of neutron densities and time scales into one convenient measuring variable. Throughout this paper we express  $\sigma$  in millibarns; accordingly the unit for  $\tau$  is  $10^{27}$  neutrons/cm<sup>2</sup>.

It is important to keep in mind that Eq. (5) applies only to that part of the abundance at atomic weight  $A$  which takes part in the  $s$ -process. The light elements are at present thought to be formed mainly by charged particle reactions. The elements in the abundance peak at the iron group are thought to be formed in the equilibrium process as discussed by B<sup>2</sup>FH. It is for the production of elements of atomic weight greater than sixty that the process of neutron capture must be invoked. The large abundances of the iron group nuclei are therefore envisioned as a starting point for the capture of neutrons produced in light element reactions. Neutron capture may then proceed in an unbroken chain of increasing atomic weight until Bi<sup>209</sup> captures a neutron, whereupon alpha decay to the lead isotopes takes place. Equation (5) may thus be thought to apply to

the *s*-process chain between these two terminal regions. Further complication is necessary because many of the nuclei of the *s*-process chain may be created in other processes, such as when only one stable isobar exists at atomic weight *A*. In these cases  $N_A$  of eq. (5) applies only to the fraction of that abundance which is created in the *s*-process.

The resulting situation can be described as follows; a group of nuclei, peaked in abundance at  $\text{Fe}^{56}$ , is exposed to unknown numbers of neutrons, characterized by a range of value in the exposure parameter  $\tau$ . An important building block of our analysis consists in the observation that the general problem may be reduced to superpositions of a much cleaner problem, that of one seed nucleus exposed to an integrated neutron flux characterized by a single value for  $\tau$ . The solution in this case may be generalized to several seed nuclei by superimposing the single seed solutions weighted proportionally to the initial relative abundances of the seed nuclei. Further generalization can be made to nonuniform exposure conditions by superimposing solutions for different  $\tau$ 's. The second type of superposition (that of different exposures) will in fact be more important, for the observed and calculated (equilibrium model) abundances seem to indicate clearly that the initial distribution consists primarily of  $A = 55, 56,$  and  $57$ , with  $N_{55} \simeq N_{57} \simeq 0.1 N_{56}$ . The long exposure distributions resulting from this seed group will not differ greatly from that produced by an exposure of  $\text{Fe}^{56}$  alone. Thus the simpler problem that we consider is, "What are the abundance distributions for different neutron exposures of  $\text{Fe}^{56}$ ?"

We will at first neglect the fact that there is recycling due to alpha-decay at the end, and consider that every time  $\text{Bi}^{209}$  captures a neutron, no further capture occurs and nuclei simply pile up at  $A = 210$ . Later we will return to the problem of the redistribution of these nuclei among the lead and bismuth isotopes. Thus the equations to be solved are

$$\begin{aligned} \frac{dN_{56}}{d\tau} &= -\sigma_{56} N_{56}, \\ \frac{dN_A}{d\tau} &= -\sigma_A N_A + \sigma_{A-1} N_{A-1}, \quad 57 \leq A \leq 209, \\ \frac{dN_{210}}{d\tau} &= \sigma_{209} N_{209}. \end{aligned} \quad (6)$$

The boundary conditions are

$$N_A(0) = \begin{cases} N_{56}(0) & A = 56 \\ 0 & A > 56 \end{cases}.$$

## IV. THE SEARCH FOR A SOLUTION

Bateman (9) who served many years on the faculty of this Institute, found long ago that exact solutions to this problem can be easily written down. If one changes the numbering index to  $k = A - 55$ , so that the index for the seed nucleus is  $k = 1$  and the process begins with  $N_1(0)$  nuclei having  $k = 1$ , then

$$N_k(\tau) = N_1(0) \sum_{i=1}^k C_{ki} e^{-\sigma_i \tau}. \quad (7)$$

By substituting back into the equations, it follows that

$$C_{ki} = \frac{\sigma_1 \sigma_2 \sigma_3 \cdots \sigma_{k-1}}{(\sigma_k - \sigma_i)(\sigma_{k-1} - \sigma_i) \cdots (\sigma_2 - \sigma_i)(\sigma_1 - \sigma_i)}, \text{ omitting } \left( \frac{1}{\sigma_i - \sigma_i} \right). \quad (8)$$

For example:

$$\begin{aligned} C_{11} &= 1, \\ C_{21} &= \frac{\sigma_1}{\sigma_2 - \sigma_1}, \quad C_{22} = \frac{\sigma_1}{\sigma_1 - \sigma_2}, \\ C_{31} &= \frac{\sigma_1 \sigma_2}{(\sigma_3 - \sigma_1)(\sigma_2 - \sigma_1)}, \quad \text{etc.} \end{aligned} \quad (9)$$

There are two severe difficulties with this exact solution: (1) The functional form is incorrect as it stands when any  $\sigma_m = \sigma_n$ ,  $n \neq m$ , in which case a limiting process as  $\sigma_m \rightarrow \sigma_n$  must be performed. In fact, many of the cross sections are equal within experimental error. (2) Even if all the cross sections were arbitrarily made to differ slightly, the numerical evaluation of this solution is prohibitive from the consideration of time required, and not easily corrected for changes in cross section estimates or measurements.

Before discarding this method, we would point out for later use that there is one interesting case for which the series is easily summable;  $\sigma_k = \gamma k$ ,  $\gamma = \text{constant}$ . Then

$$\begin{aligned} C_{ki} &= \frac{(k-1)!(-1)^{i-1}}{(k-i)!(i-1)!}, \quad \text{and} \\ N_k(\tau) &= N_1(0)(k-1)! \sum_{i=1}^k \frac{(-1)^{i-1} e^{-\gamma i \tau}}{(k-i)!(i-1)!} = N_1(0) e^{-\gamma \tau} (1 - e^{-\gamma \tau})^{k-1}. \end{aligned} \quad (10)$$

This exact solution will be used later as a quantitative check on an approximate solution to be presented.

To obtain a qualitative feeling for the nature of the solution, Fowler *et al.* (10) examined the solutions for constant cross section, which are easily seen

to be

$$N_k(\tau) = \frac{N_1(0)}{(k-1)!} (\sigma\tau)^{k-1} e^{-\sigma\tau}. \quad (11)$$

The nature of this function is a Poisson-like distribution in  $k$  with a maximum at  $k = \sigma\tau + 1$  given approximately by

$$N_k(\text{max}) \simeq \frac{N_1(0)}{(2\pi\sigma\tau)^{1/2}}, \quad (12)$$

and which must therefore have a width of  $\sim(2\pi\sigma\tau)^{1/2}$ . Thus as the distribution moves out in  $k$  or  $A$ , its height decreases and its width increases *due to the randomness of the capture processes* by a factor proportional to  $(\sigma\tau)^{1/2}$ . These observations are, of course, not quantitatively useful if the cross sections are not appreciably constant. However, it can be seen that if the cross sections are increasing, for example, that the spreading of the packet will become even more pronounced as  $\tau$  increases, and that there will tend to be a long tailing off on the high  $k$  side of the maximum (an observation which may be verified by examining the previous solution for  $\sigma = \gamma k$ ).

Hoyle (11) suggested a manner in which the effect of variable cross sections could be ascertained. If one defines  $\psi_A(\tau) = \sigma_A N_A(\tau)/N_1(0)$ , a practice which shall be followed for the rest of this paper, then the set of differential equations (5) becomes

$$\frac{1}{\sigma_A} \frac{d\psi_A}{d\tau} = -\psi_A + \psi_{A-1} \quad (13)$$

The set of values  $\psi_A$  delineate a smooth curve and thus can be interpreted as a smooth function  $\psi(A)$ . Using this property of good behavior, the difference in the  $\psi$ 's can be written as a partial derivative to yield

$$\frac{1}{\sigma_A} \frac{\partial\psi(A, \tau)}{\partial\tau} \simeq -\frac{\partial\psi(A, \tau)}{\partial A}, \quad (14)$$

If in addition, the values of the cross sections  $\sigma_A$  can be thought of as delineating another function  $\sigma(A)$ , the equation can be written entirely as a functional partial differential equation

$$\frac{\partial\psi(A, \tau)}{\partial\tau} + \sigma(A) \frac{\partial\psi(A, \tau)}{\partial A} = 0. \quad (15)$$

This equation may be solved in a well-known manner by a change of variable  $A$  to  $A'$  such that

$$\sigma(A) \frac{\partial}{\partial A} = \sigma_1 \frac{\partial}{\partial A'} \quad (16)$$

where  $\sigma_1$  is a constant, arbitrarily chosen to equal  $\sigma(A = 56)$  so that initially  $(\partial/\partial A)_{A=56} = (\partial/\partial A')_{A=56}$ . Then in integrated form  $A' = \sigma_1 \int^A (dA/\sigma(A))$ . Under this transformation, Eq. (15) becomes the well-known hydrodynamical flow equation

$$\frac{\partial \psi(A', \tau)}{\partial \tau} + \sigma_1 \frac{\partial \psi(A', \tau)}{\partial A'} = 0 \quad (17)$$

with solutions  $\psi(A', \tau) = \psi(A' - \sigma_1 \tau)$ . This approximate solution asserts that if  $\psi(A, 0)$  is the initial distribution in  $A$  at  $\tau = 0$ , its evolution in time is given by the following steps:

1. Convert  $\psi(A, 0)$  to  $\psi(A', 0)$  by  $A' = \sigma_1 \int^A (dA/\sigma(A))$ , a transformation yielding a unique one to one correspondence of  $A'$  to  $A$  once a lower limit on the integrand is arbitrarily chosen.

2. To obtain the distribution at  $\tau$  transport the initial distribution to

$$A'_\tau = A'_{\tau=0} + \sigma_1 \tau.$$

3. Convert the resulting  $\psi(A'_\tau)$  back to  $\psi(A, \tau)$  by the coordinate transformation.

The transformation itself may be evaluated by a sum starting, for simplicity, at  $A = 56$ .

$$A' = \sigma_1 \int^A \frac{dA}{\sigma(A)} \simeq \sigma_1 \sum_{A=56}^A \frac{1}{\sigma_A}. \quad (18)$$

Thus  $\sigma_1 = \sigma(A' = 1) = \sigma(A = 56)$  and  $A' = 1$  when  $A = 56$ . The physical significance of this transformation is evident after some thought, but let it be pointed out here that if  $A$  is plotted as a function of  $A'$ , the slope,

$$dA/dA' = \sigma(A)/\sigma_1,$$

yields the ratio of capture rate at  $A$  to the capture rate of the original seed nuclei (iron group). High values of this slope over a region of  $A$  will tend to equalize  $\psi(A)$  through this region. Figure 5 displays such a curve plotted with experimentally estimated cross sections to be discussed later and with  $\sigma_1 = 15$  mb. Notice that a smooth curve in  $A'$  will be greatly modified by transformation to  $A$  coordinates. In the regions of large slope,  $94 < A < 135$  and  $142 < A < 200$ , the value of the function  $\psi(A)$  will tend to be nearly constant, whereas large changes in  $\psi(A)$  for a fixed  $\tau$  may occur in the regions where  $\sigma(A)$  is small. Small cross sections are observed for nuclei with closed shells of neutrons at the "magic" numbers,  $N = 50, 82,$  and  $126$ . This investigation reveals the manner in which changing cross sections might be expected to affect the spreading of a distribution as it advances in  $A$ . However, it still does not represent a quantitatively accurate description of the capture chain, for in changing the  $A$  dependence of the equation from a difference to a partial derivative, the spreading

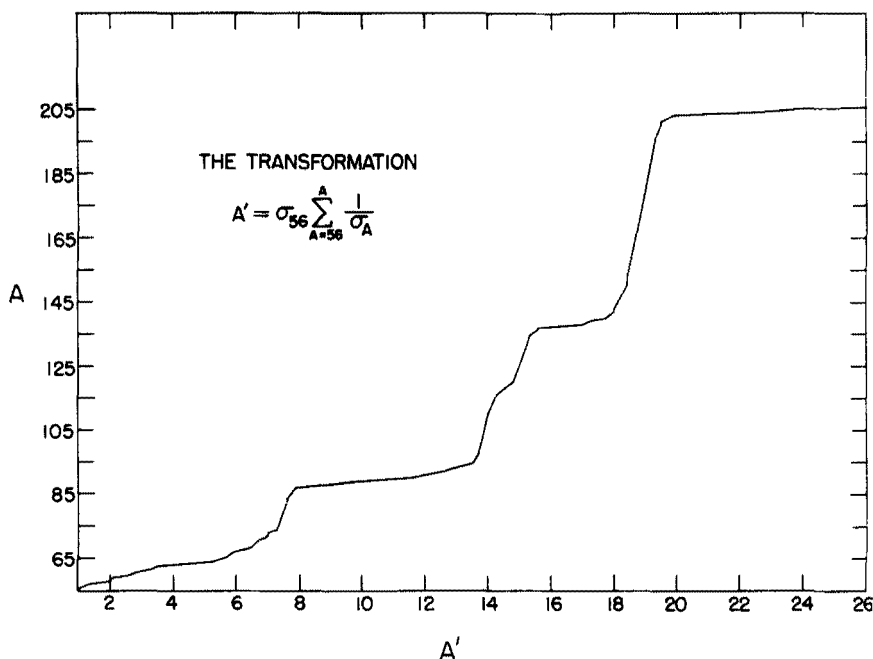


FIG. 5. The transformation yielding a one-to-one correspondence of  $A$  to  $A'$ . Approximate  $\psi_A$  solutions for the capture chain are obtained by transforming solutions  $\psi_{A'}$  for constant cross section into  $A$  coordinates.

due to random capture is neglected. This is most easily seen by examining the situation in which  $\sigma$  is a constant, making  $A = A' - 55$ . This situation would give a transition of a packet of nuclei to increasing  $A$  without any spreading at all, whereas it is known from the constant cross section case that the packet will spread as it moves out in  $A$ .

When a group of nuclei are exposed to a neutron flux, the resulting distribution will be spread over some range of  $A$ , centered approximately at the appropriate point given by the mean increase in atomic weight. The various sources of this spread may be summarized here.

- a. The initial distribution may be spread over a region in  $A$ .
- b. The random nature of discrete neutron captures, based as it is on probabilities, tends to diffuse any initial concentration of nuclei. This type of spreading increases monotonically with increasing neutron exposure.
- c. The cross sections of the capture chain determine the capture rate at each value of  $A$ . Different capture rates at points along the path alter the distribution by speeding up or retarding capture events relative to the average capture rate of the distribution as a whole. The final distribution is expanded or contracted depending on whether the cross sections increase or decrease with  $A$ .

Effect (a) may be easily handled in all solutions by superposition of distributions resulting from unique seed nuclei. Effect (b) may be isolated by considering the exact solutions for constant cross section. Effect (c) may be isolated by considering the hydrodynamic flow analogy of the last section. It now remains to incorporate effects (b) and (c) into one approximate solution.

In an earlier disclosure (12) we proposed an approximate solution based on the following considerations. The equation for the abundances  $N_A$  for constant cross section when written as a partial differential equation is the same as the partial differential equation for  $\psi$  in  $A'$  coordinates.

$$\left(\frac{\partial}{\partial \tau} + \sigma_1 \frac{\partial}{\partial A}\right) N(A, \tau) = 0 \quad \text{and} \quad \left(\frac{\partial}{\partial \tau} + \sigma_1 \frac{\partial}{\partial A'}\right) \psi(A', \tau) = 0. \quad (19)$$

Both quantities satisfy the same boundary conditions in the case of a peak at  $A = A_1$  at  $\tau = 0$ . Thus it appears that  $\psi(A', \tau)$  for varying cross sections and  $N(A, \tau)$  for constant cross section will be very similar. For this reason we calculated  $\psi_{A'}(\tau)$  with Eq. (11) as

$$\psi_{A'}(\tau) = \psi_1(0) \frac{(\sigma_1 \tau)^{A'-1}}{(A'-1)!} e^{-\sigma_1 \tau}. \quad (20)$$

The smooth curve drawn through these values, calculated for integral  $A'$  at a given value of  $\tau$ , yields  $\psi(A', \tau)$ . The transformation  $A'$  to  $A$  of Fig. 5 was then

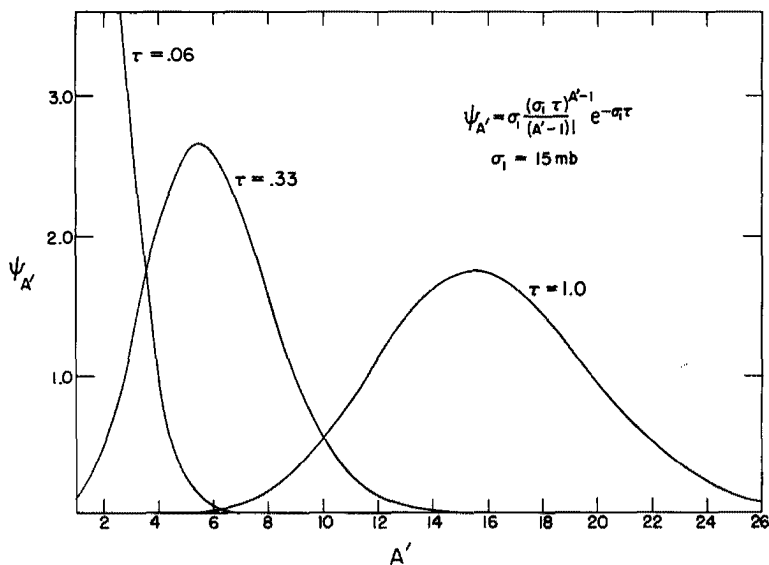


FIG. 6. The quantity  $\psi_{A'} = \sigma_1 n_A$ , for constant cross section, chosen to be  $\sigma_1 = 15$  mb. The distributions are normalized to one initial seed nucleus at  $A' = 1$ .

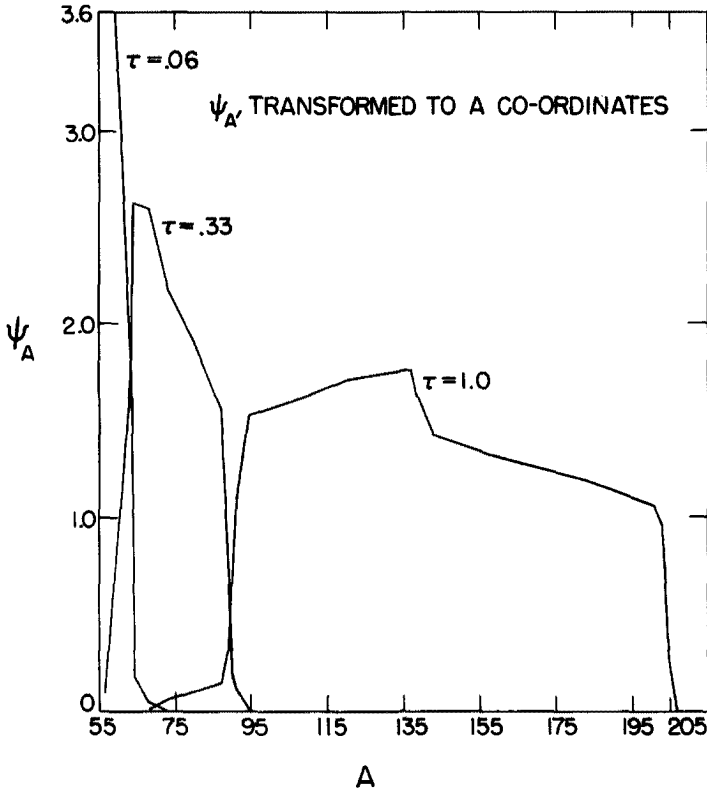


FIG. 7. The quantity  $\psi_A$  obtained by transforming the distributions of Fig. 6 into  $A$  coordinates using the coordinate transformation of Fig. 5.

employed to convert to  $\psi(A, \tau)$ . Examples of this procedure are shown in Figs. 6 and 7. Figure 6 shows  $\psi(A', \tau)$  calculated by Eq. (20) for three values of  $\tau$  corresponding to  $\sigma_1\tau = 1, 5,$  and  $15$  ( $\tau = 1/15, 1/3, 1$ ). Figure 7 shows the same three distributions after transformation to  $A$  coordinates. Recall that  $\psi$  represents the normalized distribution resulting from the exposure of one seed nucleus ( $N_1(0) = 1$ ); therefore  $\psi_1(0) = \sigma_1 N_1(0) = \sigma_1 = 15$ . The curves generated have approximately correct properties, and this method may be used to extract a great deal of useful information. We will drop this method here, however, for the examination of a more precise method of calculations which constitutes the main body of this effort.

There is little doubt that direct numerical integration of Eq. (5) would yield the most accurate approximation to the exact solution. But the solutions of the s-process chain do not require great accuracy as much as they require ease of calculation and interpretation with perhaps ten per cent error. However, there

were also two main objections to the numerical approach. First of all the numerical integration has to proceed in small steps so that relatively long calculations would be needed to obtain solutions for large  $\tau$ . We did not know in advance which values of  $\tau$  would be of greatest interest, and so it was very convenient to have a method which will quickly produce solutions for any value of  $\tau$ . The second objection is that errors "grow" in numerical calculation, which means that more accurate solutions would be obtained for small  $\tau$  than would be obtained for large  $A$  and large  $\tau$ . The method to be presented now has the advantage of simpler calculation than the numerical integration as well as almost uniform error for any value of  $\tau$ . There is the further added advantage of a functional solution for  $\psi_A$  in which the dependence on each capture cross section is explicit. These features enable swifter evaluation as new cross-section data become available.

#### V. AN APPROXIMATE SOLUTION OF HIGH RELIABILITY

If the Laplace transforms of the functions representing the abundances are defined as

$$\bar{N}_k(s) = \int_0^{\infty} e^{-s\tau} N_k(\tau) d\tau,$$

Eqs. (6) become

$$\begin{aligned} s\bar{N}_1(s) &= -\sigma_1\bar{N}_1(s) + N_1(0), \\ s\bar{N}_2(s) &= -\sigma_2\bar{N}_2(s) + \sigma_1\bar{N}_1(s), \\ s\bar{N}_k(s) &= -\sigma_k\bar{N}_k(s) + \sigma_{k-1}\bar{N}_{k-1}(s). \end{aligned} \tag{21}$$

Solving algebraically

$$\begin{aligned} \bar{N}_k(s) &= N_1(0) \frac{\sigma_{k-1}\sigma_{k-2}\cdots\sigma_2\sigma_1}{(s+\sigma_k)(s+\sigma_{k-1})\cdots(s+\sigma_2)(s+\sigma_1)}, \quad \text{or} \\ \bar{\psi}_k(s) &= \frac{\sigma_k\bar{N}_k(s)}{N_1(0)} = \frac{1}{\left(\frac{s}{\sigma_k} + 1\right)\left(\frac{s}{\sigma_{k-1}} + 1\right)\cdots\left(\frac{s}{\sigma_1} + 1\right)}. \end{aligned} \tag{22}$$

It has already been seen that the exact inversion of this transform is unwieldy and depends on the number of higher order poles ( $\sigma_i - \sigma_j$ , etc). The object of this approach is to find an easily calculable inverse that closely approximates the exact inverse. It will be found profitable to investigate the possibility of doing this by approximating the Laplace transform. Motivated by our previous solution, we consider the corresponding problem where all cross sections are the

same and equal to  $\lambda$  (reserving  $\sigma$  for actual cross sections) for which

$$\frac{\lambda \bar{N}_m^*(s)}{N_1(0)} = \frac{1}{\left(\frac{s}{\lambda} + 1\right)^m}, \quad (23)$$

where  $N_m^*$  is the abundance for constant cross section and  $m$  is a new numbering index analogous to  $k$ . An effort will be made to approximate the Laplace transform of the exact solution of Eq. (22) by the Laplace transform of Eq. (23). Our task is then to choose, for each  $k$ , values of  $m_k$  and  $\lambda_k$  in Eq. (23) such that

$$L^{-1} \frac{1}{\left(\frac{s}{\lambda_k} + 1\right)^{m_k}} \text{ "best" approximates} \quad (24)$$

$$L^{-1} \frac{1}{\left(\frac{s}{\sigma_k} + 1\right) \left(\frac{s}{\sigma_{k-1}} + 1\right) \cdots \left(\frac{s}{\sigma_1} + 1\right)},$$

where

$$\psi_k(\tau) = L^{-1} \bar{\psi}_k(s) = \frac{1}{2\pi i} \int_{-i\infty}^{i\infty} e^{s\tau} \bar{\psi}_k(s) ds. \quad (25)$$

When this choice has been made, we shall write

$$\psi_k(\tau) = \frac{\sigma_k N_k(\tau)}{N_1(0)} \simeq L^{-1} \frac{1}{\left(\frac{s}{\lambda_k} + 1\right)^{m_k}} = \lambda_k \frac{(\lambda_k \tau)^{m_k-1}}{\Gamma(m_k)} e^{-\lambda_k \tau} \quad (26)$$

Two apparent advantages of this method of investigation immediately appear:

a. A glance at Eq. (22) shows that  $\bar{\psi}_k(s)$ , and hence  $\psi_k(\tau)$ , depend only on the magnitudes  $\sigma_1, \sigma_2, \dots, \sigma_k$ , and not upon the order in which they occur. Consequently  $m_k$  and  $\lambda_k$  will be chosen for each  $k$  independent of the ordering of the cross sections up to and including  $\sigma_k$ . Moreover, it will be seen later that an important justification of the approximation procedure depends crucially on this fact.

b. The Laplace transforms are valid for any  $\sigma_1, \sigma_2, \dots$ , including those special cases in which some are equal.

The theory of functions reveals the well known fact that the behavior of a function for very small  $\tau$  and the behavior for very large values of  $\tau$  correspond, respectively, to the behavior of its Laplace transform for very large and very small values of  $s$ . An attempt at a best approximation is therefore dependent upon the range of interest of  $\tau$ . For the  $s$ -process interest lies principally in moderate to large values of  $\tau$ . Thus, it is expected that the best approximation

should be chosen to make the Laplace transforms equal for small values of  $s$ . The error in calculating  $\psi_k(\tau)$  is

$$E_k = \frac{1}{2\pi i} \int_{-i\infty}^{i\infty} e^{s\tau} \left[ \frac{1}{\left(\frac{s}{\lambda_k} + 1\right)^{m_k}} - \frac{1}{\left(\frac{s}{\sigma_k} + 1\right) \cdots \left(\frac{s}{\sigma_1} + 1\right)} \right] ds \quad (27)$$

$$= \frac{1}{2\pi i} \int_{-i\infty}^{i\infty} e^{s\tau} \frac{\sum_{h=1}^k B_{kh} s^h ds}{\left(\frac{s}{\lambda_k} + 1\right)^{m_k} \left(\frac{s}{\sigma_k} + 1\right) \cdots \left(\frac{s}{\sigma_1} + 1\right)},$$

where

$$B_{k1} = -\frac{m_k}{\lambda_k} + \sum_{i=1}^k \frac{1}{\sigma_i},$$

$$B_{k2} = -\frac{m_k(m_k - 1)}{1 \cdot 2} \frac{1}{\lambda_k^2} + \sum_{\substack{i,j=1 \\ i < j}}^k \frac{1}{\sigma_i \sigma_j}, \quad (28)$$

$$B_{k3} = -\frac{m_k(m_k - 1)(m_k - 2)}{3!} \frac{1}{\lambda_k^3} + \sum_{\substack{i,j,f=1 \\ i < j < f}}^k \frac{1}{\sigma_i \sigma_j \sigma_f}.$$

The major contribution to the error  $E_k$  comes from the integrand near  $s = 0$ . It is then desirable to have the coefficients of the smaller powers of  $s$  in the numerator vanish. Our approximation is the "best" in the sense that we choose  $m_k$  and  $\lambda_k$  such that the first two coefficients  $B_{k1}$  and  $B_{k2}$  vanish. This means

$$\frac{m_k}{\lambda_k} = \sum_{i=1}^k \frac{1}{\sigma_i} = k \left\langle \frac{1}{\sigma} \right\rangle_k. \quad (29)$$

In the last expression we drop the subscript  $i$  and the average is to be taken over all nuclei up to  $k$ . We also have

$$\frac{m_k(m_k - 1)}{2\lambda_k^2} = \sum_{\substack{i,j=1 \\ i < j}}^k \frac{1}{\sigma_i \sigma_j}. \quad (29')$$

Solving these two equations for  $m_k$  and  $\lambda_k$  yields

$$m_k = \frac{\left(\sum_{i=1}^k \frac{1}{\sigma_i}\right)^2}{\sum_{i=1}^k \frac{1}{\sigma_i^2}} = k \frac{\left\langle \frac{1}{\sigma} \right\rangle_k^2}{\left\langle \frac{1}{\sigma^2} \right\rangle_k}, \quad \lambda_k = \frac{\sum_{i=1}^k \frac{1}{\sigma_i}}{\sum_{i=1}^k \frac{1}{\sigma_i^2}} = \frac{\left\langle \frac{1}{\sigma} \right\rangle_k}{\left\langle \frac{1}{\sigma^2} \right\rangle_k}. \quad (30)$$

Note that the sums in  $m_k$  and  $\lambda_k$  range up to and include  $k$ . Hence  $\psi_k(\tau)$  includes a dependence on  $\sigma_k$ .

Then  $\lambda_k$  and  $m_k$  may be calculated for all values of  $k$ , from which  $\psi_k(\tau)$  may be calculated by Eq. (26). It can be seen that this is really an extension of the method presented earlier, where  $m_k = A' = \sigma_1 \sum_{i=1}^k 1/\sigma_i$ . In the present method, however,  $\sigma_1$  is replaced by  $\lambda_k$ , taking advantage thereby of one additional degree of freedom to make the error smaller.

It can be shown that both the exact and approximate solutions for  $\psi_k(\tau)$  have only one maximum for a given  $k$  as a function of  $\tau$ , approaching zero asymptotically for large and small  $\tau$  (excepting  $\psi_1(\tau)$  which has its maximum at  $\tau = 0$ ). It is also evident that the approximate  $\psi_k(\tau)$  has its maximum value at  $\tau_k(\max)$  given by

$$\begin{aligned} \lambda_k \tau_k(\max) &= m_k - 1, \\ \tau_k(\max) &= \frac{m_k}{\lambda_k} - \frac{1}{\lambda_k} = \sum_{i=1}^k \frac{1}{\sigma_i} - \frac{1}{\lambda_k} \simeq \sum_{i=1}^k \frac{1}{\sigma_i} = \sum_{i=1}^k (\Delta\tau)_i, \end{aligned} \quad (31)$$

where  $(\Delta\tau)_i = 1/\sigma_i$ , which is the average exposure required for the  $i$ th nucleus to capture a neutron. This approximate maximum occurs, then, at the place one would intuitively expect, i.e., the maximum occurs for nucleus  $k$  when the exposure  $\tau$  is just the average exposure necessary to transform the seed nucleus ( $k = 1$ ) into the nucleus  $k$ . But what information can be specifically concluded about the manner in which the approximate solution "approaches" the real solution?

It is helpful at this point to recall that the Laplace transform is a moment generating function.

$$\begin{aligned} L\psi(\tau) &= \int_0^{\infty} e^{-s\tau} \psi(\tau) d\tau \\ &= \int_0^{\infty} \psi(\tau) d\tau - s \int_0^{\infty} \tau\psi(\tau) d\tau + \frac{s^2}{2} \int_0^{\infty} \tau^2\psi(\tau) d\tau \dots \end{aligned} \quad (32)$$

The power series expansion of the reciprocal of a polynomial begins

$$\frac{1}{1 + ax + bx^2 + \dots} = 1 - ax + (a^2 - b)x^2 + \dots \quad (33)$$

Thus, making the pair of numbers,  $a$  and  $b$ , for the approximate Laplace transform equal the corresponding pair for the exact Laplace transform insures that

the first and second moments of  $\psi_k(\tau)$  in  $\tau$  are equal. These may be evaluated

$$\frac{1}{\left(\frac{s}{\sigma_k} + 1\right)\left(\frac{s}{\sigma_{k-1}} + 1\right) \cdots \left(\frac{s}{\sigma_1} + 1\right)} = 1 - s \sum_{i=1}^k \frac{1}{\sigma_i} + s^2 \left[ \left( \sum_{i=1}^k \frac{1}{\sigma_i} \right)^2 - \sum_{\substack{i,j=1 \\ i < j}}^k \frac{1}{\sigma_i \sigma_j} \right] + \cdots, \quad (34)$$

$$\frac{1}{\left(\frac{s}{\lambda_k} + 1\right)^{m_k}} = 1 - s \frac{m_k}{\lambda_k} + s^2 \left[ \left( \frac{m_k}{\lambda_k} \right)^2 - \frac{m_k(m_k - 1)}{2\lambda_k^2} \right] + \cdots.$$

But by our choice we made

$$\frac{m_k}{\lambda_k} = \sum_{i=1}^k \frac{1}{\sigma_i}, \quad \frac{m_k(m_k - 1)}{2\lambda_k^2} = \sum_{i < j}^k \frac{1}{\sigma_i \sigma_j};$$

thus the first three moments are equal for approximate and true solutions and have the values

$$\int_0^\infty \psi_k(\tau) d\tau = 1,$$

$$\int_0^\infty \tau \psi_k(\tau) d\tau = \sum_{i=1}^k \frac{1}{\sigma_i}, \quad (35)$$

$$\int_0^\infty \tau^2 \psi_k(\tau) d\tau = 2 \left[ \left( \sum_{i=1}^k \frac{1}{\sigma_i} \right)^2 - \sum_{i < j}^k \frac{1}{\sigma_i \sigma_j} \right] = \left[ \left( \sum_{i=1}^k \frac{1}{\sigma_i} \right)^2 + \sum_{i=1}^k \left( \frac{1}{\sigma_i} \right)^2 \right].$$

The first integral shows only that all nuclei pass through a given  $k$  at some value of  $\tau$ . The second integral reveals that, although the location of the single maximum of the real solution is unknown, its centroid is the same as that of the approximate solution, which is also very near the maximum of the approximate solution as seen in Eq. (31). The third equality yields added assurance that contributions of the tails (known to smoothly approach zero) to the second moment are equal.

It would be desirable, at this point, to check this method against some known yardstick before proceeding to its actual application. Calculations were made with this method using  $\sigma_k = \gamma k$  with  $\gamma = 1$  since it is only a scale factor. These solutions were compared with the exact solutions for such a case calculated earlier (Eq. 10). Figure 8 shows plots of  $\psi_k$  versus  $k$  for two values of  $\tau$  from both the approximate and exact solutions. The comparisons are seen to be quite good in light of the strenuous demands made by this assumption for the cross sections.

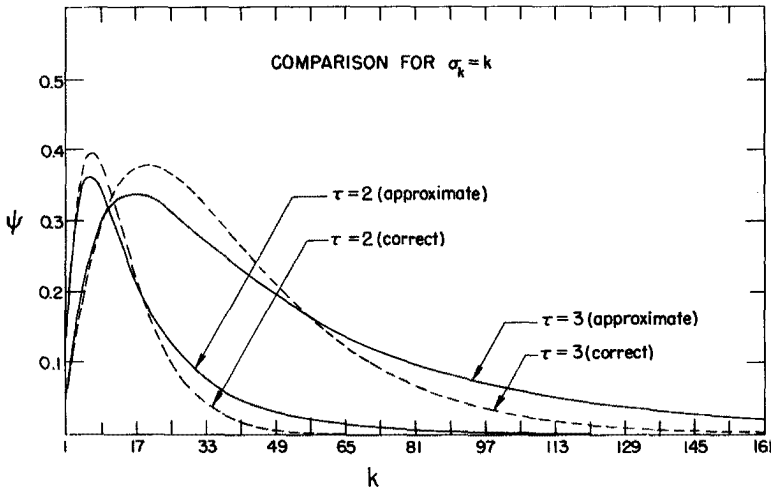


FIG. 8. Comparison of exact and approximate solutions for  $\sigma_k = k$ . The dashed curves show the exact solution for certain  $\tau$ , whereas the solid curves show the approximate solution for the same value of  $\tau$ . The approximate solutions adhere well to the correct physical properties of the exact solutions, but the value of the maximum appears to be underestimated by about 10 per cent.

One might rightly question the validity of this test for a more perplexing case in which one or two small cross sections occur in the neighborhood of large ones, as is the actual case for nuclei with closed neutron shells. This doubt may be partially dispelled by the following imaginary problem. Suppose

$$[\sigma_1, \sigma_2, \sigma_3 \cdots \sigma_{10}] = [1, 4, 2, 6, 7, 8, 9, 5, 3, 10].$$

We have seen that the exact solution for  $\psi_k(\tau)$  is independent of the ordering of the cross sections  $\sigma_{m \leq k}$ . Thus the solution for  $\psi_9$  with  $\sigma_9 = 3$  is exactly the same as in the case of  $\sigma_k = k$  (the abundances  $N_k = \psi_k/\sigma_k$  will of course be different). For  $\psi_5$  with  $\sigma_5 = 7$ , solutions will be approximately that for  $\sigma_k = \frac{7}{5}k$  and so on. Extensions of this observation can be quite general. In solving the s-chain, one can, for each value of  $k$ , renumber all the cross sections up to and including the  $k$ th one, and find rough linearity in many cases. This fact assures that the error in the calculation of  $\psi_k$  is of the same order as the error for the exactly linear case.

Further confidence may be gained by noting that superpositions of various exposures tend to decrease the relative error in  $\psi_k$  rather than to change the error in an arbitrary or statistical manner. If  $\rho(\tau)$  represents the number of seed nuclei exposed to a flux  $\tau$  in the interval  $d\tau$ , then after the superposition

$$\sigma_k N_k = \int_0^{\infty} \rho(\tau) \psi_k(\tau) d\tau. \quad (36)$$

From the moment generating nature of the Laplace transform, it was found that the error in  $\sigma_k N_k$  is in fact zero for any  $\rho(\tau)$  of the form  $a + b\tau + c\tau^2$ . The manner in which errors may cancel upon superposition can also be seen from Fig. 8 which shows at  $k = 33$ , for example, an underestimation for  $\tau = 3$  and an overestimation for  $\tau = 2$ . Such observations as these build our confidence in the general validity of the approximation procedure. Discussion of the practical application of Eq. (36) to observations on  $\sigma N$  will be postponed until Section X.

## VI. APPLICATION TO PROBLEM WITH EXPERIMENTAL CROSS SECTIONS

To apply the previous development to the *s*-process it is necessary to assume numerical values for each of the cross sections in the *s*-process neutron capture chain. This requires that a choice be made for the temperature of the stellar interior where the neutron production and capture is taking place. The cross sections depend on the neutron energy and thus on the temperature of the material in which the neutrons are produced, thermalized, and captured. From considerations based on possible neutron sources such as  $C^{13}(\alpha, n)$ ,  $Ne^{21}(\alpha, n)$ , and  $C^{12} + C^{12}$ ,  $B^2FH$  give a most probable value of  $T \sim 10^8$  to  $10^9$  °K. From detailed considerations, Reeves and Salpeter (13) conclude that the carbon

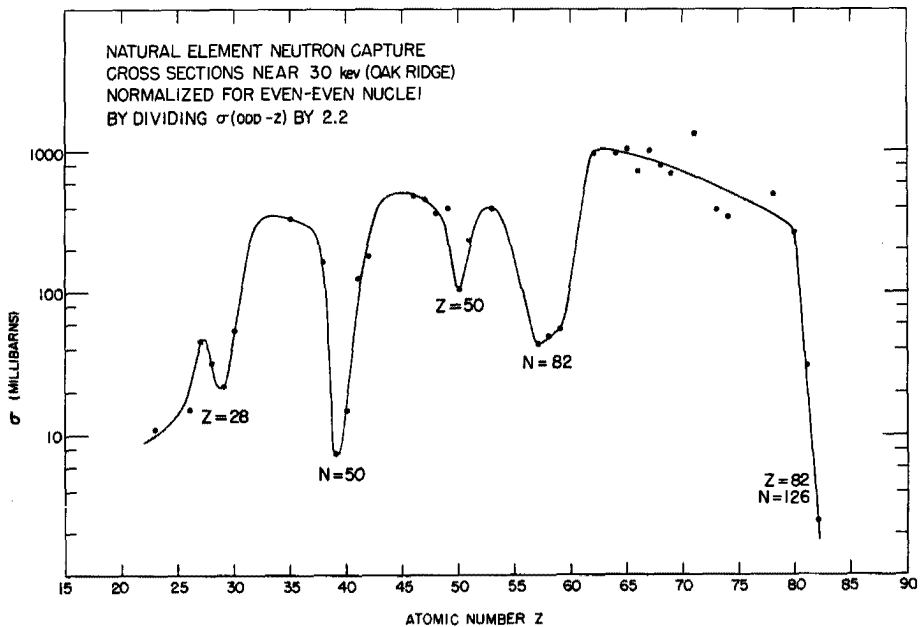


FIG. 9. The average neutron capture cross section for the elements in their natural abundances near 30 keV. The cross sections for the odd *Z* nuclei have been divided by 2.2. Taken from Oak Ridge data (27, 28).

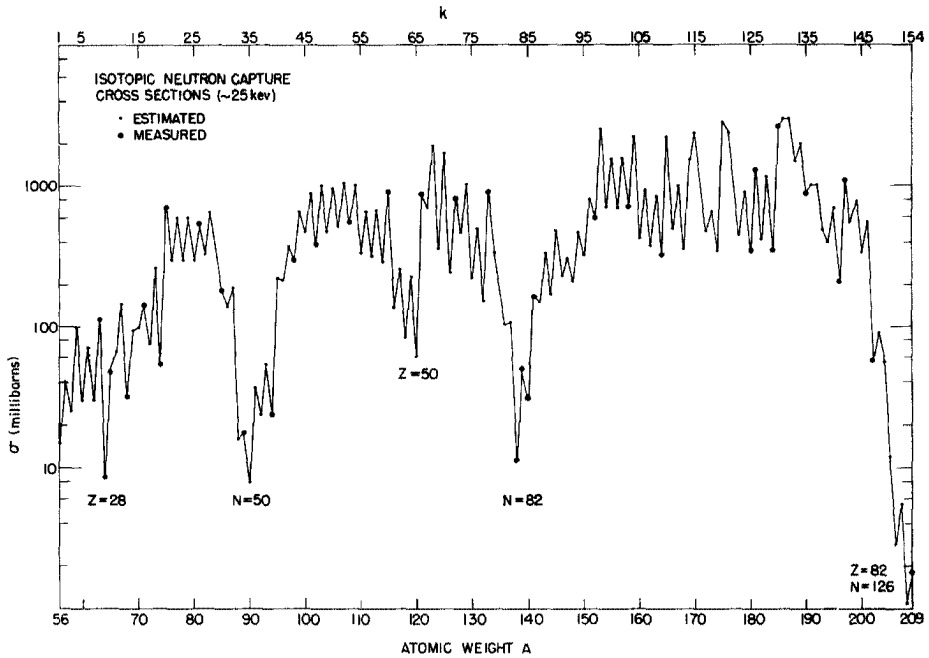


FIG. 10. The isotopic neutron capture cross sections for nuclei lying on the *s*-process path. Cross sections indicated by heavy circles are measured near 25 keV (25, 26). All other points represent values estimated in a manner described in Appendix A. These cross sections are the ones used in calculating the *s*-process distributions.

burning reactions could effectively produce neutrons at temperatures of about  $6 \times 10^8$  °K. Temperatures of  $10^8$  to  $10^9$  °K correspond to thermal energies from 10 to 100 keV.

For the actual calculation of the present problem it is not feasible to select the temperature arbitrarily. Rather the choice must be made on the basis of available experimental measurements of the neutron capture cross sections. A selected survey of this cross-section data is presented in the appendix to this paper. References are given there. Much of the information on isotopic cross sections has been obtained using an Sb-Be neutron source, producing neutrons of about 25 keV. A large body of data on the cross sections for elements in their natural abundances has been reported at 30 keV. The average energy dependence of the cross sections in this range of energies indicates that  $\sigma(25 \text{ keV})$  is only about 10 per cent greater than  $\sigma(30 \text{ keV})$ . Since the measurements at 25 keV cover the most extensive range in *A* for isotopic cross sections we have chosen to correct all cross sections to 25 keV and to interpolate in *A* where experimental values are not available. It is evident then that we have chosen a thermal

energy of about 25 keV ( $T \sim 3 \times 10^8$ ) for this work. This energy falls in the independently estimated temperature range for neutron production discussed above. It might be mentioned here that if the energy dependence of the cross sections is more or less the same for the heavy elements in question, moderate changes in energy of the  $s$ -process neutrons could be interpreted as a simple change of scale in the flux-time exposure  $\tau$ . That is, if all cross sections were reduced 20 per cent, the resulting distributions would be the same as before but for  $\tau$ 's greater by 20 per cent. No great error will be made if a  $\sigma \sim 1/v$  law is used in extending our calculations at 25 keV to other energies in the 10- to 100-keV range. Some caution is warranted in the lower energy range since individual resonances may become important for some of the lighter nuclei involved in the capture chain.

From Table 3 in the Appendix we have plotted the cross-section data. Figure 9 shows the cross section for elements in their natural isotopic abundances plotted against the atomic number. Figure 10 shows the isotopic cross sections for the members of the  $s$ -process chain plotted against the atomic weight. The solid points of Fig. 10 are values estimated by interpolation as shown in the Appendix, whereas the heavy circles represent actual isotopic measurements. It is this set of values of  $\sigma_k$  shown in Fig. 10 that is used in calculating  $m_k$  and  $\lambda_k$  in the manner prescribed in the previous section. Figure 11 shows the values of

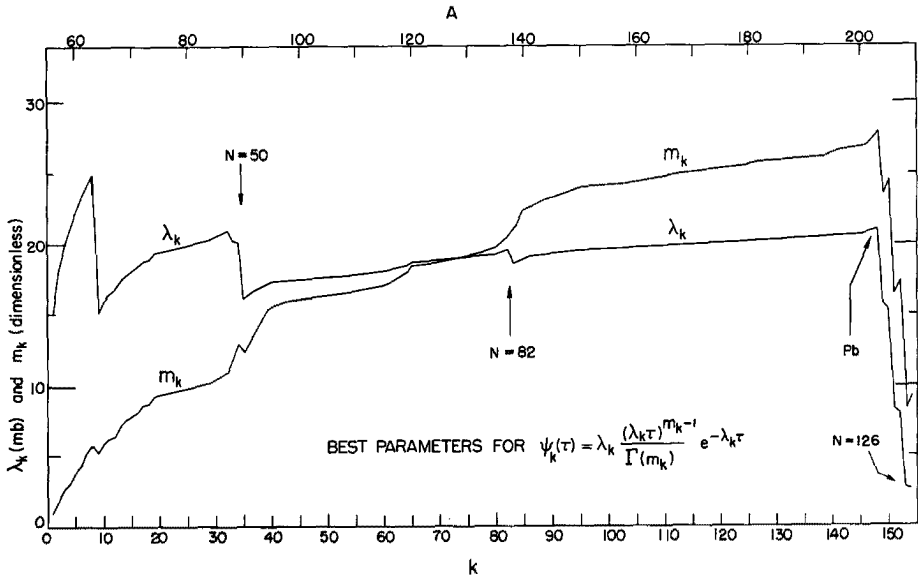


FIG. 11. The best choice of parameters for calculation of the approximate solutions. The value of 8.7 is used here for  $\sigma_{e4}$  and is reflected as a large irregularity in  $\lambda_{e4}$ . The effect of small cross sections in the magic neutron number nuclei and lead isotopes is apparent.

$m_k$  and  $\lambda_k$  versus  $k$ . The calculation of  $m_k$  and  $\lambda_k$  was incorporated into a program on a Datatron 205 computer which also calculated the resulting distributions. For facility of programming, Eq. (26) was re-written using

$$\Gamma(m) \simeq \sqrt{\frac{2\pi}{m}} \left(\frac{m}{e}\right)^m \left(1 + \frac{1}{12m}\right),$$

so that

$$\psi_k(\tau) = \lambda_k \frac{(\lambda_k \tau)^{m_k-1} e^{-\lambda_k \tau}}{\Gamma(m_k)} \simeq \left[\frac{\lambda_k e \tau}{m_k}\right]^{m_k} \sqrt{\frac{m_k e^{-\lambda_k \tau}}{2\pi \tau}} \left(1 + \frac{1}{12m_k}\right). \quad (37)$$

These functions,  $\psi_k$ , were calculated for values of  $\tau$  from 0.1 to 2.9 in steps of  $\Delta\tau = 0.1$ . For physical applications it is more useful to plot  $\psi_k$  versus  $k$  with the neutron flux-time exposure,  $\tau$ , as a curve parameter. The implications of these curves will be developed later. More mathematical investigations are first required to accomplish the following results:

- a. Account must be taken of the branch in the  $s$  path at  $A = 64$ .
- b. The nuclei stored at  $A = 210$  as a function of  $\tau$  must be properly redistributed among the lead and bismuth isotopes.
- c. It will be useful to establish the relationship between  $\tau$ , the flux-time exposure, and  $n_c$ , the average number of neutron captures per initial seed nucleus, for each distribution.

#### VII. THE BRANCH AT ATOMIC WEIGHT 64

When  $\text{Cu}^{63}$  captures a neutron, the resulting  $\text{Cu}^{64}$  is beta-active with a short half-life of 12.8 hours. The branch in the activities is 42 per cent  $EC$ , 19 per cent  $\beta^+$ , and 39 per cent  $\beta^-$ . On a long time scale the result of the neutron capture is then 61 per cent  $\text{Ni}^{64}$  and 39 per cent  $\text{Zn}^{64}$ . When either of these branches captures a neutron, the resultant nucleus has short lived activity to  $\text{Cu}^{65}$ , thereby returning to a unique path.

If the neutron capture cross sections for  $\text{Ni}^{64}$  and  $\text{Zn}^{64}$  were approximately equal, this branching could be ignored as far as the rest of the distribution is concerned. In fact, however,  $\sigma(\text{Ni}^{64})$  is measured as 8.7 mb, whereas  $\sigma(\text{Zn}^{64})$  should be much larger since  $\text{Ni}^{64}$  has a closed proton shell and  $\text{Zn}^{64}$  has two fewer neutrons. Therefore the nuclei will pass considerably more slowly through  $\text{Ni}^{64}$  than through  $\text{Zn}^{64}$ , with considerable resultant effect upon the abundance distributions.

Because the differential equations for the abundances are linear, this problem may evidently be handled by a simple superposition. To obtain the correct distribution normalized to one initial seed nucleus for a given  $\tau$ , the distributions are calculated as if all nuclei pass through  $\text{Ni}^{64}$  with 0.61 initial seed nuclei and as if all nuclei pass through  $\text{Zn}^{64}$  with 0.39 initial seed nuclei, and added at the

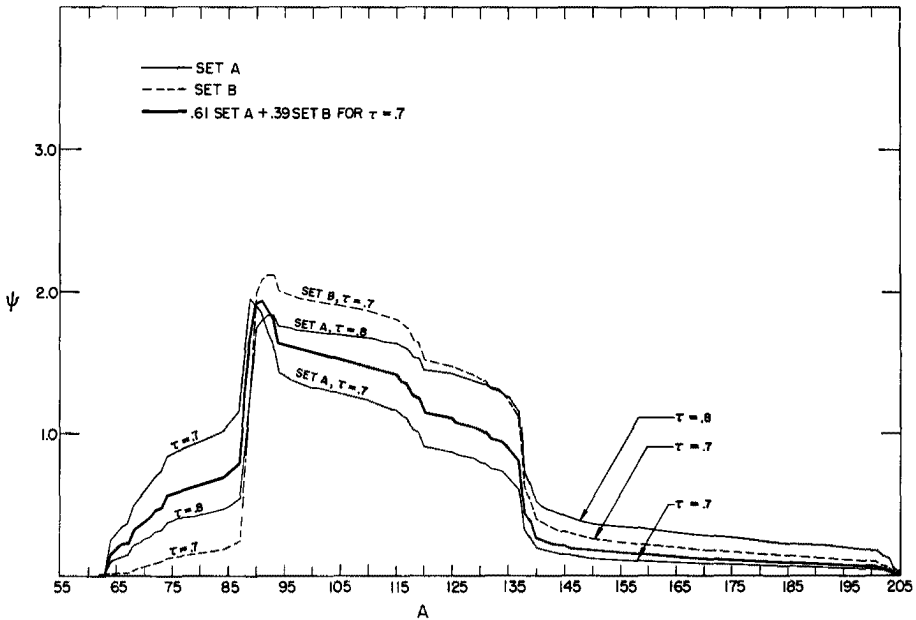


FIG. 12. The effect of the branch at atomic weight 64. Set A is calculated with  $\sigma_{64} = 8.7$  and plotted as a solid line. Set B is calculated with  $\sigma_{64} = 87$  and plotted as a dashed line. The heavy solid line is the proper superposition of Set A and Set B determined by the branching ratio at atomic weight 64. The Set A distribution for  $\tau = 0.8$  is also plotted because of its similarity to Set B for  $\tau = 0.7$ , a fact explained by the  $\Delta\tau = 0.1$  shift of A relative to B due to the different cross section at atomic weight 64.

desired value of  $\tau$ . Because of interest in comparing the resultant distributions from the two branches, we calculated both sets of distributions normalized to one initial nucleus and weighted them later for superposition to the correct expected distributions. The set of distributions obtained by passing all nuclei through  $\text{Ni}^{64}(\sigma_{64} = 8.7)$  we call set A, and the set obtained by passing all nuclei through  $\text{Zn}^{64}(\sigma_{64} = 87)$  we call set B. The correct combination to use for actual applications is then  $0.61 A + 0.39 B$ .

Figure 12 shows the effect involved here, where we have plotted, for  $\tau = 0.7$ , distributions A, B, and the superposition indicated above. The large effect of the different cross section is clearly evident. We have in addition plotted the distribution A for  $\tau = 0.8$ , and observe its close resemblance to distribution B for  $\tau = 0.7$ . The explanation of this last observation is quite simple. The exposure required for a nucleus to pass from  $k$  to  $k + 1$  is approximately  $1/\sigma_k$ , so for  $k$ 's greater than 64, distribution A should be *retarded* relative to distribution B by  $|\Delta\tau| = (1/8.7) - (1/87) = 0.10$ . Thus a useful rule is obtained, stating that the effect of changing one cross section on higher values of  $k$  may, to first

order, be thought of as a  $\tau$  shift given by  $\Delta\tau = -\Delta\sigma_k/\sigma_k(\sigma_k + \Delta\sigma_k)$ . This observation enables an estimate to be made of the effect of a new cross section value without actually recalculating the distributions. Thus the distributions  $\psi(A)$  finally obtained will only require relabelling in  $\tau$  as new experimental cross sections become available in the future. Eventually of course, an entire new calculation will be warranted but in the meantime approximate estimates can be made quickly and easily.

### VIII. TERMINATION OF THE S-PROCESS

For  $\tau$ 's greater than 1.0, the number of nuclei in the range  $A = 56$  to  $A = 209$  begins to decrease. Capture of a neutron by  $\text{Bi}^{209}$  produces a nucleus of atomic weight  $A = 210$  ( $k = 155$ ) and so far no account has been made of the subsequent alpha decays back to the lead isotopes. To correct this effect it is necessary to solve the recirculation equations attendant to the alpha decays.

Just as  $\psi$  represents the expected cross section times abundance normalized to one initial nucleus, so it is convenient to define the abundances associated with a given  $\psi$  and therefore with one initial nucleus as

$$n_A(\tau) = \frac{\psi_A(\tau)}{\sigma_A} = \frac{N_A(\tau)}{N_{56}(0)}. \quad (38)$$

Examination of the solutions before recycling was taken into account revealed that  $\psi_{209}(\tau)$  was nearly linear and could be approximated for  $0.9 < \tau < 2.7$  by

$$\psi_{209} = \sigma_{209}n_{209} = \alpha\tau', \quad (39)$$

where  $\alpha = 0.19$ ,  $\tau' = \tau - 0.9$ . The linearity of  $\psi_{209}$  for this range of  $\tau$  is a fortunate result of the semiempirical values we have taken for the neutron capture cross sections. The value  $\tau = 2.1$  is required to process almost all the initial nuclei to atomic weights  $A > 205$ , but the very small cross sections for  $A > 205$  retard  $\psi_{209}$  such that it is still in a nearly linear rise for  $\tau$ 's as great as 2.7. As a result the quantity  $\psi_{209}$  can be assumed to be a known driving term for the recirculation equations and equal to  $\alpha\tau'$ . This approximation will be valid as long as the additions to  $\psi_{209}$  from recirculation remain much smaller than the value of  $\psi_{209}$  without recirculation. This condition, too, was adequately fulfilled for  $\tau \leq 2.7$ . Under the assumption of a linear rise in  $\tau$  for  $\psi_{209}$  the recirculation equations can be approximately solved in a closed functional form.

Since the differential equations for the abundances are linear, the problem of the redistribution of the nuclei stored at  $A = 210$  can be solved independently of the arrival of nuclei from smaller atomic weight. We will call  $n_A'$  the *additional* abundance at atomic weight  $A$  resulting from the redistribution of the nuclei at  $A = 210$ . The computed  $n_A'$  will then be added to the abundance predicted by the previous calculations. Note especially that *this complication affects only the last four nuclei of the s-chain*,  $A = 206$  to  $A = 209$ . The gross aspects of the

abundance distributions for smaller  $A$  are already solved and need no further correction.

B<sup>2</sup>FH have discussed in detail the processes involved in the termination of the  $s$ -process. There is a branch in the neutron capture by Bi<sup>209</sup> leading 44 per cent of the time to a nearly stable (half-life =  $2.6 \times 10^6$  years) ground state of Bi<sup>210</sup> and 56 per cent of the time to an isomeric state which has a 5-day electron emission to Po<sup>210</sup>. The Po<sup>210</sup> alpha-decays (half-life = 138 days) to Pb<sup>206</sup>. The ground state of Bi<sup>210</sup> is assumed to live long enough to capture a neutron proceeding to Bi<sup>211</sup> which then rapidly alpha decays (half-life = 2 min) to Pb<sup>207</sup> through Tl<sup>207</sup> and a quick beta decay (half-life = 5 min). If all alpha and beta decays are rapid compared to the neutron capture times, and if the capture cross section for the ground state of Bi<sup>210</sup> is much greater than  $\sigma_{209}$ ,<sup>2</sup> then the differential equations for the additional (primed) abundances due to recirculation may be simply written as follows:

$$\begin{aligned} \frac{dn'_{206}}{d\tau} + \sigma_{206} n'_{206} &= 0.56 \sigma_{209} n_{209} \\ &= 0.56 \alpha \tau', \end{aligned} \quad (40a)$$

$$\begin{aligned} \frac{dn'_{207}}{d\tau} + \sigma_{207} n'_{207} &= \sigma_{206} n'_{206} + 0.44 \sigma_{209} n_{209} \\ &= \sigma_{206} n'_{206} + 0.44 \alpha \tau', \end{aligned} \quad (40b)$$

$$\frac{dn'_{208}}{d\tau} + \sigma_{208} n'_{208} = \sigma_{207} n'_{207}, \quad (40c)$$

$$\frac{dn'_{209}}{d\tau} + \sigma_{209} n'_{209} = \sigma_{208} n'_{208}. \quad (40d)$$

These equations have simple functional solutions. Using the cross sections in millibarns listed in the appendix ( $\sigma_{206} = 2.8$ ,  $\sigma_{207} = 5.5$ ,  $\sigma_{208} = 1.1$ ,  $\sigma_{209} = 1.8$ ), and defining  $P(\sigma_n \tau') = (\sigma_n \tau' - 1 + e^{-\sigma_n \tau'})$ , the numerical answers are

$$\begin{aligned} n'_{206} &= 0.01358 P(2.8 \tau'), \\ n'_{207} &= -0.0008840 P(5.5 \tau') + 0.01407 P(2.8 \tau'), \\ n'_{208} &= 0.2679 P(1.1 \tau') + 0.001105 P(5.5 \tau') \\ &\quad - 0.04554 P(2.8 \tau'), \\ n'_{209} &= -0.2753 P(1.8 \tau') + 0.4210 P(1.1 \tau') \\ &\quad - 0.000221 P(5.5 \tau') + 0.01789 P(2.8 \tau'). \end{aligned} \quad (41)$$

<sup>2</sup> Since Bi<sup>209</sup> is neutron magic ( $N = 126$ ), it might be expected to have a considerably smaller neutron capture cross section than does Bi<sup>210</sup>. Measurements report  $\sigma(\text{Bi}^{209}) = 1.8$  mb.

These additive corrections were calculated and added to the distributions generated directly from lower atomic weight. In principle increased accuracy for the recirculated abundances could be obtained by returning to Eqs. (40a) and (40b) and replacing  $\sigma_{209} n_{209}$  by  $(\alpha\tau' + \sigma_{209} n'_{209})$  instead of  $\alpha\tau'$ . This degree of precision is unwarranted for  $\tau \leq 2.7$ .

It should be mentioned here that B<sup>2</sup>FH intimated that this termination process creates ever increasing quantities of lead and bismuth. This is, of course, not true once all of the original seed nuclei have been transformed to lead and bismuth, for the total number of heavy nuclei remains a constant. Continual exposure has the effect of creating alpha particles from neutrons, simultaneously driving the abundance distribution of the lead and bismuth isotopes to an equilibrium configuration.

An interesting appendage to the foregoing calculations may be obtained by a related investigation. For  $\tau$ 's greater than 2.5 effectively all the nuclei have reached the lead and bismuth isotopes. For very large  $\tau$ 's, a steady state or equilibrium flow between these isotopes and the regeneration by alpha decay will occur. It is possible to answer the question, "Given an arbitrary initial distribution of nuclei among the lead isotopes, how great an exposure must occur before a good approximation to equilibrium is reached?"

If all the heavy nuclei are concentrated at atomic weights greater than 205, Eqs. (40) are applicable to the exact total abundances  $n_A$  if the exact value of  $\sigma_{209} n_{209}$  is used. These equations form a simple matrix equation

$$d \begin{bmatrix} \psi_{206} \\ \psi_{207} \\ \psi_{208} \\ \psi_{209} \end{bmatrix} = \begin{bmatrix} -\sigma_{206} & 0 & 0 & 0.56 \sigma_{206} \\ \sigma_{207} & -\sigma_{207} & 0 & 0.44 \sigma_{207} \\ 0 & \sigma_{208} & -\sigma_{208} & 0 \\ 0 & 0 & \sigma_{209} & -\sigma_{209} \end{bmatrix} \begin{bmatrix} \psi_{206} \\ \psi_{207} \\ \psi_{208} \\ \psi_{209} \end{bmatrix}. \quad (42)$$

At equilibrium, the left-hand side of Eq. (42) vanishes giving for the terminal  $\psi_T$ :

$$\psi_T = \psi_{209} = \psi_{208} = \psi_{207} = \frac{1}{0.56} \psi_{206}. \quad (43)$$

The value of  $\psi_T$  depends on the values assumed for the cross sections of these nuclei. But the sum of the abundances resulting from one initial nucleus must be one, so  $n_{206} + n_{207} + n_{208} + n_{209} = 1$ . Using this fact

$$\psi_T = \frac{1}{\frac{0.56}{\sigma_{206}} + \frac{1}{\sigma_{207}} + \frac{1}{\sigma_{208}} + \frac{1}{\sigma_{209}}}. \quad (44)$$

With the same values of the cross sections as before the equilibrium distributions become

$$\psi_{206} = 0.30, \psi_{207} = \psi_{208} = \psi_{209} = 0.54 \quad (45)$$

or

$$n_{206} = 0.11, \quad n_{207} = 0.10, \quad n_{208} = 0.49, \quad n_{209} = 0.30.$$

Equation (42) has four independent decay modes to equilibrium, whose rates  $\lambda$  are given by the secular equation

$$\begin{vmatrix} -(\sigma_{206} + \lambda) & 0 & 0 & 0.56 \sigma_{206} \\ \sigma_{207} & -(\sigma_{207} + \lambda) & 0 & 0.44 \sigma_{207} \\ 0 & \sigma_{208} & -(\sigma_{208} + \lambda) & 0 \\ 0 & 0 & \sigma_{209} & -(\sigma_{209} + \lambda) \end{vmatrix} = 0. \quad (46)$$

Solutions of (46) give

$$\begin{aligned} \lambda_1 &= 0 \text{ (equilibrium solution),} \\ \lambda_2 &= -5.77, \\ \lambda_3 &= -2.72 + 1.02\sqrt{3} i, \\ \lambda_4 &= -2.72 - 1.02\sqrt{3} i. \end{aligned} \quad (47)$$

The slowest decays are seen to be oscillatory but even so it is indicated that initial deviations from equilibrium will decay to  $e^{-1}$  for an exposure

$$\Delta\tau = 1/2.72 \simeq 0.4.$$

Figure 13 shows three curves for  $\psi$  in this region. Those labeled  $\tau = 2.3$  and  $\tau = 2.7$  are calculated by the methods previously outlined, whereas that one labeled  $\tau = \infty$  is the equilibrium case. It can be seen that deviations of  $\psi$  from equilibrium at  $\tau = 2.3$  have decayed by  $e^{-1}$  for  $\Delta\tau = 0.4$  ( $\tau = 2.7$ ).

#### IX. NEUTRON REQUIREMENTS FOR THE ABUNDANCE DISTRIBUTIONS

Although the sequence of distributions generated by different integrated flux-time exposures,  $\tau$ , is of interest in itself, the average number of heavy element neutron captures per initial iron nucleus, which we call  $n_c$ , is also of interest. This  $n_c$  is obviously related to the amount of free neutrons produced by light element reactions and to the relative densities of the seed nuclei and the neutron producing nuclei. This number was calculated for each distribution in the following manner. The sum,

$$\sum_{A=56}^{A=209} (A - 56)n_A = \sum_{A=56}^{A=209} (A - 56) \frac{\psi_A}{\sigma_A},$$

equals the number of neutron captures required for each  $\tau$  to produce the corresponding distribution. This sum does not quite equal the desired  $n_c$  because the total number of nuclei fluctuates about the initial normalized value of unity due to approximations of the calculations. We thus normalized the number of neutron

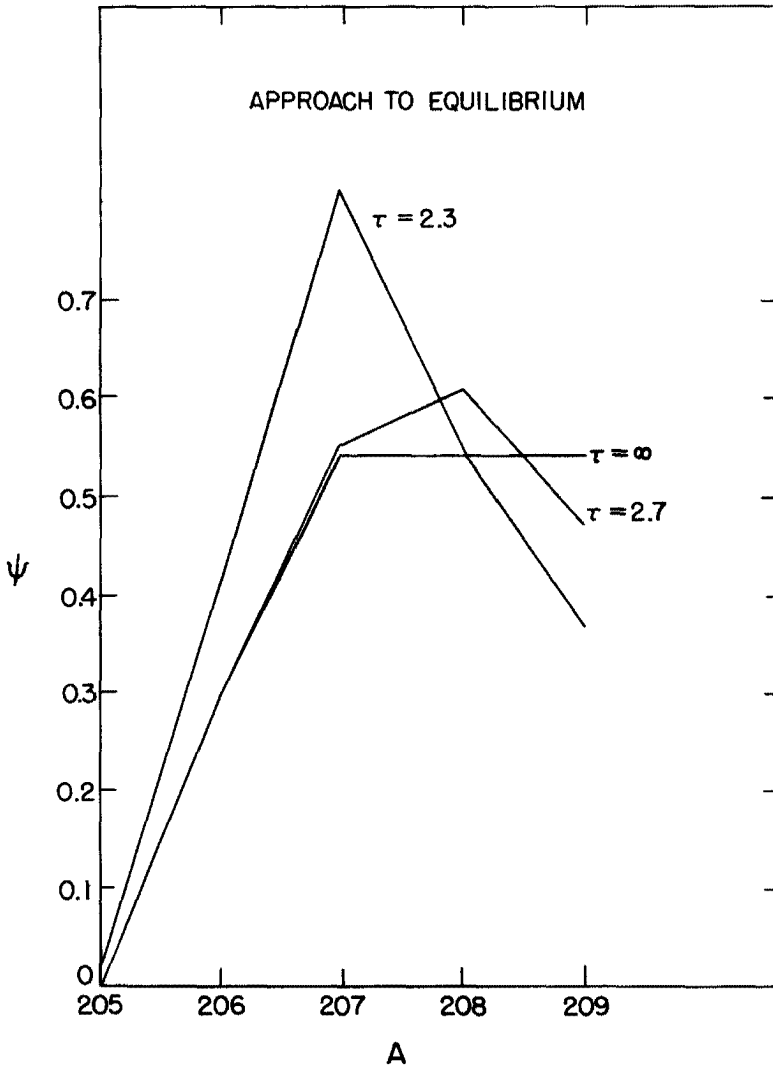


FIG. 13. The approach to equilibrium. The curves labeled  $\tau = 2.3$  and  $\tau = 2.7$  are calculated by adding the contributions of the alpha decay to the initially generated distributions and renormalizing to one total nucleus. The curve labeled  $\tau = \infty$  is the equilibrium distribution for one seed nucleus. The amplitudes for the deviation from equilibrium have decayed by about  $1/e$  for  $\Delta\tau = 0.4$ .

captures by dividing by  $\sum n_A$ , which fluctuated between the limits of 0.925 and 1.080. This calculation was incorporated into the computer program, yielding

$$n_c(\tau) = \frac{\sum_{A=56}^{209} (A - 56)n_A(\tau)}{\sum_{A=56}^{209} n_A(\tau)}. \quad (48)$$

From this set of numbers two other quantities of interest were numerically calculated. The instantaneous capture rate of the total distribution is

$$\bar{\sigma}(\tau) = \frac{\Delta n_c(\tau)}{\Delta\tau} = \frac{n_c(\tau + 0.1) - n_c(\tau - 0.1)}{0.2}. \quad (49)$$

The average capture rate for the interval 0 to  $\tau$  is

$$\bar{\sigma}(0 \rightarrow \tau) = \frac{n_c(\tau)}{\tau}. \quad (50)$$

Table II shows these numbers for all the calculated values of  $\tau$  based on the correct superposition of set *A* and set *B*.

TABLE II  
NEUTRON REQUIREMENTS FOR SINGLE EXPOSURE DISTRIBUTIONS<sup>a</sup>

$\tau$	$n_c$	$\frac{\Delta n_c}{\Delta\tau}$	$\frac{n_c}{\tau}$	$\tau$	$n_c$	$\frac{\Delta n_c}{\Delta\tau}$	$\frac{n_c}{\tau}$
0.1	2.8		28.3	1.6	145.2	34.1	90.8
0.2	6.9	49.6	34.4	1.7	147.9	20.8	87.0
0.3	12.8	65.9	42.5	1.8	149.4	12.3	83.0
0.4	20.1	71.7	50.2	1.9	150.7	7.6	79.1
0.5	27.1	70.2	54.2	2.0	151.4	4.9	75.5
0.6	34.1	78.0	56.8	2.1	151.9	3.2	72.0
0.7	42.7	100.0	61.0	2.2	152.3	2.4	68.9
0.8	54.1	127.7	67.6	2.3	152.5	2.2	66.0
0.9	68.2	149.2	75.8	2.4	152.8	2.0	63.3
1.0	83.9	156.7	83.9	2.5	153.1	1.7	60.9
1.1	99.6	149.0	90.5	2.6	153.3	1.5	58.6
1.2	113.7	130.0	94.8	2.7	153.5	1.3	56.5
1.3	125.6	104.4	96.6				
1.4	134.6	77.4	96.2				
1.5	141.0	53.1	94.0				

<sup>a</sup> The average number of neutrons captured,  $n_c$ , per initial seed nucleus; the instantaneous capture rate,  $\bar{\sigma}(\tau) = \frac{\Delta n_c}{\Delta\tau}$ , for the resulting distribution; the average capture rate,  $\bar{\sigma}(\tau) = \frac{n_c}{\tau}$ , for the resulting distribution are listed respectively for each step in  $\tau$  made in the calculations of this paper. The correspondence is valid only for the cross sections listed in Appendix A, *i.e.*, near 25 kev.

The distribution of Fig. 13 for  $\tau = 2.7$ ,  $n_c = 153$ , shows at most a ten per cent deviation from the equilibrium distribution. For this reason we arbitrarily take  $n_c = 153$  to mark the approximate onset of equilibrium. The remaining variations from equilibrium will have decreased by a factor  $1/e$  by

$$\tau = 3.1(\Delta\tau = 0.4).$$

Since  $dn_c = d\tau \sum_A \psi_A$ , and since  $\sum_{206}^{209} \psi_A \simeq 2$  at equilibrium, an exposure of  $\Delta\tau = 0.4$  requires only 0.8 additional neutron captures. The cross sections drop so markedly at  $\text{Pb}^{206}$  that all of the nuclei are swept into the range  $206 \leq A \leq 209$  by almost the minimum number of neutron captures possible. Beyond  $n_c = 155$  practically no change in the heavy element distribution occurs and additional neutrons are only converted into helium nuclei.

Figures 14 and 15 show a selected few of the calculated distributions as a function of  $A$  with  $n_c$  as a curve parameter. Figure 16 shows  $n_c$ ,  $\Delta n_c / \Delta\tau$ , and  $n_c / \tau$  as functions of  $\tau$ . Note that  $n_c$  increases very slowly for  $\tau > 3$  because

$$dn_c/d\tau = \bar{\sigma}(\tau) = \sum_{206}^{209} \psi_A = 2$$

for the equilibrium configuration among the lead and bismuth nuclei.

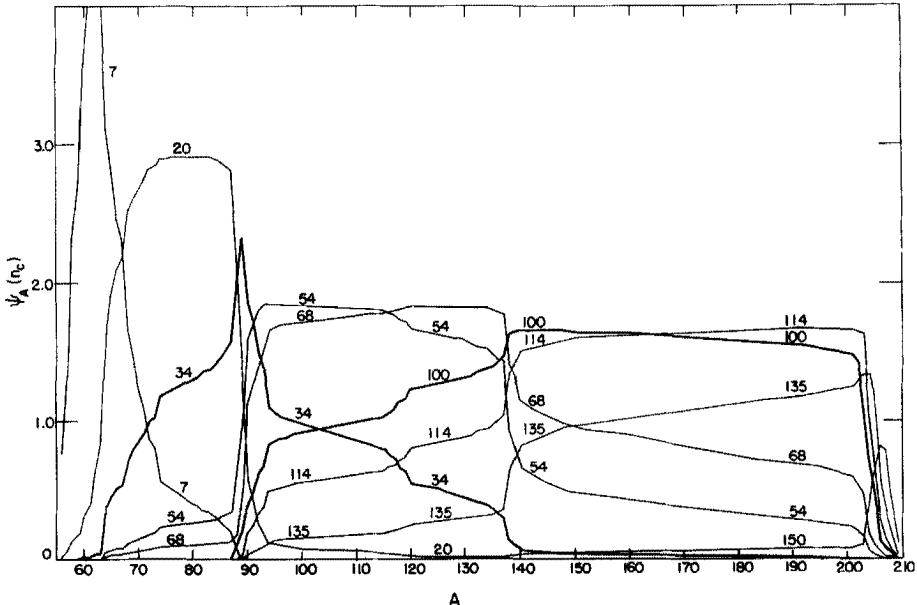


FIG. 14. The distribution in  $\psi_A = \sigma_A n_A$  for various uniform exposures. Each curve is labeled by  $n_c$ , the average number of neutron captures per initial iron seed required to generate the distribution.

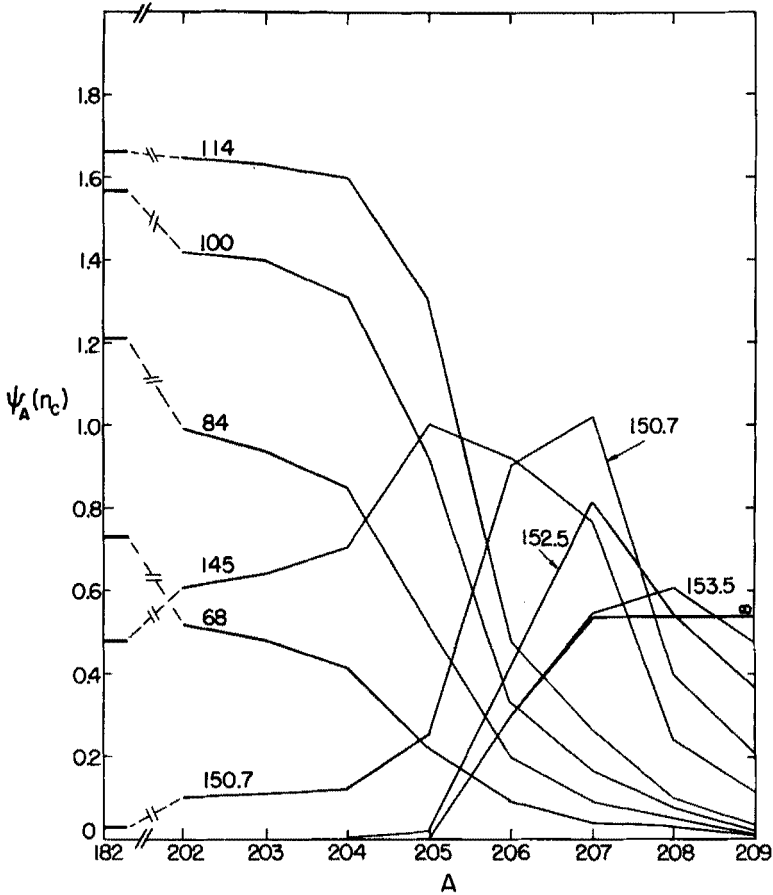


FIG. 15. The distribution in  $\psi_A = \sigma_A n_A$  for various neutron exposures for  $A > 202$ . Each curve is labeled by  $n_c$ .

Equation (26) revealed that each  $\psi_k(\tau)$  is a Poisson function. The centroid of  $\psi_k(\tau)$  is at  $\tau_c(k) = m_k/\lambda_k = \sum_{i=1}^k (1/\sigma_i)$  and the width about the centroid is  $\Delta\tau(k) \simeq \sqrt{2\pi m_k/\lambda_k}$ . The relationship between  $n_c$  and  $\tau$  of Fig. 16 enables the interpretation of the functions  $\psi_k$  with  $n_c$  as the independent variable. In Fig. 17 the  $\psi_A$  for  $A = 70, 115, 139, 204, 206,$  and  $208$  are exhibited as a function of the number of neutrons,  $n_c$ , captured per initial seed nucleus. Figure 18 shows  $\psi_A$  for  $A$  from 202 to 209 for large values of  $n_c$ . It will be noted in Fig. 17 that in general  $\psi_A$  rises to a maximum when  $n_c \simeq A - 55$ , which is approximately the value of  $n_c(\tau)$  at  $\tau_c(k)$ , and then decreases. The width at half maximum is given

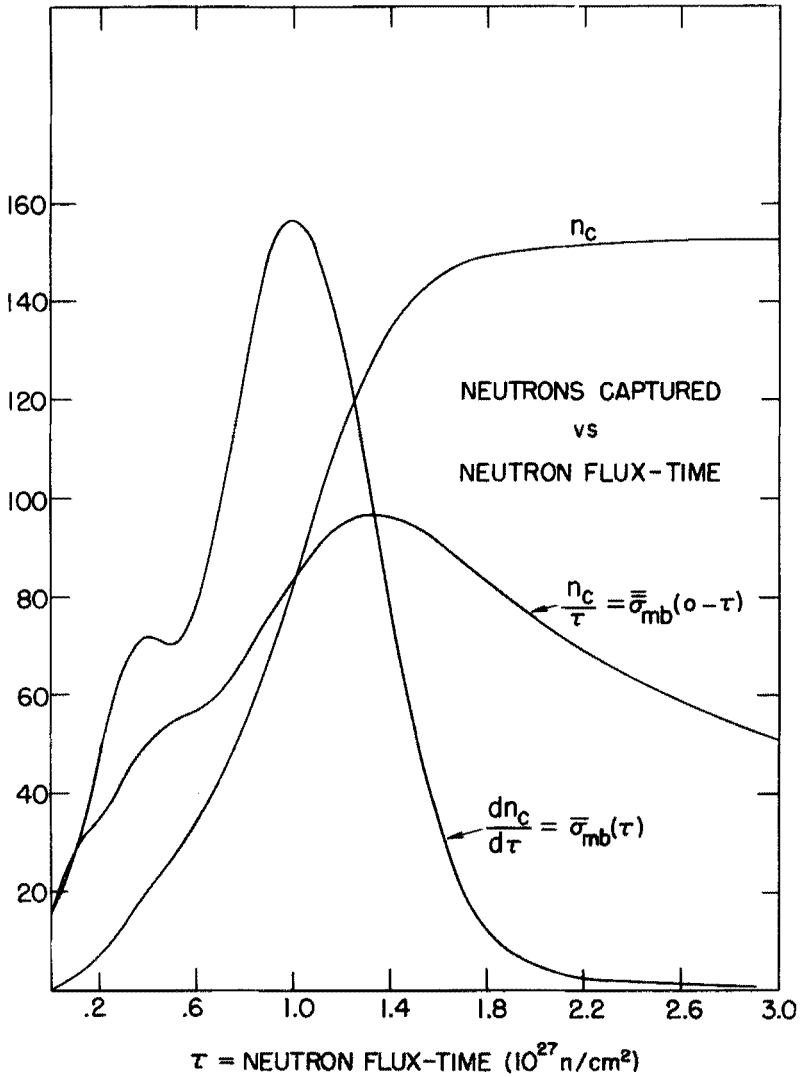


FIG. 16. The average number of neutrons captured per initial iron seed nucleus versus the flux-time exposure  $\tau$ . The derivative  $dn_c/d\tau = \bar{\sigma}$  is the instantaneous capture rate of the overall distribution of nuclei as a function of  $\tau$ . The ratio  $n_c/\tau = \bar{\sigma}$  is the average rate of capture of the distribution during the interval  $0-\tau$ . As a rule of thumb,  $\bar{\sigma} \sim 50$  to  $100$  for  $\tau > 0.4$ .

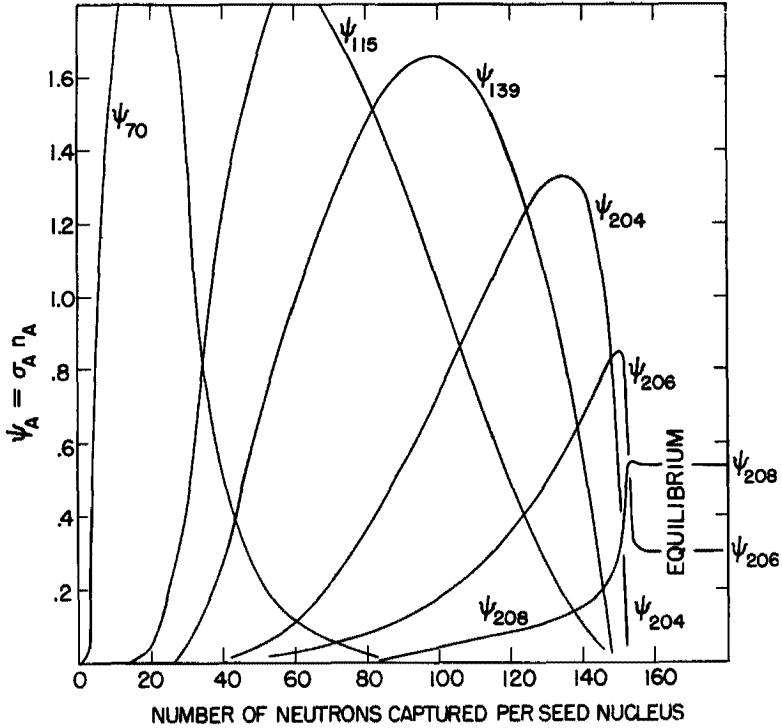


FIG. 17. The product  $\sigma_A n_A = \psi_A$  is plotted as a function of  $n_c$  for  $A = 70, 115, 139, 204, 206,$  and  $208$ . These distributions have heights and widths that can be approximately and imply predicted as in Eqs. (51) and (52).

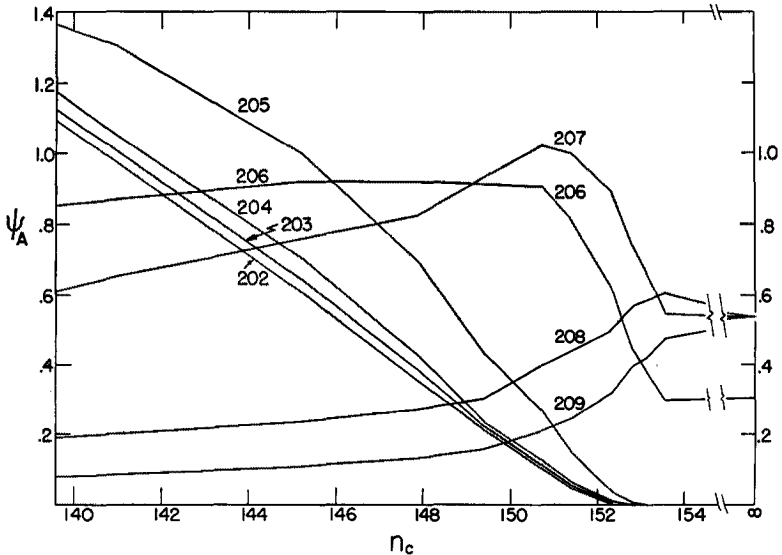


FIG. 18. The product  $\sigma_A n_A = \psi_A$  is plotted as a function of large  $n_c$  for  $A = 202$  to  $209$ .

approximately by

$$\Delta n_c(k) = \left( \frac{dn_c}{d\tau} \right)_{\tau_c(k)} \Delta\tau(k), \quad (51)$$

The nonconstancy of  $dn_c/d\tau$  prohibits any simple and accurate estimate of  $\Delta n_c(k)$  in terms of  $m_k$  and  $\lambda_k$ , as can be done for  $\Delta\tau(k)$ . However for

$$n_c < 100, \quad dn_c/d\tau \simeq 1.5 n_c/\tau,$$

from which

$$\Delta n_c(k) \simeq 1.5 \frac{n_c(\tau_c)}{\tau_c} \Delta\tau(k) = 1.5 \frac{n_c(\tau_c)}{m_k/\lambda_k} \frac{\sqrt{2\pi m_k}}{\lambda_k} = \sqrt{\frac{14}{m_k}} n_c(\tau_c). \quad (52)$$

Thus for  $n_c < 100$ , which corresponds to  $A < 155$ , it is approximately true that  $\psi_A$  has a max at  $n_c = A - 55$ , and a width at half maximum of

$$\Delta n_c(A) = \sqrt{\frac{14}{m_k}} n_c = \sqrt{\frac{14}{m_k}} (A - 55).$$

Since  $m_k$  is of the order of 15 for many  $A$ 's (see Fig. 11) it is surprisingly true that  $\Delta n_c \simeq n_c$ . These deductions are evident from  $\psi_{70}$ ,  $\psi_{115}$ , and  $\psi_{139}$  of Fig. 17.

For the larger  $\tau$ 's required to reach larger  $A$  values,  $dn_c/d\tau$  drops rapidly, which contracts the width  $\Delta n_c(k)$  of (51). For  $A$ 's greater than 200 the value of  $\psi_A(n_c)$  drops precipitously after reaching its maximum, as seen in  $\psi_{204}(n_c)$ . The same behavior occurs for  $A = 206$  except that  $\psi_{206}$  falls to its final equilibrium value, 0.30, rather than zero. In the case  $A = 208$ ,  $\psi_A$  reaches its maximum for  $n_c = 153$  and then falls slightly to its final equilibrium value of 0.54.

#### X. APPLICATIONS TO THE OBSERVED $\sigma N$ CURVE

In the preceding sections we have discussed methods for determining

$$\psi_A = \sigma_A n_A$$

as a function of  $\tau$ , the integrated neutron exposure, or of  $n_c$ , the average number of neutrons captured per seed nucleus. In particular, we have calculated  $\psi_A$  for one  $\text{Fe}^{56}$  seed nucleus. For clarity we have designated the abundances by  $n_A$  in this case. For comparison with observations on  $\sigma_A N_A$  as given in Fig. 1, it has been convenient to plot  $\psi_A$  as a function of  $A$  with  $n_c$  as parameter as shown in Figs. 14 and 15, respectively. We have used  $N_A$  to represent abundances on the standard Suess-Urey scale. Questions of normalization aside, it will be clear that the observed curve does not correspond in detailed form to any of the calculated  $\psi_A$  curves. As noted previously, this can be attributed to two causes:

(1) Other light and intermediate weight nuclei in addition to  $\text{Fe}^{56}$  have served as seed nuclei. This may have been the case and the superposition of curves for various seed nuclei similar to those shown in Figs. 14 and 15 could probably be made to give a reasonable caricature of the observed curve. How-

ever, we are inclined to believe that the iron group nuclei have served primarily as the seed for heavy element synthesis and among these  $\text{Fe}^{56}$  is by far the most abundant. Thus we neglect the effect on  $\psi_A$  due to this cause.

(2) The seed nuclei have been subjected to varying overall neutron exposures. We regard this second cause as the more important of the two and some elaboration of the astrophysical mechanisms of nucleosynthesis involved in this regard will now follow.

The abundances used in the data on which Fig. 1 is based are primarily characteristic of the elements found in the solar system. It is a basic premise of the B<sup>2</sup>FH theory of nucleosynthesis in stars that these elements were produced in many stars which evolved over the history of the Galaxy, prior to the formation of the solar system. Heavy elements were produced at various locations in the interiors of these stars whenever neutrons became available and were eventually ejected into the interstellar medium of the Galaxy by gradual or sudden mass loss by the star. Rapid mixing on a time scale of  $\sim 10^8$  years took place in the spiral arms throughout the history of the Galaxy so that the solar system formed some  $4.5 \times 10^9$  years ago from well-mixed contributions from many stars. Contributions from evolving stars occurred over an interval prior to the formation of the solar system of the order of  $10 \times 10^9$  years (14). It is not to be expected that the neutron exposure of the seed nuclei was uniform from star to star nor for that matter from place to place nor from time to time within a given star. Thus it is clear that we must try to make up the observed  $\sigma N$ -curve by superimposing curves corresponding to different neutron exposures for varying numbers of seed nuclei. This will lead to the understanding of the "history" of neutron exposures in the evolved stars of the Galaxy. There must be no confusion here with the exposure history of a given seed nucleus. As emphasized previously, the time variation of the neutron exposure for a given seed nucleus does not matter since Eqs. (6) are linear. It is only the total integrated neutron flux or total number of neutrons made available for capture which are important in determining the final abundance distribution. However, individual seed nuclei have been subjected, as noted above, to quite different  $\tau$  and  $n_c$  and it is in this sense which we must now superimpose our previous solutions.

Let  $\rho(\tau)$  represent the number of iron group nuclei exposed to the integrated neutron flux,  $\tau$ , in the interval  $d\tau$ . Numerically,  $\rho(\tau)$  is adjusted to the Suess and Urey abundance scale for which  $\text{Si} = 10^6$  is the standard. On this scale,  $N_e = 6.4 \times 10^5$  where  $N_e$  stands for the abundance of the iron group nuclei ( $\text{V}^{50}$  to  $\text{Ni}^{62}$ ) produced in the  $e$ -process. Similarly, let  $g(n_c)$  represent the number of iron group nuclei which have been exposed to  $n_c$  neutrons in the interval  $dn_c$  per seed nucleus. Then  $g(n_c) dn_c = \rho(\tau) d\tau$  and

$$\int_0^{\infty} g(n_c) dn_c = \int_0^{\infty} \rho(\tau) d\tau = N_e. \quad (53)$$

Equation (53) is indicative of our procedure in normalizing to Suess and Urey abundances and thus must include those iron group nuclei which have *not* been subjected to neutron exposure. If we *exclude* these nuclei then we will find in what follows that the remainder of the integrals are relatively very small indeed. We can represent this result as follows:

$$\int_{>0}^{\infty} g(n_c) dn_c = \int_{>0}^{\infty} \rho(\tau) d\tau \ll N_e. \quad (54)$$

There is some ambiguity in the exact value for the lower limit of integration. However, as indicated in Fig. 1 we concern ourselves only with  $A \geq 62$  whereas for most of the seed nuclei  $A = 56$ . To reach  $A = 62$  requires on the average six neutrons,  $n_c = 6$ , and as a practical matter few nuclei reach  $A = 62$  for  $n_c \leq 1$ . In this practical sense Eq. (54) is to be taken to indicate that only a small fraction of the iron group nuclei have been subjected to neutron exposure since their primary formation. Thus the iron group abundance distributions have remained characteristic of the equilibrium process in which they were produced. Astrophysically this must be taken to mean that the iron group nuclei found in the solar system have not been condensed into the deep interiors of the stars in between their primary formation and their incorporation into the various objects of the solar system. Those nuclei which have been through the deep interior of evolving stars have almost certainly at one time or another been exposed to a neutron flux.

With  $g(n_c)$ ,  $\rho(\tau)$ , and  $\psi_A$  defined as above it is now possible to express the observed  $\sigma_A N_A$  as the following integrals:

$$\sigma_A N_A = \int_0^{\infty} g(n_c) \psi_A(n_c) dn_c = \int_0^{\infty} \rho(\tau) \psi_A(\tau) d\tau \quad A \geq 62. \quad (55)$$

In principle then the problem resolves itself into the "unfolding" of  $g(n_c)$  or  $\rho(\tau)$  from the observed  $\sigma_A N_A$  using the calculated  $\psi_A$ . There is no ambiguity in using zero for the lower limit of integration in these integrals since unexposed nuclei do not contribute to  $\sigma_A N_A$ . However, for  $A \leq 62$  the abundances have been determined by the equilibrium process and it is meaningless to compare  $\sigma_A N_A$  with integrals over the  $\psi_A$  calculated for neutron capture.

It is worthwhile at this point to emphasize one aspect of the use of Eq. (55). Consider, for example, the situation which will occur when an experimental cross section value  $\sigma_A$  for a given atomic weight becomes available and replaces the estimate given in Table III. In principle  $\psi_A$  depends on  $\sigma_A$ . However, moderate changes in  $\sigma_A$  do not change  $\psi_A$  appreciably, especially if  $\sigma_A$  is large. As a consequence  $\sigma_A N_A$  does not depend critically on  $\sigma_A$  and one can have some confidence in calculating  $N_A$  simply by using the general average of  $\sigma_A N_A$  near  $A$  and dividing by the experimental  $\sigma_A$ . Similarly the  $g(n_c)$  or  $\rho(\tau)$  derived from (55) are primarily dependent on a given  $\sigma_A$  through the product  $\sigma_A N_A$  rather

than through  $\psi_A$ . In case  $\sigma_A$  is small, as for a nucleus with a closed neutron shell, these remarks do not apply and detailed calculations are required when new data becomes available.

Some insight into the meaning of Eq. (55) results from the use of the hydrodynamical approximation (see Eq. 17) with no initial spread in seed nuclei, i.e., one seed nucleus only. In this approximation  $\psi_A$  is proportional to a  $\delta$ -function according to  $\psi_A(n_c) = \sigma_A \delta(A = A_1 + n_c)$  and hence  $\sigma_A N_A = \sigma_A g(A - A_1)$  or  $N_A = g(A - A_1)$ . This obvious relation tells us that if there were no statistical spreading in the capture process then  $g(A - A_1)$  would just indicate the number of nuclei which had captured  $A - A_1$  neutrons. Hydrodynamical flow is a poor approximation but even so if we average over a region covering the statistical spreading, then the total  $N_A$  in this region is roughly the number of seed nuclei which have on the average captured  $A - A_1$  neutrons. As can be seen in the curve for  $n_c = 100$  in Fig. 14, the spread is in some cases so large that this approximation is of little use in practical application.

There is a general property of  $\psi(\tau)$  which leads to an interesting consequence. We refer to Eq. (35) which indicates, when  $k$  is replaced by  $A = k + A_1$ , that

$$\int_0^{\infty} \psi_A(\tau) d\tau = 1. \quad (56)$$

In the case that  $\rho(\tau)$  is a constant given by  $\rho(\tau) = N_e/\tau_{\max}$  for  $0 \leq \tau \leq \tau_{\max}$  we see from (55) and (56) that

$$\sigma_A N_A \simeq N_e/\tau_{\max} \quad \text{for} \quad 56 \leq A < A_{\text{lim}}. \quad (57)$$

This equation states that  $\sigma_A N_A$  will also be approximately constant up to a limiting value of  $A$ , designated  $A_{\text{lim}}$ , which can be calculated for any  $\tau_{\max}$ . At  $A_{\text{lim}}$ ,  $\sigma_A N_A$  will decline rapidly to zero. Interest in this point is prompted by the constancy of  $\sigma_A N_A$  in the region  $90 < A < 200$  shown in Fig. 1. It might be argued that this experimental behavior implies  $\rho(\tau) \sim \text{const}$  over the relevant range in  $\tau$ . This does not of course follow rigorously from the "unfolding" process and indeed we will find in what follows that  $\rho$  can be discontinuous, i.e., superpositions of the calculated curves for several discrete  $\tau$  will fit the observed curves within the experimental errors.

We now turn our attention to the details of Fig. 1 and attempt to synthesize it from the curves of Fig. 14 in the spirit of the first integral relationship given in Eq. (55). It is immediately evident, as previously emphasized, that none of the calculated curves of Fig. 14 resembles the observed curve in entirety. Thus we can immediately eliminate the possibility that the observed  $\sigma N$  curve is the result of the exposure of iron group nuclei to a uniform integrated neutron flux. The relatively large values of  $\sigma N$  for  $A < 90$  and the large negative slope in this range implies that the largest fractions of the seed nuclei were exposed to a

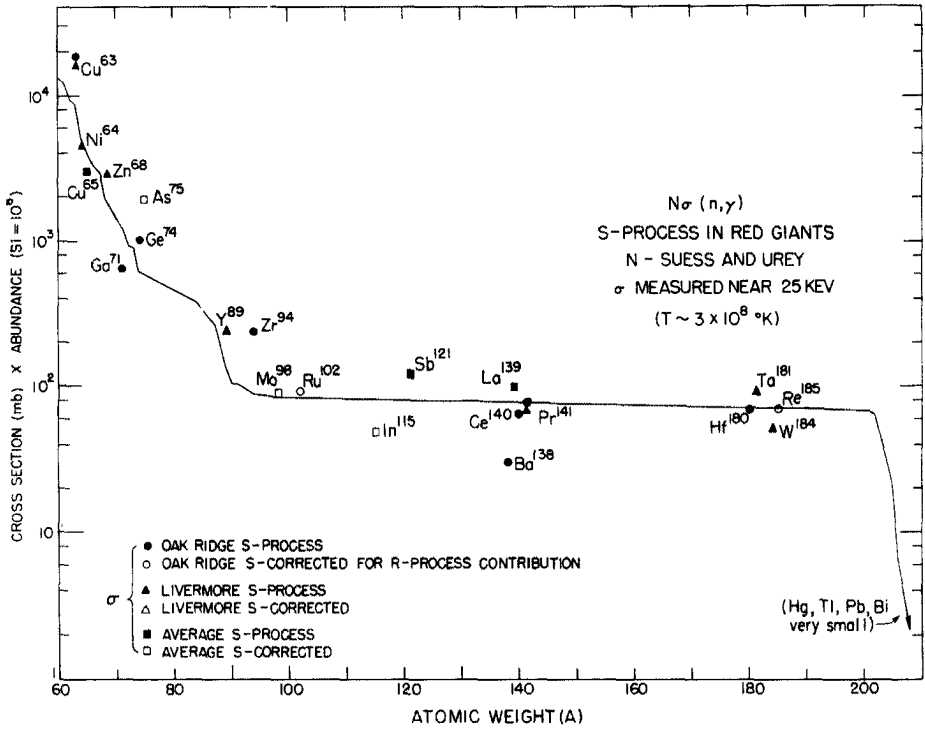


FIG. 19. A superposition of exposures to approximately fit the observed  $\sigma N$  data curve. The format is identical to Fig. 1, but the curve is a calculated one,  
 $\sigma_A N_A = 2160 \psi(n_c = 2.8) + 990 \psi(n_c = 6.9) + 45 \psi(n_c = 34) + 45 \psi(n_c = 100)$   
 See Eqs. (58) and (59) in the text.

limited neutron supply resulting in a total exposure characterized by  $\tau \sim 0.1$  or  $n_c \sim 3$ . It has already been noted that over the range  $90 < A < 200$ , the  $\sigma N$  curve remains relatively constant. Discussion of the behavior of the curve beyond  $A \sim 200$  will be postponed until later sections.

One of the many ways in which  $\sigma N$  for  $62 < A < 200$  could be approximately synthesized is shown in Fig. 19 where we have plotted

$$\begin{aligned}
 \sigma N &= 2160\psi(\tau = 0.1) + 990\psi(\tau = 0.2) + 45\psi(\tau = 0.6) \\
 &\quad + 45\psi(\tau = 1.1) \\
 &= 2160\psi(n_c = 2.8) + 990\psi(n_c = 6.9) + 45\psi(n_c = 34) \\
 &\quad + 45\psi(n_c = 100).
 \end{aligned}
 \tag{58}$$

In these equations the numbers on the right-hand side represent the number of iron group nuclei exposed to the indicated values of  $\tau$  or  $n_c$ . These numbers

are on the customary abundance scale fixed by  $N(\text{Si}) = 10^6$  on which

$$N_e = 6.4 \times 10^5.$$

Relative to  $N_e$  this becomes

$$\begin{aligned} \sigma N/N_e = & 3.9 \times 10^{-3} \psi(n_c = 2.8) + 1.8 \times 10^{-3} \psi(n_c = 6.9) \\ & + 8.2 \times 10^{-5} \psi(n_c = 34) + 8.2 \times 10^{-5} \psi(n_c = 100). \end{aligned} \quad (59)$$

It will be noted immediately that only a small fraction (0.59 per cent) of the iron group nuclei has been exposed to neutron capture. Even a smaller fraction, 0.15 per cent, was converted into *s*-process nuclei with  $A \geq 63$ . The great bulk of these iron group nuclei have not been subject to neutron capture since their formation in the *e*-process. The iron group abundances are thus correctly given by the theory of the *e*-process as shown by B<sup>2</sup>FH.

Although Eq. (58) represents by no means a unique synthesis of the observed  $\sigma N$ -curve nonetheless its two major features will be characteristic of any distribution in available neutrons per seed nucleus which fits the observations. These two features are (1) relatively large exposures to  $n_c \sim 3-7$  and (2) small and equal exposures to  $30 < n_c < 70$  and  $70 < n_c < 140$ . Certain types of variation for  $\sigma N$  versus  $A$  would appear to be quite impossible on the basis of our calculations. Since the  $\psi(n_c)$  tend to be nearly constant in the range  $90 < A < 140$  and also in the range  $140 < A < 200$ , the resultant  $\sigma N$  will be nearly constant in the same regions for any superposition of the  $\psi(n_c)$ . Large changes in the  $\psi(n_c)$  occur only at nuclei with abnormally small capture cross sections, which are in general those with magic numbers (closed shells) of neutrons, viz:  $N = 50, 82, 126$  and  $A \sim 89, 138, 208$ . Thus discontinuities in the  $\sigma N$  curve will occur only near these values for  $A$ . The apparent rapid decrease in  $\sigma N$  above  $A \sim 200$  will be discussed in this connection in Section XIII. With nearly equal  $\sigma N$  levels on both sides of a region of closed shell nuclei, as is observed at  $A \sim 138$ , only slightly different  $\sigma N$  values may occur in the closed shell region depending on the superposition used to produce the equal levels on either side. In any event, the  $\sigma N$  value in the closed shell region must be approximately equal to the mean of the  $\sigma N$  levels on the two sides. In case additional discontinuities are established in the  $\sigma N$  curve in the future the most likely explanation will be the occurrence of an abnormally small cross section among the nuclei at the discontinuity. The probability of this occurring at other than the closed shells would seem to be rather small.

## XI. NEUTRON ECONOMY

The overall problem of the production of the abundance distribution from the neutron exposure of iron group nuclei conveniently resolves itself into two nearly independent parts: (a) the resultant abundances from a given distribution of

integrated neutron flux-time exposures  $\rho(\tau)$ , (b) the stellar mechanisms for production of neutrons with the resultant  $\rho(\tau)$ . This paper has investigated only the first part of the problem. Such an approach seems justifiable in light of the fact that *once a temperature for the s-process is selected*, the experimental determinations of abundances and neutron capture cross sections should allow an unfolding of  $\rho(\tau)$  in the sense of Eq. (55). This  $\rho(\tau)$  then represents a given set of conditions to be explained by the second part of the overall problem.

The lack of independence of these two parts of the problem is evident from the temperature dependence of the s-process. The identification of abundance curves such as Fig. 14 with a given  $\tau$  depends upon the temperature assumed for the process. This is because of the energy and thus temperature dependence of the neutron capture cross sections. As a simple example it is evident that if all the  $\sigma_A$  are decreased by a factor of two, a value of  $\tau$  twice as large is needed to produce the same abundance distribution. On the other hand, the temperature of the star is closely related to the neutron production mechanism of the second part of the problem. Thus the unfolding of  $\rho(\tau)$  from observed data is practically impossible unless a nearly constant temperature can be assumed for the s-process.

This same difficulty may be viewed in yet a slightly different way. The second part of the problem may be attacked first by detailed calculations of the free neutron density from the total composition and temperature of the star. From this type of calculation, such as made by Reeves and Salpeter (13),  $\tau = \int n_n(t)v dt$  may be extracted; however, that may not be identified with the  $\tau$  of this paper due to the temperature difference of the two calculations. In such a case, the simplest approximation is to assume that in the tens of kilovolts energy region all the neutron capture cross sections have roughly the same energy dependence. With that approximation, the respective  $\tau$  values of two calculations may be temperature corrected by the same scale factor as the cross sections. The hard truth of the matter is however, that the s-process calculation depends strongly on the exact magnitudes of the smallest cross sections in the chain and it is the energy dependence of those cross sections which largely determine the temperature dependence of the s-process. Appendix B elaborates on a related aspect of the temperature dependence of the capture process.

In order to have a more nearly temperature independent representation of the abundance distributions we have for the most part, considered  $n_c$  as an independent variable in place of  $\tau$ . It is quite clear, for instance, that in case a uniform scale factor is applied to all the  $\sigma_A$ , the resulting abundances are unaltered as a function of  $n_c$ . Thus we hope that curves such as Fig. 14 when labeled with  $n_c$  are reasonably independent of the temperature of the s-process. The temperature dependence is then largely contained in the relationship of  $n_c$  to  $\tau$ . To produce a desired  $n_c$  will require a  $\tau$  which is quite dependent upon the temperature of the process.

The variable  $\tau$  is related to the total number of neutrons liberated per  $\text{cm}^3$  in the stellar interior, which can be quite different than  $n_c$ , the average number captured by each heavy seed nucleus. Since values of  $\tau$  are very difficult to calculate, it is instructive to turn to the comparison of neutrons produced,  $n$ , and neutrons captured,  $n_c$ , by the heavy elements per original seed nucleus. Recall that there is always just one heavy nucleus produced per initial seed nucleus. For any  $\tau$ ,  $n_c = \bar{\sigma}_H \tau$ , where  $\bar{\sigma}_H$  is the cross section averaged first over the heavy elements produced for a given  $\tau$  and then over  $\tau$ . If  $\alpha_L$  is the number of light nuclei per original seed nucleus or per final heavy nucleus, then  $n = \bar{\sigma}_H \tau + \alpha_L \bar{\sigma}_L \tau$  where  $\bar{\sigma}_L$  is a comparable average cross section for the light nuclei. In general each light nucleus captures few neutrons. The  $\bar{\sigma}_L$  is an average over the initial and final nuclei in the neutron producing reactions as well as any light nuclei which are present but which are inert insofar as neutron production is concerned. Then

$$\frac{n_c}{n} = \frac{\bar{\sigma}_H}{\bar{\sigma}_H + \alpha_L \bar{\sigma}_L}. \quad (60)$$

Now suppose the number of neutrons produced,  $n$ , is some fraction  $\beta$  of the number of light nuclei so that  $n$  per heavy nucleus is  $\beta \alpha_L$ . Then

$$n_c = \frac{\bar{\sigma}_H \beta \alpha_L}{\bar{\sigma}_H + \alpha_L \bar{\sigma}_L} \leq \beta \frac{\bar{\sigma}_H}{\bar{\sigma}_L} \quad \text{and} \quad \leq \beta \alpha_L. \quad (61)$$

It is thus apparent that the number of heavy element captures,  $n_c$ , is limited not only by the neutron supply but also by the fact that the source nuclei also capture neutrons. As an example, suppose it takes five light nuclei, with average  $\bar{\sigma}_L = 0.1$  mb, to produce one neutron. Then for  $\bar{\sigma}_H = 50$  mb, we have

$$n_c \leq \frac{1}{5} \frac{50}{0.1} \sim 100. \quad (62)$$

Such a simple consideration as this one may be the key to the rapid drop-off in Fig. 19 for  $A > 200$ . Be that as it may, it is essential to use  $n_c$  as the independent variable. Then  $\tau$  can be calculated and then  $n$ , the actual number of neutrons which must be produced in order to make  $n_c$  neutrons available for heavy element capture.

## XII. NEW AND REVISED ABUNDANCES

Neutron activation analysis has in recent years led to new abundance determinations in meteorites. In this section we will make use of new determinations by Schmitt *et al.* (15) and by Reed *et al.* (16) in whose papers references to the other work in this field are given. On the basis of these new determinations and with some revision of Suess and Urey data we have prepared Fig. 20 which is presented as a very tentative, but possible alternative to Fig. 1.

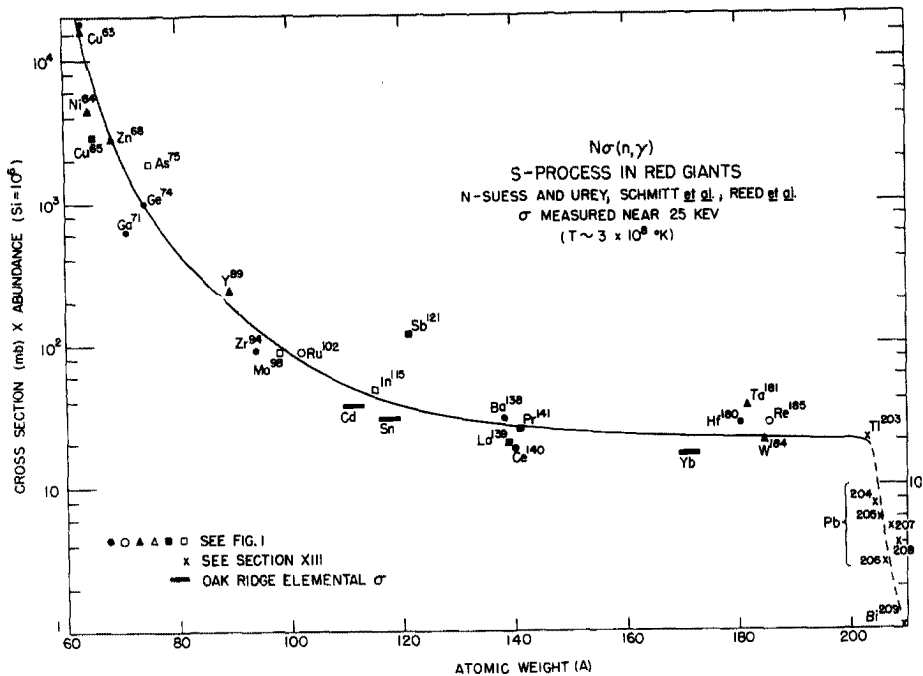


FIG. 20. A revision of Fig. 1 based on new abundance evidence obtained by neutron activation techniques. In addition the Suess and Urey abundances for Zr and Hf through Au have been lowered by a factor of 2.5. The points corresponding to the isotopes of Tl, Pb, and Bi are calculated in a manner described in Section XIII.

Schmitt *et al.* have determined the abundances of the rare earth elements in chondritic meteorites. They find the abundances of the closed shell isotopes La<sup>139</sup>, Ce<sup>140</sup>, and Pr<sup>141</sup> to be considerably less than the Suess-Urey abundances. An average of measurements on the meteorites Allegan and Richardton yields the abundances 0.40, 0.55, and 0.15 compared to the Suess-Urey values of 2.00, 2.00, and 0.40, respectively. These new measurements lower the  $\sigma N$  values for these three from  $\sim 80$  to  $\sim 20$  making them closer to the closed shell nucleus Ba<sup>138</sup> as seen in Fig. 20, which is to be compared with Fig. 1.

In order to supplement this new data we have also plotted in Fig. 20 average  $\sigma N$  values for elements which have several s-process isotopes, namely Cd, Sn, and Yb. Elemental capture cross sections are available in these cases as indicated in Table III. In the case of Cd and Sn we have used Suess and Urey abundances. For Yb we use the new determination of Schmitt *et al.* We have also noted that Suess and Urey chose an abundance value for Re 2.5 times that estimated from observations on the iron phase of meteorites. Their value for Hf was determined from the observational ratio relative to Zr. We note that

lowering  $Zr^{94}$  by a factor of 2.5 will place it closer to the curve through  $Y^{89}$ ,  $Mo^{98}$ , and  $Ru^{102}$ . We thus feel that it is not out of the question to lower  $Zr^{94}$ ,  $Hf^{190}$ , and  $Re^{185}$  by a factor of 2.5. Lowering these nuclear species means that all isotopes of Zr, Hf, and Re must be lowered. Since Ta and W were interpolated by Suess and Urey between Hf and Re we also lower  $Ta^{181}$  and  $W^{184}$ . Finally, in order to maintain the smoothness of the Suess and Urey curves, we lower by a factor of 2.5 the abundance of all the elements and their isotopes from Hf through Au. We note that similar, but not identical, abundance revisions have been made by Cameron (8). The  $\sigma N$  curve thus tapers off near  $A \sim 200$  at a value near 20 rather than 70. We note that this is very similar to the  $\sigma N$  curve drawn through widely varying "empirical" points by B<sup>2</sup>FH in 1957.

Reed *et al.* confirm the abundance of Ba chosen by Suess and Urey. However, for the heavy elements Hg, Tl, Pb, and Bi they find very much lower abundances in the chondritic meteorites but at the same time roughly the Suess-Urey values in enstatite and carbonaceous chondrites. The only exception in these chondrites is Hg for which they find rather large values to which they attribute considerable uncertainty.

Presumably these low melting point elements were removed in the formation of the ordinary chondrites in which relatively high temperature processes were involved but not in the formation of the enstatite and carbonaceous chondrites in which the order of 50 per cent of the material has clearly not been involved in high temperature events. Reed *et al.* thus suggest that solar system abundances of Tl, Pb, and Bi relative to Si are most reliably estimated from these latter meteorites. Using the data of Reed *et al.* on the Orgueil and Mighei carbonaceous meteorites to calculate abundances relative to the actual Si which they contain (lower than in ordinary chondrites) and correcting for the probable removal of lead from 50 per cent of the meteorite and from 75 per cent in the case of Tl and Bi we find  $Tl = 0.74$ ,  $Pb = 6.5$  and  $Bi = 0.92$  on the  $Si = 10^6$  scale. We are grateful to Professor L. Anders for suggesting this procedure. The values for Tl and Bi are probably lower limits in view of the ease with which these elements can be lost from meteorites (witness the ordinary chondrites). With our cross section estimate for  $Tl^{203}$  we find  $\sigma N \sim 20$ . As will be discussed in the next section, we find  $\sigma N$  for  $Pb^{204, 6, 7, 8}$  approximately equal to 5 and for  $Bi^{209}$ ,  $\sigma N \sim 1$ . There would thus seem to be a drop in  $\sigma N$  above  $A \sim 200$  and this will be discussed more fully in the next section. As emphasized above, we present Fig. 20 with considerable hesitancy. However, it differs from Fig. 1 essentially only in a lower level for  $\sigma N$  at large  $A$  and can be synthesized by changing the coefficients of  $\psi(n_c = 34)$  and  $\psi(n_c = 100)$  in Eq. (58) from 45 to 13 and in Eq. (59) from  $8.2 \times 10^{-5}$  to  $2.3 \times 10^{-5}$ . There exists the remote possibility that  $\sigma_A N_A$  remains near 70 for  $90 < A < 138$  and then drops to 20 in the range  $138 \leq A \leq 141$  and remains constant to  $A \sim 200$ . In this case only the coefficient for  $\psi(n_c =$

100) need be changed as indicated above. Inspection of Fig. 20 would appear to indicate that either  $\sigma$  or  $N$  or both may be high for  $\text{Sb}^{121}$ .

The following remarks on the neutron economy (see preceding section) may well be significant. If all the isotopes of C, N, O, and Ne were converted in hydrogen and helium burning<sup>3</sup> into  $\text{Ne}^{22}$  and the two excess neutrons in this nucleus were released by successive  $(\alpha, n)$  reactions, the maximum ratio of neutrons to iron group nuclei would be slightly over 100 using Suess-Urey abundances ( $\text{CNO}/\text{Fe-group} = 63$ ). This may mean that  $n_c$  rarely exceeds 100 and the drop in  $\sigma N$  above  $A = 200$  is real.

### XIII. LEAD AND BISMUTH ABUNDANCES

Correlations between empirical and theoretical abundances of bismuth and the isotopes of lead are of considerable importance because these two elements represent the end of the line for both the slow process and the rapid process of neutron capture and subsequent radioactive decays. There is the additional fact that the abundances of the lead isotopes are closely connected with methods of determining the time and duration of the processes of nucleosynthesis. This is because the abundances of  $\text{Pb}^{206}$ ,  $\text{Pb}^{207}$ ,  $\text{Pb}^{208}$  are in part radiogenic as the end products of the decay of  $\text{U}^{238}$ ,  $\text{U}^{235}$ , and  $\text{Th}^{232}$ . Cosmoradiogenic contributions occurred before the formation of the earth and georadiogenic contributions thereafter. Cosmoradiogenic process also contributed to the abundance of  $\text{Bi}^{209}$ . The general problem was analyzed in some detail by B<sup>2</sup>FH and an extended and revised study was made by Fowler and Hoyle (14). We are not in a position to propose a definitive solution of the lead and bismuth abundance problem but wish at this point to present the current situation as succinctly as possible. We are primarily interested in illustrating how observed abundances may be eventually corrected for  $r$ -process contributions in order to make a correlation with  $s$ -process calculations possible.

From a concordant solution based on observed and computed ratios both for  $\text{U}^{235}/\text{U}^{238}$  and  $\text{Th}^{232}/\text{U}^{235}$ , Fowler and Hoyle concluded that  $r$ -process nucleosynthesis in supernovae in the Galaxy occurred over an interval starting  $12 \times 10^9$  years ago and terminating in so far as the solar system was concerned  $4.7 \times 10^9$  years ago. As a result of their calculations they were able to give  $r$ -process contributions, primary, cosmoradiogenic, and georadiogenic, to the abundances of  $\text{Pb}^{206}$  through  $\text{Bi}^{209}$ .

The relative  $r$ -process abundances calculated by Fowler and Hoyle ought to be

<sup>3</sup> B<sup>2</sup>FH have shown that this is closely the case in the main line of hydrogen and helium burning (see especially Fig. 2.1 of this reference). In the CNO-cycle, C and O are largely converted into  $\text{N}^{14}$ . Then in subsequent helium burning,  $\text{N}^{14}$  is converted into  $\text{Ne}^{22}$  by  $\text{N}^{14}(\alpha, \gamma)\text{F}^{18}(\beta^+\nu)\text{O}^{18}(\alpha, \gamma)\text{Ne}^{22}$ . Furthermore, in the NeNa-cycle,  $\text{Ne}^{20}$  is at least partially converted into  $\text{Ne}^{22}$ .

fairly reliable. The absolute values were essentially adjusted by the methods of B<sup>2</sup>FH and of Becker and Fowler (17) to the empirical abundances of the osmium, iridium, and platinum isotopes which occur in the *r*-process abundance peak centered near  $A = 195$  and which are produced almost entirely in the primary *r*-process (no radiogenic contributions and very little from the *s*-process.) In what follows we include a factor  $r$  in the stated *r*-process abundances. Explicitly this factor will be unity if the Suess and Urey abundances<sup>4</sup> Os = 1.00, Ir = 0.823, and Pt = 1.625 on the scale Si = 10<sup>6</sup> are correct and if the calculations give the correct dependence on atomic weight over the range  $A = 195$  to 255. We estimate a relative decrease by a factor of three from the calculated trend might be possible over this range and in addition the Os, Ir, Pt abundances might be high by a factor of  $\sim 2.5$  as indicated in the previous section. There seems to be little possibility that  $r$  could exceed unity so we estimate  $0.1 < r < 1$  and adopt  $r = 0.4$  for certain of our calculations. Recent activation analysis of Th and U in chondrites by Bate *et al.* (18) and Hamaguchi *et al.* (19) substantiate this choice.

The lead isotope, Pb<sup>204</sup>, is produced only in the *s*-process and in particular has no radiogenic contributions. Accordingly we will express all abundances relative to the abundance of this isotope. In general we will have for the isotope of element  $Z$  with atomic weight  $A$ :

$$\frac{Z^A}{\text{Pb}^{204}} = \frac{Z_s^A}{\text{Pb}_s^{204}} + \frac{Z_r^A}{\text{Pb}_r^{204}}, \quad (63)$$

where the subscripts  $s$  and  $r$  represent slow and rapid process contributions, respectively. The  $Z_r^A$  will be taken from Table III of Fowler and Hoyle (14) while the  $Z_s^A$  will eventually be calculable from the methods described in the present paper when experimental cross sections for bismuth and the lead isotopes are available. The  $Z_s^A$  are just the quantities  $N_A$  given in Eq. (55). It is our belief that the cross sections used in this paper are correct to order of magnitude and that the  $\psi_A$ -values calculated are substantially correct with an important exception to be discussed in the next paragraph. The  $\psi_A$  for  $A = 202$  to 209 as a function of  $n_c$ , the neutron exposure per seed nucleus, are shown in Figs. 15 and 18. To test the insensitivity of the  $\psi$ -function to an individual cross section, we also calculated  $\psi_{204}$  and  $\psi_{205}$  for  $\sigma_{204} = 5.5$  instead of the value 55 used in this paper. These trial calculations resulted in only nominal changes in the  $\psi$  values as a function of  $n_c$  and will not be considered further. However, the final values for  $Z_s^A$  depend inversely on  $\sigma_A$  so the importance of accurate cross section values in any particular case is apparent.

It will be clear from Eq. (55) for  $N_A = Z_s^A$  that in principle we will also need

<sup>4</sup> Here and in what follows we let chemical symbols represent atomic abundance.

to know  $g(n_c)$ . In addition we must treat the equilibrium contributions for  $n_c > 153$  in a somewhat special manner, this being the exception in regard to our determination of  $\psi_A$  mentioned in the previous paragraph. Accordingly we will divide contributions to  $Z_s^A$  into two physically distinct parts corresponding to the contributions from  $g(n_c)$  for  $n_c < 153$  and from  $g(n_c)$  for  $n_c > 153$ , since  $n_c = 153$  marks the approximate onset of equilibrium. Define a terminal neutron exposure as

$$G_T = \int_{153}^{\infty} g(n_c) dn_c \quad (64)$$

and let  $I_A$  stand for

$$I_A = \int_0^{153} g(n_c)\psi_A(n_c) dn_c. \quad (65)$$

Then

$$Z^A = \frac{1}{\sigma_A} I_A + \frac{1}{\sigma_A} G_T \psi_T + Z_r^A, \quad (66)$$

where  $\psi_T$  is given by Eq. (44). For  $A = 206$ , the second term on the right must be multiplied by 0.56 and for  $A < 206$  it should be disregarded.

Applying the above considerations to bismuth and the lead isotopes yields the following set of equations for the indicated ratios *at the present time*:

$$\begin{aligned} \frac{\text{Pb}^{206}}{\text{Pb}^{204}} &= \frac{\sigma_{204} I_{206} + 0.56 G_T \psi_T}{\sigma_{206} I_{204}} + \frac{0.652 r}{\text{Pb}_{204}} + \frac{0.114 r}{\text{Pb}_{204}} f_U \\ &= 9.46 \text{ (iron met.)}; 19.38 \text{ (chondrites)}; \\ &\quad 18.93 \text{ (recent terr.)}; 50.28 \text{ (Nuevo Laredo)}. \end{aligned} \quad (67)$$

$$\begin{aligned} \frac{\text{Pb}^{207}}{\text{Pb}^{204}} &= \frac{\sigma_{204} I_{207} + G_T \psi_T}{\sigma_{207} I_{204}} + \frac{0.964 r}{\text{Pb}^{204}} + \frac{0.066 r}{\text{Pb}^{204}} f_U \\ &= 10.29 \text{ (iron met.)}; 15.86 \text{ (chondrites)}; \\ &\quad 15.73 \text{ (recent terr.)}; 34.86 \text{ (Nuevo Laredo)}. \end{aligned} \quad (68)$$

$$\begin{aligned} \frac{\text{Pb}^{208}}{\text{Pb}^{204}} &= \frac{\sigma_{204} I_{208} + G_T \psi_T}{\sigma_{208} I_{204}} + \frac{0.386 r}{\text{Pb}^{204}} + \frac{0.110 r}{\text{Pb}^{204}} f_{Th} \\ &= 29.21 \text{ (iron met.)}; 38.63 \text{ (chondrites)}; \\ &\quad 38.80 \text{ (recent terr.)}; 67.97 \text{ (Nuevo Laredo)}. \end{aligned} \quad (69)$$

$$\frac{\text{Bi}^{209}}{\text{Pb}^{204}} = \frac{\sigma_{204} I_{209} + G_T \psi_T}{\sigma_{209} I_{204}} f_{Bi} + \frac{0.939 r}{\text{Pb}^{204}} f_{Bi}. \quad (70)$$

The first terms on the right-hand side of these equations represent the *s*-process contributions, the second terms are the primary and cosmogenic *r*-process contributions (line 7, Table III, Fowler and Hoyle, 1960) while the last terms are the georadiogenic *r*-process contributions (line 9). For reasons which will become clear below, we express the *r*-process terms relative to  $\text{Pb}^{204}$  rather than  $\text{I}^{204}/\sigma_{204}$ . The numerical lead isotope ratios for iron meteorites, chondritic meteorites, recent terrestrial ocean sediments, and the Nuevo Laredo meteorite are taken from data of Patterson *et al.* (20), Tilton *et al.* (21) and Patterson (22).

The  $f$ 's in Eqs. (67) to (70) have been introduced to represent the fractionation of U, Th, and Bi relative to Pb at the time of formation of a specified object (meteorite, terrestrial object, sun, etc.). It would seem reasonable that no fractionation occurred in the formation of the sun so  $f_{\text{sun}} = 1$  for all elements. The iron meteorites have the lowest  $\text{Pb}^{206, 7, 8}/\text{Pb}^{204}$  ratios which have been discovered and accordingly are thought to contain no georadiogenic lead. Thus it is assumed that they formed with no U or Th and hence  $f_{\text{U,Th}}(\text{iron met}) = 0$ . With this relation it is a simple matter to calculate  $f_{\text{U}}$  and  $f_{\text{Th}}$  for other objects from each of the first three equations above using the numerical ratios indicated in each case. In each case we find approximately the same solution from all three equations and also find  $f_{\text{U}} = f_{\text{Th}}$  as might be expected from the chemical similarity of these two elements. The average results are:

$$\frac{r}{\text{Pb}^{204}} f_{\text{U,Th}} = 84 \text{ (recent terr); } 86 \text{ (chondrites); } 361 \text{ (Nuev Laredo)}. \quad (71)$$

That the three equations give consistent solutions in each case is a result of the facts that Patterson *et al.* find a common age for the meteorites and the earth's crust and that Fowler and Hoyle were able to find a *concordant* solution for the duration of nucleosynthesis in the Galaxy using their *r*-process production ratios for  $\text{U}^{235}/\text{U}^{238}$  and  $\text{Th}^{232}/\text{U}^{238}$  and the present day values of these ratios.

To find the  $f$ -values we use our previously adopted value  $r = 0.4$  and obtain  $\text{Pb}^{204}$  in the following way:  $\text{Pb} = 6.5$  in carbonaceous chondrites in which  $f_{\text{U,Th}} \sim 1$  so that  $\text{Pb} = 6.5 - 0.4 (0.114 + 0.066 + 0.110) = 6.4$  exclusive of georadiogenic contributions. Iron meteorites are taken as giving the relative isotopic abundances exclusive of these contributions. In the iron meteorites  $\text{Pb}^{204}/\text{Pb} = 0.02$ . Thus

$$f_{\text{U,Th}} = 27 \text{ (recent terr); } 28 \text{ (chondrites); } 116 \text{ (Nuevo Laredo)}. \quad (72)$$

These large values are most probably due to depletion of Pb in the formation of the earth's crust and the meteorites some  $4.5 \times 10^9$  years ago although in the case of the Nuevo Laredo meteorite some enhancement of U and Th probably occurred.

The above considerations would seem to indicate reasonably consistent lead isotope ratios in various objects of the solar system. Since the iron meteorites require the minimum  $r$ -process corrections we set  $f_{U,Th} = 0$  in what follows, and use lead isotope ratios from the iron meteorites. In order to discuss the behavior of the  $\sigma N$ -curve through lead and bismuth we require absolute abundances for which we use the new carbonaceous chondrite values given in the previous section; as a matter of principle we make the trivial correction  $Pb = 6.4$  rather than 6.5 when iron meteorite isotope ratios are used. Since Tl precedes Pb and since  $Tl^{205}$  results from the decay of the  $s$ -process  $Pb^{205}$  (half-life  $\sim 5 \times 10^7$  years) we include Tl in our discussion. The adopted abundances are  $Tl^{203} = 0.11/f_{Tl}$ ,  $Tl^{205} = 0.26/f_{Tl}$ ,  $Pb^{204} = 0.13$ ,  $Pb^{206} = 1.21$ ,  $Pb^{207} = 1.32$ ,  $Pb^{208} = 3.74$ ,  $Bi^{209} = 0.46/f_{Bi}$ . We retain  $f_{Tl} \leq 1$  and  $f_{Bi} \leq 1$  to remind us that Tl and Bi may be depleted relative to Pb even in carbonaceous chondrites. We now write the  $s$ -process abundances directly rather than as ratios to  $Pb^{204}$ , as follows (assuming no  $r$ -process contributions to Tl):

$$Tl^{203} = Tl_s^{203} = \frac{I_{203}}{\sigma_{203}} = \frac{0.11}{f_{Tl}} = 0.22, \quad (73)$$

$$Pb^{204} = Pb_s^{204} = \frac{I_{204}}{\sigma_{204}} = 0.13, \quad (74)$$

$$Tl^{205} = Pb_s^{205} = \frac{I_{205}}{\sigma_{205}} = \frac{0.26}{f_{Tl}} = 0.52, \quad (75)$$

$$Pb_s^{206} = \frac{0.56 G_T \psi_T}{\sigma_{206}} + \frac{I_{206}}{\sigma_{206}} = 1.21 - 0.652 r = 0.95, \quad (76)$$

$$Pb_s^{207} = \frac{G_T \psi_T}{\sigma_{207}} + \frac{I_{207}}{\sigma_{207}} = 1.32 - 0.964 r = 0.93, \quad (77)$$

$$Pb_s^{208} = \frac{G_T \psi_T}{\sigma_{208}} + \frac{I_{208}}{\sigma_{208}} = 3.74 - 0.386 r = 3.59, \quad (78)$$

$$Bi_s^{209} = \frac{G_T \psi_T}{\sigma_{209}} + \frac{I_{209}}{\sigma_{209}} = \frac{0.46}{f_{Bi}} - 0.939 r = 0.54. \quad (79)$$

In the final numerical values we have set  $r = 0.4$  and set  $f_{Tl}$  and  $f_{Bi}$ , the fractionation of Tl and Bi relative to Pb equal to 1/2.

An aside on the above equations is in order at this point. In discussing lead and bismuth abundances B<sup>2</sup>FH assumed  $G_T = 0$  and  $I_A = \sigma_A N_A = \text{constant}$ . In other words they extrapolated the  $\sigma N$  curve for  $A < 200$  to  $A > 200$ . As a result they found order of magnitude discrepancies for lead and bismuth relative to the amounts found in ordinary chondrites. It would now seem that lead and bismuth have been substantially depleted in ordinary chondrites and that

carbonaceous chondrites give much larger and more reasonable values. However a glance at Fig. 15 and the above equations will indicate that the problem is much more complicated than assumed by B<sup>2</sup>FH. Figure 15 shows that for  $n_c \leq 100$ ,  $\psi_A$  drops rapidly in the range of interest and thus  $I_A$  may do likewise. Furthermore  $\sigma_A N_A$  is not given by  $I_A$  alone but the  $G_T \psi_T$  terminal terms must be included where appropriate. Thus the lead and bismuth isotope abundances (*s*-process) may be given almost entirely by the  $G_T \psi_T$  terms and be completely independent from a nuclear standpoint of the  $\sigma_A N_A$  behavior at lower  $A$ . They would then provide information on the ratio of neutron exposures for which  $n_c > 153$  relative to neutron exposure for which  $n_c < 100$  in the *s*-processes in stars of the Galaxy which contributed to solar system abundances.

Eventually all of the necessary neutron capture cross sections will be measured and the problems raised in the previous paragraph will be amenable to solution. As an example of how the calculations will go, let us use the adopted cross sections of Table III. For simplicity let us assume that  $I_A$  for  $A \geq 206$  is negligible and that  $r = 0.4$ . We recall that for  $A \sim 182$ ,  $I_A = \sigma_A N_A \sim 20$  and that 13  $\psi_A(n_c = 100)$  fits the  $\sigma_A N_A$  curve with *new* abundance determinations. Then we find from

Eq. (73): with  $\sigma_{203} = 90$ ,  $I_{203} = 20$ . This would indicate no decrease in  $I_A$  from  $A \sim 182$  to  $A = 203$  and justifies our choice of  $f_{T1} = 1/2$  made previously.

Eq. (74): with  $\sigma_{204} = 55$ ,  $I_{204} = 7.2$ . This decrease is somewhat greater than expected from the curve for  $n_c = 100$  in Fig. 15. It even exceeds that expected for  $n_c = 84$  or  $n_c = 68$ . Possible explanations can be listed as follows (1) the cross section for Pb<sup>204</sup> is greater than 55 mb, (2) the abundance of Pb is greater than 6.5 and Pb<sup>204</sup> accordingly greater than 0.13, (3) there is a small capture cross section at an atomic weight between  $A = 182$  and  $A = 204$ . The difficulty can not be definitely resolved with our present knowledge.

Eq. (75): with  $\sigma_{206} = 11$  (Pb),  $I_{206} \sim 6$ . This result is again consistent with  $\psi_A(n_c = 84)$  in Fig. 15.

Eq. (76): with  $\sigma_{206} = 2.8$  and neglecting  $I_{206}$  we find  $G_T \psi_T = 4.8$ . The neglect of  $I_{206}$  is probably not justified in this case but at least  $G_T \psi_T$  is correct to a factor of 2 or 3.

Eq. (77): with  $\sigma_{207} = 5.5$ ,  $G_T \psi_T = 5.1$  in good agreement with the results of Eq. (76).

Eq. (78): with  $\sigma_{208} = 1.1$ ,  $G_T \psi_T = 4.0$  in good agreement with the results of Eq. (76) and (77). Since  $\psi_T = 0.56$ , we find  $G_T \sim 8$  which is the same order of magnitude as the coefficient = 13 found for  $\psi_A(n_c = 100)$  previously. The drop in the  $\sigma_A N_A$  curve occurs primarily because  $\psi_T < \psi(n_c = 100)$ .

Eq. (79): with  $\sigma_{209} = 1.8$ ,  $G_T \psi_T = 0.83/f_{Bi} - 0.38 = 1.3$  using  $f_{Bi} = 1/2$ . This rather low value for  $G_T \psi_T$  may indicate that  $f_{Bi}$  is still smaller than the value we have adopted. It would imply that in some carbonaceous chondrites  $Bi \sim 2$  to 3 relative to  $Si = 10^6$ , ought to be found.

In all of the preceding, we have concentrated upon meteoritic abundances. A comment on solar abundances is now in order. In this case all of the  $f$ 's are most certainly equal to unity. Thus, we expect  $Pb = 6.5 \pm 3$  on the  $Si = 10^6$  scale where we had made a reasonable estimate of the probable error of our calculation. The most probable value,  $Pb = 6.5$ , is taken as being consistent with the meteoritic value. However, the range  $Pb = 3.5$  to  $9.5$  is determined quite independently on the basis of the variation of  $\sigma N$  with  $A$ , which can be reasonably expected from the analysis we have made in this paper. Goldberg *et al.* (23) give solar  $Pb = 10$  to  $20$  but Aller (24) has recently given a revised value,  $Pb = 0.36$ . The abundance depends critically, of course, on  $f$ -values assumed for Pb-spectral lines. Solar values for Tl and Bi are not available.

It will be clear from the above, that the  $\sigma N$ -correlation problem cannot be resolved at the present time. Clearly, we are at the mercy of our ignorance of neutron capture cross sections in the kev range for the Tl, Pb, and Bi isotopes and our ignorance of abundances for these elements. We await, in both regards, the results of accurate measurements. In the meantime, we present this paper as a "Handbuch der Ezzprocess".

*Note added in Proof.* T. M. Helliwell of the California Institute of Technology has informed us privately that he has recently calculated certain  $f$ -values for lead and the lead abundance in the Sun. He has submitted his results for publication in the *Astrophysical Journal*. Helliwell finds excellent agreement with the experimental  $f$ -values for the Pb I line  $\lambda$  2833 determined by G. D. Bell and R. B. King of this Institute who have also submitted their results to the *Astrophysical Journal*. On the  $Si = 10^6$  scale Helliwell finds  $Pb = 5.0 \begin{matrix} +2.4 \\ -1.7 \end{matrix}$ . This is in excellent agreement with the value,  $Pb = 6.5 \pm 3.0$ , deduced in this paper. It is very satisfying that Helliwell's value falls within the limits  $Pb = 3.5$  and  $Pb = 9.5$  which were determined by us on the basis of a reasonable behavior of  $\sigma N$  at large  $A$ .

#### APPENDIX A. THE NEUTRON CAPTURE CROSS SECTIONS

Every effort has been made to rely on experimentally measured cross sections wherever possible. Isotopic activation measurements near 25 kev come from Macklin *et al.* (25) at Oak Ridge and Booth *et al.* (26) at Livermore. Cross sections for the elements in their natural abundances are reported from Oak Ridge by capture tank (27) at 30 kev and spherical shell absorption techniques (28) at 24 kev. Gibbons *et al.* (27) (hereafter designated GM<sup>2</sup>N) published also a graph of the capture cross sections for the elements, with cross sections for odd  $Z$  divided by 2.4, and found a fairly smooth curve showing strong shell effects. Where no other information was available, we often demanded that the cross sections for the natural elements be close to this curve, which is reproduced in Fig. 9.

Table III contains much of this information. The table is constructed according to elements, with the several isotopes of each element listed by mass number in the second column. Those mass numbers lying on the  $s$ -process path are followed by the letter  $s$ , with the combination  $sb$  indicating the branch in the path at  $A = 64$ . The third column lists several items. Enclosed in parentheses opposite the chemical symbol for the element is the abundance we have adopted for the element. These abundances are of four types for reasons explained earlier in this paper. As a superscript following each elemental abundance we include one of four letters which indicate, respectively: (a) abundances obtained by neutron activation analysis principally by Schmitt *et al.* (15) or Reed *et al.* (16), (b) Suess and Urey (6), (c) four-tenths Suess and Urey for reasons explained in Section XII, (d) an activation measurement corrected for probable fractionation. The number in column three opposite each isotope of an element represents the fraction by number which that isotope constitutes of the total element abundance. All abundances are on the scale  $\text{Si} = 10^6$ . The fourth column lists the formation process for each isotope as in  $\text{B}^2\text{FH}$ . The fifth column lists the cross section for the natural element as measured by  $\text{GM}^2\text{N}$ . All cross section values are expressed in units of millibarns. We used values of the cross sections for the natural element as an aid in estimating many isotopic cross sections to be used in our calculations. The numbers we actually used for this estimate are not those listed in column four, which represent the latest values, but are those given in earlier publications by  $\text{GM}^2\text{N}$ . It is also this earlier data which is plotted in Fig. 9. The sixth and seventh columns respectively indicate the isotopic activations of Macklin *et al.* and of Booth *et al.* The eighth column lists the cross section we have adopted near 25 kev for the  $s$ -process calculation for those isotopes in the  $s$ -path.

The final column lists the product  $\sigma N$ , where  $N$  is the abundance normalized to  $10^6$  for silicon. Note particularly that all the numbers in this column do not correspond directly to the  $\sigma N$  of the  $s$ -process correlation; only those isotopes which are formed predominantly in the  $s$ -process ( $s$ -only or  $s$ ) have a  $\sigma N$  which is immediately meaningful for the  $s$ -process curve. If one-half of the abundance of a given nucleus is estimated to be formed by the  $s$ -process, then its  $\sigma N$  should be divided by two to give the  $s$ -process number. Those  $\sigma N$  values for isotopes formed in the  $s$ -process whose isotopic cross sections have been measured are enclosed in parentheses, for these are the experimentally valid points which are plotted to determine the behavior of the  $\sigma N$  curve. Also enclosed in parentheses are those  $\sigma N$  values corresponding to the revised abundance data which is plotted in Fig. 20. Where only an estimated fraction ( $\frac{1}{2}$  or  $\frac{2}{3}$ ) of the abundances of those isotopes can be attributed to the  $s$ -process, that fraction is explicitly written in front of the parentheses to indicate the fraction of the value in parentheses that has been plotted. Question marks appear after the  $\sigma N$  values that

TABLE III

Element	Mass Number	Element Abundance Fraction of Element	Formation Process	$\sigma_{\text{Natural}}$ (30 keV)* ORNL	$\sigma_{\text{Isotopic Activation}}$ (25 keV) ORNL      Livermore		$\sigma_{\text{Adopted}}$ (25 keV)	$\sigma_N$
$^{26}\text{Fe}$		$(6.00 \times 10^5)^b$		12				
	54	.059	e					
	56s	.915	$< \frac{1}{2} \text{ s(e)}$				15	
	57s	.023	$< \frac{1}{2} \text{ s(e)}$				40	
$^{27}\text{Co}$		$(1800)^b$		88				
	59s	1.00	$< \frac{1}{2} \text{ s(e)}$				98	
$^{28}\text{Ni}$		$(2.74 \times 10^4)^b$		16				
	58	.679	e					
	60s	.262	$< \frac{1}{2} \text{ s(e)}$				30	
	61s	.013	$< \frac{1}{2} \text{ s(e)}$				70	
	62s	.037	$< \frac{1}{2} \text{ s(e)}$				30	
	64sb	.012	s			8.7	8.7	$(4.5 \times 10^3)$
$^{29}\text{Cu}$		$(212)^b$		39				
	63s	.689	s		116	114	115	$(1.7 \times 10^4)$
	65s	.311	s		46	48	47	$(3.1 \times 10^3)$
$^{30}\text{Zn}$		$(486)^b$		31				
	64sb	.490	s-only				87	$5.3 \times 10^4$
	66s	.276	s				66	$8.8 \times 10^3$
	67s	.041	s				144	$2.9 \times 10^3$
	68s	.185	s			32	32	$(2.9 \times 10^3)$
	70	.007	r					

\* Increase by ~10% to obtain  $\sigma(25 \text{ keV})$

TABLE III--Continued

Element	Mass Number	Element Abundance Fraction of Element	Formation Process	$\sigma_{\text{Natural}}$ (30 kev)* ORNL	$\sigma_{\text{Isotopic Activation}}$ (25 kev) ORNL	Activation Livermore	$\sigma_{\text{Adopted}}$ (25 kev)	OT
$^{31}\text{Ga}$		(11.4) <sup>b</sup>						
	69s	.602	s				93	640
	71s	.398	s		142		142	(650)
$^{32}\text{Ge}$		(50.5) <sup>b</sup>						
	70s	.206	s-only				97	1000
	72s	.273	s				75	1000
	73s	.076	s				262	1000
	74s	.369	s		54		54	(1000)
	76	.077	r				.40	
$^{33}\text{As}$		(4.0) <sup>b</sup>						
	75s	1.00	$\frac{2}{3}\text{s}$		740	650	695	$\frac{2}{3} (2.8 \times 10^3)$
$^{34}\text{Se}$		(18.8) <sup>a</sup>						
	74	.0096	p					
	76s	.091	s-only				300	500
	77s	.0750	$\frac{1}{2}\text{s}$				600	830?
	78s	.237	$\frac{1}{2}\text{s}$				300	1300?
	79s	active	s				600	
	80s	.500	$\frac{1}{2}\text{s}$				300	$2.8 \times 10^3?$
	82	.089	r					
$^{35}\text{Br}$		(13.4) <sup>b</sup>		650				
	79	.506	r, s-decay					
	81s	.494	$\frac{1}{2}\text{s}$		550		550	$3.6 \times 10^3?$

TABLE III—Continued

Element	Mass Number	Element Abundance Fraction of Element	Formation Process	$\sigma_{\text{Natural}}$ (30 kev) ORNL	$\sigma_{\text{Isotopic Activation}}$ (25 kev) ORNL    Livermore	$\sigma_{\text{Adopted}}$ (25 kev)	$\sigma_N$
$^{36}\text{Kr}$		(51.3) <sup>b</sup>					
	78	.0034	p				
	80	.022	s-only				
	82s	.115	s-only			330	$1.9 \times 10^3$
	83s	.115	$\Lambda \frac{1}{2}^-$ s			660	$3.9 \times 10^3?$
	84s	.571	$\Lambda \frac{1}{2}^-$ s			300	$8.0 \times 10^3?$
$^{37}\text{Rb}$	86	.174	r				
		(4.4) <sup>a</sup>					
	85s	.728	$\Lambda \frac{1}{2}^-$ s		181	181	580?
$^{38}\text{Sr}$	87	.272	r		75		
		(18.9) <sup>b</sup>		155			
	84	.0056	p				
	86s	.098	s-only			140	260
	87s	.070	s-only			190	260
$^{39}\text{Y}$	88s	.825	s-magic			16	260
		(8.9) <sup>b</sup>		13.5			
$^{40}\text{Zr}$	89s	1.00	s-magic		13    28	18	(180)
		(21.8) <sup>c</sup>		14			
	90s	.514	s-magic			8	90
	91s	.112	s			37	90
	92s	.171	s			24	90
	93s	active	s			53	
	94s	.174	s		24	24	(90)
96	.028	r			24		

TABLE III—Continued

Element	Mass Number	Element Abundance Fraction of Element	Formation Process	$\sigma$ Natural (30 kev) ORNL	$\sigma$ Isotopic Activation (25 kev) ORNL      Livermore	$\sigma$ Adopted (25 kev)	$\sigma N$	
$^{41}\text{Nb}$		(1.00) <sup>b</sup>		264		264		
	93	1.00	r,s-decay					
$^{42}\text{Mo}$		(2.42) <sup>b</sup>		140				
	92	.150	p					
	94	.093	p,s					
	95s	.160	s			224	87	
	96s	.166	s-only			217	87	
	97s	.096	s			374	87	
	98s	.240	$\frac{1}{2} s$		209	390	300	$\frac{1}{2}$ (174)
	100	.097	r		63			
$^{43}\text{Tc}$	99s	active	s			660		
$^{44}\text{Ru}$		(1.49) <sup>b</sup>						
	96	.057	p		321			
	98	.022	p					
	99	.128	$\frac{1}{2} s$ , s-decay					
	100s	.127	s-only			477	90	
	101s	.170	$\frac{1}{2} s$			880	220?	
	102s	.313	$\frac{1}{2} s$		386	386	$\frac{1}{2}$ (180)	
104	.183	r		211				
$^{45}\text{Rh}$	103s	(.27) <sup>a</sup>	$\frac{1}{2} s$			1000	270?	
$^{46}\text{Pd}$		(.675) <sup>b</sup>		454				
	102	.008	p					
	104s	.093	s-only			480	30	

TABLE III—Continued

Element	Mass Number	Element Abundance ----- Fraction of Element	Formation Process	$\sigma_{\text{Natural}}$ (30 kev)* ORNL	$\sigma_{\text{Isotopic Activation}}$ (25 kev) ORNL	Activation Livermore	$\sigma_{\text{Adopted}}$ (25 kev)	$\sigma/N$
<sup>46</sup> Pd	105s	.228	$\Lambda$ $\frac{1}{2}t$ s				960	148?
	106s	.272	$\Lambda$ $\frac{1}{2}t$ s				520	96?
	107s	active	s				1040	
	108s	.267	$\Lambda$ $\frac{1}{2}t$ s		540	580	560	100?
	110	.135	r			> 300		
<sup>47</sup> Ag		(0.13) <sup>a</sup>		951				
	107	.515	r,s-decay					
<sup>48</sup> Ca	109s	.485	$\Lambda$ $\frac{1}{2}t$ s				1000	63?
		(0.89) <sup>b</sup>		330				(37)
	106	.012	p					
	108	.0089	p,s					
	110s	.125	s-only				337	37
	111s	.128	$\frac{1}{2}t$ s				660	$\frac{1}{2}t$ 75
	112s	.238	$\frac{1}{2}t$ s				324	$\frac{1}{2}t$ 75
	113s	.124	$\frac{1}{2}t$ s				672	$\frac{1}{2}t$ 75
	114s	.288	$\frac{1}{2}t$ s				290	$\frac{1}{2}t$ 75
	116	.076	r				250	
<sup>49</sup> In		(0.11) <sup>b</sup>		763				
	113	.042	p,s			8500		
	115s	.958	$\frac{1}{2}t$ s		805	980	900	$\frac{1}{2}t$ (94)

TABLE III—Continued

Element	Mass Number	Element Abundance Fraction of Element	Formation Process	$\sigma$ Natural (30 kev) ORNL	$\sigma$ Isotopic Activation (25 kev) ORNL	Activation Livermore	$\sigma$ Adopted (25 kev)	$\sigma$ N
$^{50}\text{Sn}$		(1.53) <sup>b</sup>		88				(26)
	112	.010	p					
	114	.0068	p,s					
	115	.0035	p,s					
	116s	.142	s-only				138	26
	117s	.077	s				258	26
	118s	.238	s				83	26
	119s	.087	s				230	26
	120s	.326	s				61	26
	122	.047	r				50	
124	.059	r				40		
$^{51}\text{Sb}$		(0.246) <sup>b</sup>		436				
	121s	.573	s		950	810	880	(124)
	123	.427	r		456	230		
$^{52}\text{Te}$		(1.83) <sup>a</sup>						
	120	.0009	p					
	122s	.025	s-only				700	32
	123s	.0089	s-only				1930	32
	124s	.047	s-only				363	32
	125s	.070	$\leq \frac{1}{2}$ s				1720	220?
	126s	.187	$\leq \frac{1}{2}$ s				245	85?
	128	.317	r				192	
130	.343	r				156		

TABLE III—Continued

Element	Mass Number	Element Abundance Fraction of Element	Formation Process	$\sigma$ Natural (30 kev) ORNL	$\sigma$ Isotopic Activation (25 kev) ORNL	Activation Livermore	$\sigma$ Adopted (25 kev)	$\sigma$ N
$^{55}\text{I}$		(0.25) <sup>a</sup>		753				
	127s	1.00	$< \frac{1}{2}$ s		820		820	190?
$^{54}\text{Xe}$		(4.0) <sup>b</sup>						
	124	.0010	p					
	126	.0009	p					
	128s	.019	s-only				470	36
	129s	.263	$< \frac{1}{2}$ s				1030	$1.1 \times 10^3?$
	130s	.041	s-only				227	36
	131s	.213	$< \frac{1}{2}$ s				500	420?
	132s	.270	$< \frac{1}{2}$ s				153	165?
	134	.105	r				115	
136	.090	r				92		
$^{55}\text{Cs}$		(0.069) <sup>a</sup>						
	133s	1.0	$< \frac{1}{2}$ s			900	900	62?
$^{56}\text{Ba}$		(3.66) <sup>b</sup>						
	130	.001	p					
	132	.001	p					
	134s	.024	s-only				337	30
	135s	.066	s				124	30
	136s	.078	s-only				105	30
	137s	.113	s				73	30
	138s	.716	s-magic			11.4	11.4	(30)
$^{57}\text{La}$		(0.40) <sup>a</sup>		55				
	138	.0009	p					
	139s	1.00	s-magic		50	49	50	(20)

TABLE III—Continued

Element	Mass Number	Element Abundance Fraction of Element	Formation Process	$\sigma_{\text{Natural}}$ (30 kev) ORNL	$\sigma_{\text{Isotopic Activation}}$ (25 kev) ORNL Livermore	$\sigma_{\text{Adopted}}$ (25 kev)	$\sigma_N$
$58^{\text{Ce}}$		(0.62) <sup>a</sup>		35			
	136	.0019	p				
	138	.0025	p				
	140s	.885	s-magic		31	31	(17)
	142	.111	r		425		
$59^{\text{Pr}}$		(0.15) <sup>a</sup>		115			
	141s	1.00	s-magic		155	170	162 (24)
$60^{\text{Nd}}$		(0.74) <sup>a</sup>					
	142s	.271	s-only magic			150	30
	143s	.121	s			335	30
	144s	.239	s			170	30
	145s	.083	s			490	30
	146s	.172	s			236	30
	148	.057	r			250	
	150	.056	r			250	
$62^{\text{Sm}}$		(0.25) <sup>a</sup>		875			
	144	.016	p				
	147s	.151	< $\frac{1}{2}$ s			320	12?
	148s	.113	s-only			213	6
	149s	.139	< $\frac{1}{2}$ s			470	16?
	150s	.074	s-only			324	6
	151s	active	s			800	
	152s	.265	< $\frac{1}{2}$ s		668	600	40?
154	.226	r		527			

TABLE III—Continued

Element	Mass Number	Element Abundance ----- Fraction of Element	Formation Process	$\sigma_{\text{Natural}}$ (30 kev) ORNL	$\sigma_{\text{Isotopic Activation}}$ (25 kev) ORNL	Activation Livermore	$\sigma_{\text{Adopted}}$ (25 kev)	$\sigma_N$
$^{63}\text{Eu}$		(0.096) <sup>a</sup>						
	151	.477	$< \frac{1}{2} \text{ s}$					
	153s	.522	$< \frac{1}{2} \text{ s}$				2560	130?
$^{64}\text{Gd}$		(0.36) <sup>a</sup>		1175				
	152	.002	p, s					
	154s	.022	s-only				710	5.6
	155s	.148	$< \frac{1}{2} \text{ s}$				1560	84?
	156s	.206	$< \frac{1}{2} \text{ s}$				710	53?
	157s	.156	$< \frac{1}{2} \text{ s}$				1560	89?
	158s	.247	$< \frac{1}{2} \text{ s}$			710	710	64?
	160	.218	r					
$^{65}\text{Tb}$		(0.055) <sup>a</sup>		1850				
	159s	1.00	$< \frac{1}{2} \text{ s}$				2280	125?
$^{66}\text{Dy}$		(0.39) <sup>a</sup>		775				
	156	.0005	p					
	158	.0009	p					
	160s	.0228	s-only				430	3.8
	161s	.189	$< \frac{1}{2} \text{ s}$				940	70?
	162s	.255	$< \frac{1}{2} \text{ s}$				380	38?
	163s	.250	$< \frac{1}{2} \text{ s}$				840	82?
	164s	.282	$< \frac{1}{2} \text{ s}$			330	330	36?
$^{67}\text{Ho}$		(0.078) <sup>a</sup>		1720				
	165s	1.00	$< \frac{1}{2} \text{ s}$				2210	170?

TABLE III—Continued

Element	Mass Number	Element Abundance Fraction of Element	Formation Process	$\sigma_{\text{Natural}}$ (30 keV) ORNL	$\sigma_{\text{Isotopic Activation}}$ (25 keV) ORNL, Livermore	$\sigma_{\text{Adopted}}$ (25 keV)	$\sigma_N$
$^{68}\text{Er}$		(0.21) <sup>a</sup>		960			
	162	.001	p				
	164	.015	p				
	166s	.329	$\sqrt{\frac{1}{2}}$ s			500	35?
	167s	.244	$\sqrt{\frac{1}{2}}$ s			1000	51?
	168s	.269	$\sqrt{\frac{1}{2}}$ s			360	20?
	170	.140	r		298		
$^{69}\text{Er}$		(0.039) <sup>a</sup>		1310			
	169s	1.00	$\sqrt{\frac{1}{2}}$ s			1530	60?
$^{70}\text{Yb}$		(0.19) <sup>a</sup>		575			(16)
	168	.0014	p				
	170s	.0303	s			2340	14
	171s	.144	$\sqrt{\frac{1}{2}}$ s			1000	$\sqrt{\frac{1}{2}}$ 28
	172s	.218	$\sqrt{\frac{1}{2}}$ s			486	$\sqrt{\frac{1}{2}}$ 20
	173s	.162	$\sqrt{\frac{1}{2}}$ s			658	$\sqrt{\frac{1}{2}}$ 20
	174s	.308	$\sqrt{\frac{1}{2}}$ s			344	$\sqrt{\frac{1}{2}}$ 20
	176	.126	r			280	
$^{71}\text{Lu}$		(0.037) <sup>a</sup>		2520			
	175s	.976	$\sqrt{\frac{1}{2}}$ s			2900	$\sqrt{\frac{1}{2}}$ 100
	176	.026	p				
$^{72}\text{Hf}$		(0.175) <sup>c</sup>					
	174	.0018	p				
	176s	.0516	s-only			2400	22
	177s	.184	$\sqrt{\frac{1}{2}}$ s			1000	$\sqrt{\frac{1}{2}}$ 32

TABLE III—Continued

Element	Mass Number	Element Abundance Fraction of Element	Formation Process	$\sigma$ Natural (30 kev) ORNL	$\sigma$ Isotopic (25 kev) ORNL	Activation (25 kev) Livermore	$\sigma$ Adopted (25 kev)	$\sigma$ N
$^{72}\text{Hf}$	178s	.272	s				456	22
	179s	.138	s				900	22
	180s	.354	s		441	260	350	(22)
$^{73}\text{Ta}$		(0.026) <sup>c</sup>		735				
	181s	1.00	s			1400, 1200	1300	(34)
$^{74}\text{W}$		(0.20) <sup>c</sup>		270				
	180	.0012	p					
	182s	.265	s				420	21
	183s	.143	$\frac{2}{3}$ s				1155	$\frac{2}{3}$ 32
	184s	.306	s			350	350	(21)
	186	.286	r		296	270, 340		
	$^{75}\text{Re}$		(0.054) <sup>c</sup>					
185s		.370	$\frac{1}{2}$ s		2650		2650	$\frac{1}{2}$ (53)
187		.630	r		970			
$^{76}\text{Os}$		(0.40) <sup>c</sup>						
	184	.0002	p					
	186s	.0159	s-only				3000	19
	187s	.0164	s-only				3000	19
	188s	.133	$< \frac{1}{2}$ s				1500	80?
	189s	.161	$< \frac{1}{2}$ s				2000	130?
	190s	.264	$< \frac{1}{2}$ s		886		886	93?
	192	.410	r					

TABLE III—Continued

Element	Mass Number	Element Abundance Fraction of Element	Formation Process	$\sigma_{\text{Natural}}$ (30 kev) ORNL	$\sigma_{\text{Isotopic}}$ Activation (25 kev) ORNL	Livermore	$\sigma_{\text{Adopted}}$ (25 kev)	$\sigma_N$
<sup>77</sup> Ir		(0.328) <sup>c</sup>						
	191s	.585	$\leftarrow \frac{1}{2} \frac{1}{2} s$				1000	125?
	193s	.615	$\leftarrow \frac{1}{2} \frac{1}{2} s$				500	100?
<sup>78</sup> Pt		(0.650) <sup>c</sup>		330				
	190	.0001	p					
	192s	.0078	s-only				1000	5.2
	194s	.3281	$\leftarrow \frac{1}{2} \frac{1}{2} s$				400	85?
	195s	.337	$\leftarrow \frac{1}{2} \frac{1}{2} s$				700	150?
	196s	.254	$\leftarrow \frac{1}{2} \frac{1}{2} s$			210	210	35?
	198	.072	r			240		
<sup>79</sup> Au		(0.058) <sup>c</sup>		515				
	197s	1.00	$\leftarrow \frac{1}{2} \frac{1}{2} s$		1120	890, 1200	1100	64?
<sup>80</sup> Hg		(0.284) <sup>b</sup>		295				
	196	.0016	p					
	198s	.1004	s-only				560	16
	199s	.169	$\frac{1}{2} \frac{1}{2} s$				780	$\frac{1}{2} \frac{1}{2} 38$
	200s	.231	$\frac{1}{2} \frac{1}{2} s$				340	$\frac{1}{2} \frac{1}{2} 23$
	201s	.132	$\frac{1}{2} \frac{1}{2} s$				560	$\frac{1}{2} \frac{1}{2} 21$
	202s	.297	s		57		57	4.8
	204	.068	r					
<sup>81</sup> Tl		(0.74) <sup>d</sup>		71				
	203s	.295	s				90	(20)
	205	.705	s (Pb <sup>205</sup> -decay)				60(11)	(6)

TABLE III—Continued

Element	Mass Number	Element Abundance Fraction of Element	Formation Process	$\sigma$ Natural (30 kev) ORNL	$\sigma$ Isotopic ORNL	Activation (25 kev) Livermore	$\sigma$ Adopted (25 kev)	$\sigma N$
$^{82}\text{Pb}$		(6.4 <sup>**</sup> ) <sup>d</sup>		3 ± 3				
	204s	.020 <sup>**</sup>	s-only				55	(7.2)
	205s	active	cycles				11.0	
	206s	.189 <sup>**</sup>	cycles (0.652r) <sup>***</sup>				2.8	(2.7)
	207s	.206 <sup>**</sup>	cycles (0.964r)				5.5	(5.3)
	208s	.585 <sup>**</sup>	cycles (0.386r) magic				1.1	(4.0)
$^{85}\text{Bi}$		(0.92) <sup>d</sup>		1 ± 4				
	209s	1.0	cycles (0.939r) magic			1.8 ± 0.7	1.8	(1)

\*\* The total Pb abundances exclusive of georadiogenic contributions. The iron meteorites are considered to give relative isotope abundances exclusive of georadiogenic contributions.

\*\*\* Cosmoradiogenic r-process contributions,  $0.1 < r < 1.0$ ; adopted  $r = 0.4$ .

are not at least  $\frac{1}{2}$  s to indicate their lack of direct bearing on the  $\sigma N$  curve. Only three exceptions to this meaning occur in the  $\sigma N$  column. One is at the branch in the s-path at  $A = 64$ . Both  $\text{Ni}^{64}$  and  $\text{Zn}^{64}$  are formed predominantly by the s-process, but their  $\sigma N$  products do not indicate the level of the s-curve because only a fraction (61 per cent for  $\text{Ni}^{64}$ , and 39 per cent for  $\text{Zn}^{64}$ ) of the s-nuclei passed through each isotope on the path to heavier nuclei. We therefore normalized these two  $\sigma N$  products to what their value would have been if all the nuclei passed through that point; that is  $\sigma(\text{Ni}^{64})N(\text{Ni}^{64})/0.61$  and  $\sigma(\text{Zn}^{64})N(\text{Zn}^{64})/0.39$ . The second exception in the  $\sigma N$  column occurs at  $\text{Tl}^{205}$ , which is believed to be formed in the s-process via the decay of  $\text{Pb}^{205}$ . Since  $\text{Pb}^{205}$  is the actual participant in the chain, the abundance of  $\text{Tl}^{205}$  must be correlated with the cross section for  $\text{Pb}^{205}$ , which we assume to be 11 mb. The third exception occurs for the  $\sigma N$  products of the isotopes of Pb and Bi. The abundances used

in calculating these products are the result of correcting the observed abundance for that part formed in the  $r$ -process as calculated by Fowler and Hoyle (14).

Since only a relative few of the  $s$ -process isotopic cross sections have been measured, we have had to estimate the others in various ways. The considerations mainly used for these estimates are the following:

1. Since the  $s$ -process seems to be a reasonably correct model, we have used the implications of such a model by assuming that the cross sections of the isotopes of certain elements vary inversely with the abundances *attributed to the  $s$ -process*. This reasoning is not at all circular. Over a small region of atomic weight the product  $\sigma N$  resulting from the uniform neutron exposure of iron nuclei will be nearly constant *if* (a) the region is sufficiently far away from the seed nuclei (say  $A > 100$ ) and (b) all the cross sections in the local region are considerably greater than the smallest of the cross sections for lower  $A$ . Under the above conditions, the group of large cross sections merely reach an equilibrium flow with the rate determined by the small cross sections in an earlier part of the chain. This type of behavior is clearly evident in the constant  $\psi$  regions of Fig. 14, all of which satisfy the above two conditions. Any superposition of exposures will have the same properties. We use this behavior to help estimate cross sections which, when thus estimated, predict the very behavior we anticipated. The solution is then *self-consistent*.

This reasoning is used frequently in the numerical cross section estimates of column eight of Table III. If the  $s$ -process abundances of the isotopes of an element satisfying the two conditions are known, we may estimate the cross sections of all of them from the measurement of only one of them.

As an example of this procedure, consider the isotopes of Ba. The isotope Ba<sup>138</sup> has a measured  $\sigma_{139} = 11.4$ . Assuming that the product  $\sigma_A N_A$  is constant for the isotopes of Ba where  $N_A$  is the abundance of isotope  $A$  which is created in the  $s$ -process, it follows

$$\sigma_{136} = \frac{N_{138}}{N_{136}} \sigma_{138} = \frac{0.716}{0.078} 11.4 = 105$$

and so forth for the other isotopes.

2. If the  $s$ -process abundances are known, but none of the isotopic cross sections have been measured, we form cross sections inversely proportional to these abundances which add up to give a measured or estimated element cross section.

As an example, consider the isotopes of tin. Because tin is proton magic, it has a large number of isotopes, five of which are formed in the  $s$ -process path. Its being proton magic will also produce cross sections smaller than the neighboring elements. The only measurement available is that of 102 mb for the elemental tin.

a. Neglect  $A = 112, 114, 115$  because their abundances are too small to contribute greatly to  $\sigma_{\text{natural}}$ .

b. Since  $A = 116 - 120$  are  $s$ -process, assume  $\sigma N$  to be constant,  $\sigma = a/N$ .

c. Assume that  $\sigma_{122}$  and  $\sigma_{124}$  are decreasing at the same rates as  $\sigma_{116}$ ,  $\sigma_{118}$ , and  $\sigma_{120}$  were decreasing.

Then we say, with  $a$  to be determined from the elemental  $\sigma$ , that

$$\sigma_{116} = \frac{a}{0.142}, \quad \sigma_{117} = \frac{a}{0.0767}, \quad \sigma_{118} = \frac{a}{0.238},$$

$$\sigma_{119} = \frac{a}{0.0865}, \quad \sigma_{120} = \frac{a}{0.326},$$

and guess

$$\sigma_{122} \sim \frac{a}{0.41}, \quad \sigma_{124} \sim \frac{a}{0.50},$$

$\sigma_{\text{natural}} = 102 = \sum_n \sigma_A(Z) N_A = [5 + (0.047/0.41) + (0.059/0.50)]a = 5.2a$ ,  $a = 19.7$ . Substituting back gives  $\sigma_{116} = a/0.142 = 19.7/0.142 = 138$ ,  $\sigma_{117} = 258$ ,  $\sigma_{118} = 83$ ,  $\sigma_{119} = 230$ ,  $\sigma_{120} = 61$ ,  $\sigma_{122} = 50$ ,  $\sigma_{124} = 40$ .

3. When the  $s$ -process abundances are unknown, we often assume general trends in cross sections observed elsewhere to be operative for the particular element in question. For instance, in the middle of a neutron shell, the cross sections generally decrease among isotopes of a given element with increasing neutron numbers. Characteristically  $\sigma_{n+2} \sim \frac{3}{4}\sigma_n$ , where  $n$  is the number of neutrons. Odd neutron number isotopes seem to have cross sections about twice as large as their even neutron neighbors in the isotopes of a given element. We use the factor 2.2 arbitrarily, because it is the factor originally used for the odd  $Z$  to even  $Z$  ratio for the element cross sections as reported by G<sup>2</sup>MN and shown in Fig. 9.

4. Many other special considerations, as well as some outright guesses were necessary to complete column eight of Table III.

The reader should be reminded that we are *not* attempting to predict neutron capture cross sections. But since our model demands cross sections for calculation, we have been forced to make estimates. In a further analysis, we hope to rely exclusively upon measured values. It must be realized too, that for the purpose of the  $s$ -process, uncertainties in large cross sections (say  $>200$  mb) are not as important as uncertainties in small ones. The difference between 15 mb and 25 mb is much more important than the difference between 500 mb and 1000 mb insofar as the resultant effect on the calculated  $\psi$  is concerned.

#### APPENDIX B. NEUTRON CAPTURE AT HIGH ENERGY

At high temperatures the  $(n, \gamma)$  capture process is opposed by the  $(\gamma, n)$  photo-disintegration reaction. The assumption of statistical equilibrium between these two reactions lowers the effective value of  $\langle \sigma v \rangle$  to be used in Eq. (1) to

$$\langle \sigma v \rangle_{\text{eff.}} = \langle \sigma v \rangle \left[ 1 - \frac{\omega_i \omega_n n_f}{\omega_f n_i n_n} \left( \frac{A_i A_n}{A_f} \right)^{3/2} \left( \frac{kT}{2\pi N_0 \hbar^2} \right)^{3/2} e^{-Q/kT} \right]. \quad (80)$$

The subscript  $i$  indicates the initial nucleus, the subscript  $f$  indicates the final nucleus, the subscript  $n$  indicates the neutron, the  $\omega$ 's are statistical factors of the order unity, the  $n$ 's are number densities per  $\text{cm}^3$  of the reactants, and the other symbols follow standard notation. The neutron binding energy in the final nucleus is a positive quantity given by  $Q = (M_i + M_n - M_f)c^2 \sim 4 - 8$  Mev for the heavy nuclei. If in Eq. (80) we set all  $\omega = 1$ ,  $A_f = A_i$ , and  $A_n = 1$ , there results

$$\langle \sigma v \rangle_{\text{eff.}} \sim \langle \sigma v \rangle \left[ 1 - \frac{n_f}{n_i n_n} \left( \frac{T_8}{3} \right)^{3/2} \times 10^{33.0 - (50.4 Q_6 / T_8)} \right], \quad (81)$$

where  $T_8$  is the temperature in  $10^8$  degrees and  $Q_6$  is the binding energy in Mev.

Now if the final nucleus is stable  $n_f$  is determined by  $\langle \sigma v \rangle$  for this nucleus and only in rare cases will  $n_f$  be an order of magnitude larger than  $n_i$ . If the final nucleus is beta active it will decay much more rapidly than it is produced and  $n_f \ll n_i$ . Consider the case  $n_f = n_i$  and  $n_n = 10^7$  and  $T_8 = 3$ . Then the second term in the brackets is less than 10 per cent for

$$50.4 \frac{Q_6}{T_8} - 27.0 > 0$$

or

$$T_8 \leq 1.8 Q_6. \quad (82)$$

For  $T_8 \sim 3$  as used in this paper no correction need ever be made for this effect since  $Q_6 > 4$  for all heavy nuclei. For  $T_8 \sim 7$  the effect must be investigated starting from the closed shell magic nuclei where the smallest neutron binding energies are found.

#### APPENDIX C. RELATIVE SOURCES OF ELEMENT ABUNDANCES

For purposes of astronomical observation it is interesting to estimate the relative amounts of elemental abundances produced in the  $r$  and  $s$  processes. This requires summing over the contributions to the abundances of each isotope of an element. Table IV contains a summary of the best estimates we have been able to make of the relative contributions of these two processes to the elements heavier than iron. The  $r$  and  $s$  processes for elements lighter than iron are complicated by uncertainties as to the seed nuclei involved and cannot be estimated at present. Three quantities are compared for each element listed in column one: (1) the observed abundance of the element is given on the scale  $\text{Si} = 10^6$  in column two; (2) the calculated ( $1, 17$ ) abundance of that element produced

TABLE IV  
RELATIVE SOURCES OF ELEMENT ABUNDANCES

Element	Abundance	r	s	r/s	Merit
<sup>29</sup> Cu	212 <sup>b</sup>	20	296	.07	A
<sup>30</sup> Zn	486 <sup>b</sup>	50	320	.2	A
<sup>31</sup> Ga	11.4 <sup>b</sup>	11	21.5	.5	B
<sup>32</sup> Ge	50.5 <sup>b</sup>	3.5	45.6	.07	A
<sup>33</sup> As	4.0 <sup>b</sup>	.9	1.3	.7	B
<sup>34</sup> Se	18.8 <sup>a</sup>	23	7.4	3	B
<sup>35</sup> Br	13.4 <sup>b</sup>	5.5	1.5	4	A
<sup>36</sup> Kr	51.3 <sup>b</sup>	15	2.6	6	A
<sup>37</sup> Rb	4.4 <sup>c</sup>	2.7	1.5	2	A
<sup>38</sup> Sr	18.9 <sup>b</sup>	1.4	16.2	.08	A
<sup>39</sup> Y	8.9 <sup>b</sup>	1.4	10.0	.1	A
<sup>40</sup> Zr	21.8 <sup>c</sup>	4.5	35.3	.1	A
<sup>41</sup> Nb	1.00 <sup>b</sup>	.9	2.6	.4	C
<sup>42</sup> Mo	2.42 <sup>b</sup>	1.1	1.7	.7	C
<sup>43</sup> Tc <sup>99</sup>	2.2x10 <sup>5</sup> yr.	SN	RG		
<sup>44</sup> Ru	1.49 <sup>b</sup>	.26	.57	.5	B
<sup>45</sup> Rh	.27 <sup>a</sup>	.07	.07	1	B
<sup>46</sup> Pd	.675 <sup>b</sup>	.19	.42	.5	B
<sup>47</sup> Ag	.13 <sup>a</sup>	.058	.11	.5	B
<sup>48</sup> Cd	.89 <sup>b</sup>	.12	.69	.2	B
<sup>49</sup> In	.11 <sup>b</sup>	.023	.048	.5	B
<sup>50</sup> Sn	1.33 <sup>b</sup>	.16	1.7	.1	A
<sup>51</sup> Sb	.246 <sup>b</sup>	.05	.04	1.3	C
<sup>52</sup> Te	1.83 <sup>a</sup>	1.55	.31	5	A
<sup>53</sup> I	.23 <sup>a</sup>	.17	.04	4	B
<sup>54</sup> Xe	4.0 <sup>b</sup>	2.1	.48	4.5	B
<sup>55</sup> Cs	.069 <sup>a</sup>	.10	.032	3	B
<sup>56</sup> Ba	3.66 <sup>b</sup>	.46	3.2	.1	A

TABLE IV—Continued

Element	Abundance	r	s	r/s	Merit
57 <sup>La</sup>	.40 <sup>a</sup>	.18	.52	.3	B
58 <sup>Ce</sup>	.62 <sup>a</sup>	.36	.81	.4	B
59 <sup>Pr</sup>	.15 <sup>a</sup>	.022	.15	.1	B
60 <sup>Nd</sup>	.74 <sup>a</sup>	.25	.53	.5	B
61 <sup>Pm</sup> <sup>147</sup>	2.6 yr.	SN	RG		
62 <sup>Sm</sup>	.25 <sup>a</sup>	.25	.35	.7	B
63 <sup>Eu</sup>	.096 <sup>a</sup>	.11	.04	3	B
64 <sup>Gd</sup>	.36 <sup>a</sup>	.28	.13	2	A
65 <sup>Tb</sup>	.055 <sup>a</sup>	.073	.010	7	B
66 <sup>Dy</sup>	.39 <sup>a</sup>	.22	.22	1	B
67 <sup>Ho</sup>	.078 <sup>a</sup>	.074	.010	7	B
68 <sup>Er</sup>	.21 <sup>a</sup>	.232	.13	2	B
69 <sup>Tm</sup>	.039 <sup>a</sup>	.046	.014	3	B
70 <sup>Yb</sup>	.19 <sup>a</sup>	.21	.17	1.2	B
71 <sup>Lu</sup>	.037 <sup>a</sup>	.027	.0076	3.5	B
72 <sup>Hf</sup>	.175 <sup>c</sup>	.07	.17	.4	B
73 <sup>Ta</sup>	.026 <sup>c</sup>	.014	.016	.9	B
74 <sup>W</sup>	.20 <sup>c</sup>	.056	.13	.4	B
75 <sup>Re</sup>	.054 <sup>c</sup>	.044	.008	5	B
76 <sup>Os</sup>	.40 <sup>c</sup>	.45	.063	7	A
77 <sup>Ir</sup>	.328 <sup>c</sup>	.33	.063	5	A
78 <sup>Pt</sup>	.650 <sup>c</sup>	.59	.21	3	A
79 <sup>Au</sup>	.058 <sup>c</sup>	.11	.019	6	B
80 <sup>Hg</sup>	.284 <sup>b</sup>	.11	.51	.2	C
81 <sup>Tl</sup>	.74 <sup>d</sup>	.044	.70	.06	B*
82 <sup>Pb</sup>	6.5 <sup>d</sup>	.90	5.6	.16	A*
83 <sup>Bi</sup>	.92 <sup>d</sup>	.38	.54	.70	A*

a. Activation analysis.

b. Suess and Urey.

c. Four-tenths Suess and Urey.

d. Activation corrected for fractionation

\*These figures of merit are primarily determined on the basis of radiogenic or closely associated contributions which are necessarily r-process.

in the  $r$ -process is given in column three; (3) the  $s$ -process abundances calculated by demanding that the  $\sigma N$  product of  $s$ -process isotopes fall near the curve in Fig. 20 is given in column four. Considerable caution must be applied in using these numbers. All three abundances are subject to rather sizeable error at present as revealed by the fact that column two is not the exact sum of columns three and four. Columns three and four are *independent* estimates of the  $r$  and  $s$ -process contributions and a comparison of their sum with the observed abundance thus serves as a check on the overall theory of heavy element production as outlined (1) by B<sup>2</sup>FH. We neglect  $p$ -process contributions.

The element abundances are of four types for reasons explained earlier in this paper. As a superscript following each abundance we include one of four letters which indicate, respectively: (a) activation analysis of meteorites, (b) Suess and Urey, (c) four-tenths Suess and Urey, (d) an activation measurement corrected for probable fractionation. Exceptions to this notation occur at the radioactive isotopes  $^{99}\text{Tc}$  and  $^{147}\text{Pm}$  where the  $r$  and  $s$  columns have the symbols  $SN$  and  $RG$  to indicate, respectively, that the observations are necessarily  $r$ -process in Type I Supernovae and  $s$ -process in Red Giants.  $\text{Tc}^{97, 98}$  are produced only in the  $p$ -process. The fifth column lists the ratio  $r/s$  of the calculated contributions from the two processes. The final column lists a symbol of merit, A, B, or C, regarding the certainty of the ratio  $r/s$  for a given element. These symbols may be roughly interpreted to mean: A-near certain, B-probable, C-questionable. These figures of merit were not primarily determined by the accuracy with which column two equals the sum of columns three and four, for such a discrepancy may be merely an error in the observed elemental abundance. Rather the merit is determined by the inner consistency of the investigations on the source of the several isotopes of each element which were listed in Table III.

RECEIVED July 15, 1960

#### REFERENCES

1. E. M. BURBIDGE, G. R. BURBIDGE, W. A. FOWLER, AND F. HOYLE, *Science* **124**, 611 (1956); *Revs. Modern Phys.* **29**, 547 (1957).  
J. L. GREENSTEIN, in "Modern Physics for the Engineer," L. N. Ridenour, ed., Chapter 10. McGraw-Hill, New York, 1954.  
A. G. W. CAMERON, *Astrophys. J.* **121**, 144 (1955).  
W. A. FOWLER, E. M. BURBIDGE, AND G. R. BURBIDGE, *Astrophys. J.* **122**, 271 (1955).  
F. HOYLE, *Astrophys. J. Suppl.* **1**, 121 (1954).  
W. A. FOWLER AND J. L. GREENSTEIN, *Proc. Natl. Acad. Sci. U. S. A.* **42**, 173 (1956).
2. GEORGE GAMOW, *Ohio J. Sci.* **35**, 406 (1935); *Phys. Rev.* **70**, 572 (1946); *Phys. Rev.* **74**, 505 (1948); *Nature* **162**, 680 (1948); *Revs. Modern Phys.* **21**, (1949).
3. R. A. ALPHER AND R. C. HERMAN, *Revs. Modern Phys.* **22**, 153 (1950); in "Annual Reviews of Nuclear Science," Vol. 2, p. 1. Annual Reviews, Stanford, 1953. See also R. A. ALPHER, H. A. BETHE, AND G. GAMOW, *Phys. Rev.* **73**, 803 (1948).
4. D. J. HUGHES, W. B. D. SPATZ, AND N. GOLDSTEIN, *Phys. Rev.* **78**, 1781 (1949).

- D. J. HUGHES, R. C. GARTH, AND J. S. LEVIN, *Phys. Rev.* **91**, 1423 (1953).
5. GEORGE GAMOW, *Sci. Am.* **195**, No. 3, 154 (1956).
  6. H. E. SUESS AND H. E. UREY, *Revs. Modern Phys.* **28**, 53 (1956).
  7. C. D. CORYELL, Laboratory for Nuclear Studies, M.I.T., Annual Report (1956).
  8. A. G. W. CAMERON, *Astrophys. J.* **129**, 676 (1959). See also G. R. BURBIDGE, *Astrophys. J.* **131**, 2, 519 (1960), and in reply A. G. W. CAMERON, *Astrophys. J.* **131**, 2, 521 (1960).
  9. H. BATEMAN, *Proc. Cambridge Phil. Soc.* **15**, 423, 1910.
  10. W. A. FOWLER, E. M. BURBIDGE, AND G. R. BURBIDGE, *Astrophys. J. Supp.* **II**, 167, Appendix II (1955).
  11. F. HOYLE (private communication).
  12. D. D. CLAYTON AND W. A. FOWLER, *Bull. Am. Phys. Soc.* [2], **3**, 407 (1958).
  13. H. REEVES AND E. E. SALPETER, *Phys. Rev.* **116**, 1505 (1959).
  14. W. A. FOWLER AND F. HOYLE, *Annals of Physics* **10**, 280 (1960).
  15. R. A. SCHMITT, R. SHARP, A. W. MOSEN, R. B. DUFFIELD, AND L. ZUMWALT (private communication). To appear in *Geochimica et Cosmochimica Acta*.
  16. G. W. REED, K. KIGOSHI, AND A. TURKEVICH, "Concentrations of Some Heavy Elements in Meteorites by Activation Analysis." Submitted to *Geochimica et Cosmochimica Acta*.
  17. R. A. BECKER AND W. A. FOWLER, *Phys. Rev.* **115**, 1410, (1959).
  18. G. L. BATE, J. R. HUIZENGA, AND H. A. POTRATZ, *Science* **126**, 612 (1957).
  19. H. HAMAGUCHI, G. W. REED, AND A. TURKEVITCH, *Geochim. et Cosmochim. Acta* **12**, 337 (1957).
  20. C. PATTERSON, H. BROWN, G. TILTON, AND M. INGRAM, *Phys. Rev.* **92**, 1234 (1953) and *Science* **121**, 69 (1955).
  21. G. TILTON, C. PATTERSON, AND G. DAVIS, *Bull. Geol. Soc. Am.* **65**, 1314 (1954).
  22. C. PATTERSON, *Geochim. et Cosmochim. Acta* **7**, 151 (1955).
  23. L. GOLDBERG, E. MÜLLER, AND L. H. ALLER, in "Handbuch of the Solar System," Vol. 4. Univ. of Chicago Press, Chicago, 1959.
  24. L. H. ALLER, "Primordial Composition of the Solar System" (prepared for presentation at the Cleveland Meeting of the American Astronomical Society) December, 1959; see also L. H. ALLER, in "Handbuch der Physik," Vol. 51, p. 324 Springer-Verlag, Heidelberg, 1958.
  25. R. L. MACKLIN, N. H. LAZAR, AND W. S. LYON, *Phys. Rev.* **107**, 504 (1957).
  26. R. BOOTH, W. P. BALL, AND M. H. MACGREGOR, *Phys. Rev.* **112**, 226 (1958).
  27. J. H. GIBBONS, R. L. MACKLIN, P. D. MILLER, AND J. H. NEILER, Submitted to *Phys. Rev.* For early results by these authors see *Bull. Am. Phys. Soc.* (2), **4**, 474 (1959).
  28. C. W. COOK AND H. W. SCHMITT, submitted to *Nuclear Phys.* For early results by these authors see *Bull. Am. Phys. Soc.* (2), **4**, 359 (1959).

## B. Calculated Abundances of the Heavy Nuclei

Physical theories pertaining to heavy element synthesis must be evaluated on two counts. In the first place, the mechanisms of production must be consistent with known physical laws. Secondly, the predictions of the formulated theory must be compared with the observed facts. It is toward the latter that this section is directed.

It has already been emphasized in Section A that most of the heavy elements are produced by the two stellar processes called the s- and r-processes, as formulated in the review article of Burbidge et al. (1). In fact the purpose of Section A\* was to formulate more quantitatively the theoretical framework of the s-process. The time is appropriate, therefore, to review the quantitative predictions of these two stellar processes in more detail than was done in Table IV of CFHZ. The object will be to compare the resulting abundance estimates with current knowledge of element abundances and isotope ratios.

Knowledge of the abundances comes from several sources. Astronomical observations of spectral line strengths yield information on element abundances in stars. In general, the most accurate determinations are those made on light from the sun (29). However, even for the sun, with a few exceptions such as  $C^{13}/C^{12}$ , it is not possible to make determinations of

---

\*Section A will hereafter be referred to as CFHZ.

the relative abundances of the isotopes of the elements. On the other hand, detailed examination of terrestrial and meteoritic material can yield relative isotopic abundances as well as relative elemental abundances.\* In this case, however, the elemental abundances are subject to chemical and physical fractionation which must be evaluated in terms of known properties of the elements and assumed histories of the objects under investigation. The comprehensive review of Suess and Urey (6) emphasizes the role of the fractionation problem in the correlation of observed abundances. With suitable qualifications, these separate lines of investigation by astrophysicists and geophysicists can be combined to give a complete abundance curve for all of the stable nuclear species. The terrestrial and meteoritic isotopic abundances may be assumed to be characteristic of those in the sun but not in other stars, and there are even a few instances in which terrestrial and meteoritic abundances might be expected to be different from those in the sun (31). Nonetheless, the abundance curve so obtained is fairly representative of solar system material. The abundances should not be taken to be "cosmic" or "universal," however, as there is at present no certain way to estimate the extent to which the primitive solar material was representative of the universe. For purposes of comparison of

---

\*W. D. Ehmann (30) has written an excellent review article of recent abundance measurements obtained by the technique of neutron activation of meteoritic samples.

semitheoretical abundances with solar abundances, however, it is only necessary that no extensive fractionation of solar material occurred during its formation.

Relative isotopic abundances are essential to an understanding of the processes of nucleosynthesis since the mechanism of formation for the individual isotopes of an element are in general quite different. In particular, the observed isotopic composition of an element whose different isotopes are produced primarily in different processes indicates the relative amount by which these processes have contributed to the synthesis of solar system material.

In the following discussion the concern will lie with the relative contributions of the r- and s-processes. The p-process will be ignored because its effects are visible only in the very rare, lightest isotopes of the heavy elements. The expectations of the r- and s-processes, taken individually, are determined primarily by observation of nuclear properties, but the relative yield of the two processes in solar material is a simple fact of history which remains only to be uncovered. In the s-process, the neutron capture cross sections of the stable (or long-lived) isotopes are the significant quantities for the determination of abundances. In the r-process, a generalized nuclear mass law is employed to determine neutron binding energies and beta-decay lifetimes which are the significant quantities in this case for the determination of abundances. The s- and r-process calculations yield relative

abundances of the isotopes which then must be normalized to observed abundances. It is this problem of normalization which is primarily the present concern. In a very general sense, the ultimate solution indicates the relative number of r-process and s-process events which contributed to the synthesis of solar system material.

From CFHZ it is evident that the normalization for the s-process contributions consists in the smooth adjustment of a theoretically reasonable  $\sigma N$ -curve to known cross sections,  $\sigma(n, \gamma)$ , and abundances,  $N$ , as a function of atomic weight. In light of the fact that only those abundances formed in the s-process can take part in this correlation, the quantity  $\sigma_A^N(s)$  is given the special symbol  $I_A$ . Theoretically allowable  $I_A$ -curves are those for which there exists some  $g(n_c)$  such that (see eq. 55 of CFHZ)

$$\sigma_A^N(s) = I_A \equiv \int_0^{\infty} g(n_c) \psi_A(n_c) dn_c \quad \text{for } A \geq 62.$$

In this equation  $g(n_c)$  represents the number of iron group nuclei that had been exposed to a neutron flux resulting in an average of  $n_c$  neutron captures per seed nucleus before mixing into the original solar material. It also follows that  $\int_0^{\infty} g(n_c) dn_c$  is approximately equal to the total number of nuclei in the solar system with  $A \geq 62$  which have been produced in the s-process.

An important general result found by CFHZ is that  $\psi_A(n_c)$ , and hence  $I_A$ , is relatively insensitive to changes in all but

the smallest of the cross sections in the s-process chain. This fact insures that an  $I_A$  calculated on the basis of the cross sections given in Table III will be approximately equal to the  $I_A$  resulting from the actual cross sections. Once a curve  $I_A$  has been chosen, it follows that the abundance produced in the s-process,  $N_A = I_A/\sigma_A$ , is inversely proportional to its neutron capture cross section. This last conclusion emphasizes the importance of accurate knowledge of these cross sections for purposes of abundance calculations. A tentative determination of  $I_A$  was presented by CFHZ in figure 20. In this section that curve is assumed to be correct, the s-process abundances being calculated from it and from the neutron capture cross sections.

An important clarification of the resulting s-process abundances must be emphasized at this point. The calculated abundances agree, of course, with the observed abundances whenever a given  $\sigma N$ -product falls on the smooth curve of figure 20. Also, the calculated and the observed isotope ratios are nearly equal for those predominately s-process elements whose isotopic neutron capture cross sections were chosen to be inversely proportional to the isotopic abundances. In neither case does the result imply that the observed abundance is more accurate than those for neighboring elements. The degree of agreement between the calculated and the observed abundances rests on the picture in the large, so to speak, rather than on isolated cases.

The method of normalization for the r-process calculations is to adjust the parameters of the model until the abundance peaks near  $A = 80, 130, \text{ and } 196$  are fitted. Errors in the mass law used will result only in minor errors in the shape of the r-process abundance distribution, but the normalization of the resultant shape rests primarily on the observed abundances of Os, Ir, Pt, Te, Xe, Se, and Kr. Considerable evidence has arisen that the Suess and Urey (6) abundances of these elements may be too large. The abundances of Se, Xe, Kr, and Te were "boot-strapped" together in their analysis. Terrestrial ratios of the rare gases were used, thereby setting Kr/Xe. The abundance of Te was determined by extrapolation from Xe and by observed ratios with Se, which in turn was determined by augmenting Se/S observations due to the slightly greater stability of Se compounds as compared with S compounds. Recent abundance measurements of meteoritic samples by the technique of neutron activation (30) have revealed that Te and Se are lower by about a factor of three in meteorites than the value given by Suess and Urey. It is, therefore, not unreasonable to reduce both of these r-process peaks by a similar factor. The activation analyses of Os and Ir have indicated that their abundances are about one-half of the Suess and Urey value. Ehmann (30) gives  $Os \approx .6$  and  $Ir = .38$ . A similar reduction for Pt would therefore be indicated. The last reductions are consistent with the factor of 2.5 by which these elements were reduced by CFHZ on the basis of

general smoothing arguments. It is also worth noting that Taylor (32) concludes that the smoothing process of Suess and Urey has overestimated the abundances of r-process elements in the rare-earth region.

For these reasons the calculations of Burbidge et al. (1) and of Becker and Fowler (17) on the r-process abundances, based as they were on normalization to Suess and Urey abundances, were uniformly reduced by a factor of 2.5. This simple assumption will have to suffice until more accurate experimental abundance information on the r-process peaks is available.

Exceptions to this general procedure of abundance calculations occur for the elements Tl, Pb, and Bi. In addition to direct formation in the r- and s-processes, these elements are in part the results of radiogenic decays. The r-process contributions, both direct and radiogenic, are taken from Fowler and Hoyle (14). The present-day Th and U abundances employed for these calculations are  $Th = 0.173$  and  $U = 0.045$ . The s-process contributions are the difference of the observed abundances and the r-process contributions. This procedure produces, of course, exact agreement of the observed abundances with  $N_r + N_s$ . Such an attitude was adopted by CFHZ to determine the behavior of the s-process  $\sigma N$  curve for  $A > 200$ . See Section XIII of CFHZ for the details.

The results of these calculations are shown in Table V. The isotopes of each element are listed by mass number beneath

the chemical symbol of the element in column one. The letter s following a mass number identifies that isotope as lying on the s-process path. Column two gives the abundances of the elements and their isotopes as used by CFHZ. The element abundance is enclosed in parentheses with superscript opposite the element symbol. The superscripts indicate the following sources for the abundance given: a, activation analysis of meteoritic samples (30); b, Suess and Urey (6) value; c, 0.4 times the Suess and Urey value for reasons indicated by CFHZ; d, activation analysis corrected for probable fractionation of the meteoritic samples used.\* The abundance of each isotope follows from the element abundance and the known isotopic composition of the elements in terrestrial material.

The expected value of  $I_A$  taken from figure 20 of CFHZ is listed in column three. The neutron capture cross sections used for calculation of the s-process abundances are given in column four. The resulting abundance,  $N_s$ , is equal to  $I/\sigma$ . The sixth column contains the renormalized r-process abundances,  $N_r$ .

The final two columns contain, respectively, the sum of the r- and s-process contributions and the ratio of the r- to s-process contributions. The sum,  $N_r + N_s$ , is the quantity

---

\*The abundances of Tl, Pb, and Bi from chondritic meteorites are much smaller than the values given here. For a discussion of this problem, see Section XIII of CFHZ.

to be compared to the observed isotopic abundance.\* The ratio,  $N_r/N_s$ , is an indication of the relative extent to which the isotopes have been formed by these two processes in the solar system. It should be noted that this ratio must not be taken to be of "cosmic" significance. Observations of extra-solar material could lead to quite different ratios. It would be expected, however, that when a similar table can be constructed for another star, all the  $N_r/N_s$  ratios will differ from the solar ratio by a constant factor over the flat portions of the  $I_A$  curve. The solar ratios can nonetheless serve as a rough guide to those elements which could most probably be seen in r- and s-process events. The ratio  $N_r/N_s$  should replace the more qualitative assignment process given originally by Burbidge et al. (1), although no major changes are required.

The comparison of the calculated abundances with the observed abundances is quite encouraging. It has been mentioned previously that good agreement will, of course, be expected for those elements which dominated the normalizations. One such example is Ba, whose heaviest isotope,  $Ba^{138}$ , falls on the  $I_A$  curve of figure 20. The cross sections for the

---

\*Recall that no account has been made of the p-process. For this reason the lightest isotopes of the elements remain completely unaccounted for in this review. Small corrections to  $N_r + N_s$  resulting from this process are also not included, but they are insignificant. See Burbidge et al. (1) for a review of the p-process.

other isotopes of Ba were chosen to give  $\sigma_N$  products equal to that at  $A = 138$ . Since the r-process contributes a relatively small amount to this element, the calculated abundances and isotope ratios agree well with the observed quantities. Future measurements of the capture cross sections for all the isotopes of Ba will remove this arbitrariness and will confirm or refute, as the case may be, the s-process calculations. Similar arguments apply to many of the elements.

The calculated abundances,  $O_s = .51$  and  $Ir = .39$ , agree well with the values  $O_s \approx .6$  and  $Ir = .38$  obtained by Ehmann (30). This fact reflects the correctness of the normalization used in the r-process calculations. The excellent agreement of the isotope ratios calculated for these elements, on the other hand, indicates the correctness of the r-process theory and the selection of parameters as formulated by Burbidge et al. (1).

More meaningful in terms of theoretical prediction is the success with an element like Gd, which did not participate in the normalization of either process. Both processes contribute substantially to its isotopes, and the resulting predictions account for the abundance of each isotope remarkably well. Unfortunately, the neutron capture cross sections used in the determination of the s-process contributions are not entirely measured values.

Some difficulties are, of course, also encountered. For example, the isotope ratios of Kr (mostly r-process) and of Mo (mostly s-process) are not very good. The element Hg may

be cited as particularly vexing. Not only is its abundance difficult to determine because of its physical properties, but isotopic capture cross sections are sorely needed.

Abundances measured by neutron activation are certainly tending to support the general attitudes taken in this work. In addition to the new abundances mentioned already in the r-process peaks, Ehmann (30) has reported the abundances of Ta and W as .019 and .11 respectively. These numbers are much nearer those calculated in this work (Ta = .030, W = .18) than to the values of Suess and Urey (Ta = .065, W = .49). The importance of these two elements lies in the somewhat arbitrary reduction of Suess and Urey abundances performed by CFHZ for determination of the  $I_A$  curve of figure 20. This reduction is now justified.

In spite of the success of these calculations, the theoretical abundances must be considered as only tentative. Continuous improvement may be hoped for from several sources. Foremost among these is the measurement of isotopic neutron capture cross sections. The cross sections used for the present calculation are mostly interpolated semiempirically from known cross sections. More known cross sections will also provide more data points for determination of the  $I_A$  curve. The shape of the r-process yields may be improved with better theoretical expressions for the binding energies of neutron-rich nuclei. Finally, the importance of continuing abundance observations must be emphasized. In particular, the normalization

of the entire r-process yield rests on the observed abundances in the r-process peaks.

The abundance calculations have been made in order to facilitate comparison with observation and not to create a new table of abundances. However, there will be some circumstances under which it is advisable to use the calculated  $N_p + N_s$  abundances which vary in a relatively smooth manner with atomic weight rather than the "observed" abundances which show discontinuities arising from different techniques in measurement. However, the calculated abundances must always be used with considerable caution.

Table V . Contributions to Isotopic Abundances

<u>Element Isotope</u>	<u>Abund.</u>	<u>I<sub>A</sub></u>	<u>σ<sub>A</sub></u>	<u>N<sub>s</sub></u>	<u>N<sub>r</sub></u>	<u>N<sub>r</sub> + N<sub>s</sub></u>	<u><math>\frac{N_r}{N_s}</math></u>
29 Cu	(212) <sup>b</sup>			296	20	316	.07
63s	146	17000	115	146	10	156	.07
65s	66	7000	47	150	10	160	.07
30 Zn	(486) <sup>b</sup>			320	40	360	.2
64sb	238	10000	50	80	0	80	0
66s	134	5000	40	125	10	135	.1
67s	20	3500	144	24	10	34	.4
68s	90	2900	32	91	10	101	.1
70	3.4				10	10	.
31 Ga	(11.4) <sup>b</sup>			21.5	11	32	.5
69s	6.9	2200	200	11.0	10	21	.9
71s	4.5	1500	142	10.5	.88	11.4	.1
32 Ge	(50.5) <sup>b</sup>			45.6	3.5	49.1	.07
70s	10.4	1700	170	10.0	0	10.0	0
72s	13.8	1400	105	13.2	.88	14.1	.06
73s	3.8	1200	310	3.9	.88	4.8	.2
74s	18.6	1000	54	18.5	.88	19.4	.05
76	3.9		40	0	.88	.88	
33 As	(4.0) <sup>b</sup>			1.30	.88	2.18	.7
75s	4.0	900	695	1.30	.88	2.18	.7

Element Isotope	Abund.	$I_A$	$\sigma_A$	$N_s$	$N_r$	$N_r + N_s$	$\frac{N_r}{N_s}$
34 Se	(18.8) <sup>a</sup>			7.4	23.5	30.9	3
74	0.18			0	0		
76s	1.7	800	300	2.7	0	2.7	0
77s	1.4	700	600	1.2	0.88	2.1	.7
78s	4.4	600	300	2.0	1.44	3.4	.7
79s	$7 \times 10^4$ yr.	500	600	(.8) <sup>*</sup>	(1.25)	2.1	
80s	9.4	440	300	1.5	17.0	18.5	11
82	1.7		300	0	4.2	4.2	r-only
35 Br	(13.4) <sup>b</sup>			1.5	5.4	6.9	4
79	6.8			<u>0.8</u> <sup>**</sup>	<u>1.25</u>	2.1	1.5
81s	6.6	400	550	0.73	4.2	4.9	6
36 Kr	(51.3) <sup>b</sup>			2.6	15.3	17.9	6
78	.17			0	0		
80	1.1			0	0		
81	$2 \times 10^5$ yr.			0	0		
82s	5.9	360	330	1.1	0	1.1	0
83s	5.9	330	600	0.55	4.2	4.8	8
84s	29.2	300	300	1.0	9.7	10.7	10
86	8.9			0	1.35	1.35	r-only

\* Isotopic Abundances in parentheses are unstable.

\*\* Underlined abundances are the products of long lived decay.

Element Isotope	Abund.	$I_A$	$\sigma_A$	$N_s$	$N_r$	$N_r + N_s$	$\frac{N_r}{N_s}$
37 Rb	(4.4) <sup>a</sup>			1.54	2.70	4.24	1.7
85s	3.2	280	181	1.54	1.35	2.89	0.9
87	1.2		75	0	1.35	1.35	r-only
38 Sr	(18.9) <sup>b</sup>			16.2	1.35	17.55	.08
84	.11			0	0		
86s	1.85	260	140	1.86	0	1.86	0
87s	1.32	240	190	1.26	0	1.26	0
88s	15.6	210	16	13.1	1.35	14.45	.1
39 Y	(8.9) <sup>b</sup>			10.0	1.35	11.35	.1
89s	8.9	180	18	10.0	1.35	11.35	.1
40 Zr	(21.8) <sup>c</sup>			35.3	4.5	39.8	.1
90s	11.2	160	8	20.0	0.9	20.9	.05
91s	2.4	150	37	4.1	0.9	5.0	.2
92s	3.7	140	24	5.8	0.9	6.7	.2
93s	$1.1 \times 10^6$ yr.	135	53	(2.6)	(0.9)	3.5	
94s	3.8	130	24	5.4	0.9	6.3	.2
96	0.61		24	0	0.9	0.9	r-only
41 Nb	(1.00) <sup>b</sup>			2.6	0.9	3.5	.4
91	long life			0	0		
93	1.00	135		<u>2.6</u>	<u>0.9</u>	3.5	.4
94	$1.8 \times 10^4$ yr.			0	0		

Element Isotope	Abund.	I <sub>A</sub>	σ <sub>A</sub>	N <sub>s</sub>	N <sub>r</sub>	N <sub>r</sub> + N <sub>s</sub>	$\frac{N_r}{N_s}$
42 Mo	(2.42) <sup>b</sup>			1.68	1.09	2.77	.7
92	.36			0	0		
94	.22			0	0		
95s	.39	120	224	0.54	0.9	1.44	1.7
96s	.40	115	217	0.53	0	0.53	0
97s	.23	105	374	0.28	0.063	0.34	.23
98s	.58	100	300	0.33	0.063	0.39	.19
100	.23			0	0.063	0.06	r-only
43 Tc	radioactive						
97	2.6x10 <sup>6</sup> yr.			0	0		
98	1.5x10 <sup>6</sup> yr.			0	0		
99s	2.1x10 <sup>5</sup> yr.	90	660	(.14)	(.063)	.20	
44 Ru	(1.49) <sup>b</sup>			0.57	0.26	0.83	.5
96	.085			0	0		
98	.035			0	0		
99	.19			<u>0.14</u>	<u>0.063</u>	0.20	.45
100s	.19	80	477	0.17	0	0.17	0
101s	.25	75	880	0.077	0.063	0.14	.8
102s	.47	70	386	0.18	0.067	0.25	.37
104	.27		211	0	0.067	0.07	r-only
45 Rh	(.27) <sup>a</sup>			0.065	0.067	0.13	1.0
103s	.27	65	1000	0.065	0.067	0.13	1.0

<u>Element Isotope</u>	<u>Abund.</u>	<u>I<sub>A</sub></u>	<u><math>\sigma_A</math></u>	<u>N<sub>S</sub></u>	<u>N<sub>r</sub></u>	<u>N<sub>r</sub> + N<sub>S</sub></u>	<u><math>\frac{N_r}{N_S}</math></u>
46 Pd	(.675) <sup>b</sup>			.415	.186	.601	.5
102	.0054			0	0		
104s	.063	65	480	.135	0	.135	0
105s	.15	62	960	.065	.067	.132	1.0
106s	.18	60	520	.115	.067	.182	.6
107s	4.5x10 <sup>6</sup> yr.	58	1040	(.055)	(.029)	.084	
108s	.18	56	560	.10	.029	.129	.3
110	.091	51		0	.023	.023	r-only
47 Ag	(0.13) <sup>a</sup>			.108	.058	.166	.5
107	0.067			<u>.055</u>	<u>.029</u>	.084	.5
109s	0.063	53	1000	.053	.029	.082	.5
48 Cd	(0.89) <sup>b</sup>			.689	.115	.804	.2
106	.011			0	0		
108	.0078			0	0		
110s	.11	51	337	.151	0	.151	0
111s	.11	49	660	.074	.023	.097	.31
112s	.21	47	324	.145	.023	.168	.15
113s	.11	45	672	.067	.023	.090	.34
114s	.26	44	290	.152	.023	.175	.15
116	.068		250	0	.023	.023	r-only

<u>Element Isotope</u>	<u>Abund.</u>	<u>IA</u>	<u><math>\sigma_A</math></u>	<u><math>N_s</math></u>	<u><math>N_r</math></u>	<u><math>N_r + N_s</math></u>	<u><math>\frac{N_r}{N_s}</math></u>
49 In	(0.11) <sup>b</sup>			.048	.023	.071	.5
113	.0046			0	0		
115s	.105	43	900	.048	.023	.071	.5
50 Sn	(1.33) <sup>b</sup>			1.721	.16	1.88	.1
112	.013			0	0		
114	.009			0	0		
115	.0047			0	0		
116s	.19	42	138	.304	0	.304	0
117s	.10	41	258	.158	.012	.170	.08
118s	.32	40	83	.482	.012	.494	.025
119s	.12	39	230	.169	.012	.181	.07
120s	.43	37	61	.608	.018	.626	.03
122	.063		50	0	.018	.018	r-only
124	.079		40	0	.084	.084	r-only
51 Sb	(.246) <sup>b</sup>			.040	.051	.091	1.3
121s	.141	35	880	.040	.018	.058	.45
123	.105		350	0	.033	.033	r-only
52 Te	(1.83) <sup>a</sup>			.307	1.55	1.86	5
120	.0018			0	0		
122s	.045	35	700	.050	0	.050	0
123s	.016	34	1930	.018	0	.018	0
124s	.085	33	363	.091	0	.091	0

<u>Element Isotope</u>	<u>Abund.</u>	<u>I<sub>A</sub></u>	<u>σ<sub>A</sub></u>	<u>N<sub>s</sub></u>	<u>N<sub>r</sub></u>	<u>N<sub>r</sub> + N<sub>s</sub></u>	<u><math>\frac{N_r}{N_s}</math></u>
52 Te (cont.)							
125s	.13	32	1720	.018	.070	.088	4
126s	.34	32	245	.130	.20	.33	1.5
128	.58		192	0	.59	.59	r-only
130	.63		156	0	.69	.69	r-only
53 I							
	(0.23) <sup>a</sup>			.038	.17	.21	4
127s	.23	31	820	.038	.17	.21	4
129	1.7x10 <sup>7</sup> yr.			0	(.47)		
54 Xe							
	(1.6) <sup>c</sup>			.477	2.13	2.61	4.5
124	.0016			0	0		
126	.0016			0	0		
128s	.030	31	470	.066	0	.066	0
129s	.42	30	1030	.029	<u>.47</u>	.50	16
130s	.064	30	227	.132	0	.13	0
131s	.34	30	500	.060	.69	.75	11
132s	.43	29	153	.190	.69	.88	4
134	.17		115	0	.10	.10	r-only
136	.14		92	0	.18	.18	r-only
55 Cs							
	(.069)			.032	.10	.13	3
133s	.069	29	900	.032	.10	.13	3
135	3x10 <sup>6</sup> yr.			0	(.10)		

<u>Element Isotope</u>	<u>Abund.</u>	<u>I<sub>A</sub></u>	<u>σ<sub>A</sub></u>	<u>N<sub>s</sub></u>	<u>N<sub>r</sub></u>	<u>N<sub>r</sub> + N<sub>s</sub></u>	<u><math>\frac{N_r}{N_s}</math></u>
56 Ba	(3.66) <sup>b</sup>			3.22	.46	3.68	.14
130	.0037			0	0		
132	.0037			0	0		
134s	.088	28	337	.083	0	.083	0
135s	.24	28	124	.226	<u>.10</u>	.33	.45
136s	.28	27	105	.257	0	.26	0
137s	.41	27	73	.371	.18	.55	.5
138s	2.62	26	11.4	2.28	.18	2.46	.08
57 La	(0.40) <sup>a</sup>			.52	.18	.70	.3
137	6x10 <sup>4</sup> yr.			0	0		
138	4x10 <sup>-4</sup> , (10 <sup>11</sup> yr.)			0	0		
139s	.40	26	50	.52	.18	.70	.3
58 Ce	(0.62) <sup>a</sup>			.81	.36	1.17	.4
136	.0012			0	0		
138	.0016			0	0		
140s	.55	25	31	.81	.18	.99	.2
142	.069		425	0	.18	.18	r-only
59 Pr	(0.15) <sup>a</sup>			.154	.022	.176	.14
141s	.15	25	162	.154	.022	.176	.14

<u>Element Isotope</u>	<u>Abund.</u>	<u>I<sub>A</sub></u>	<u>σ<sub>A</sub></u>	<u>N<sub>S</sub></u>	<u>N<sub>R</sub></u>	<u>N<sub>R</sub> + N<sub>S</sub></u>	<u><math>\frac{N_R}{N_S}</math></u>
60 Na	(0.74) <sup>a</sup>			.531	.246	.777	.5
142s	.20	25	150	.167	0	.167	0
143s	.090	24	335	.072	.022	.094	.3
144s	.18	24	170	.141	.022	.163	.1
145s	.061	24	490	.049	.022	.071	.5
146s	.13	24	236	.102	.069	.171	.7
148	.042		250	0	.069	.069	r-only
150	.041		250	0	.042	.042	r-only
61 Pm	radioactive						
145	18 yr.			0	0		
146	1 yr.			0	0		
147	2.6 yr.			0	(.069)		
62 Sm	(0.25) <sup>a</sup>			.346	.249	.595	.7
144	.004			0	0		
146	5x10 <sup>7</sup> yr.			0	0		
147s	.038	24	320	.075	<u>.069</u>	.144	.9
148s	.028	24	213	.113	0	.113	0
149s	.035	23	470	.049	.042	.091	.9
150s	.018	23	324	.071	0	.071	0
151s	93 yr.	23	800	(.029)	(.042)		
152s	.066	23	600	.038	.069	.107	2
154	.056		527	0	.069	.069	r-only

Element Isotope	Abund.	$I_A$	$\sigma_A$	$N_S$	$N_R$	$N_R + N_S$	$\frac{N_R}{N_S}$
63 Eu	(.096) <sup>a</sup>			.038	.111	.149	3
151	.046			<u>.029</u>	<u>.042</u>	.071	1.5
153s	.050	23	2560	.009	.069	.078	8
64 Gd	(0.36) <sup>a</sup>			.126	.284	.410	2
150	> 10 <sup>5</sup> yr.			0	0		
152	.0007			0	0		
154s	.008	23	710	.032	0	.032	0
155s	.053	23	1560	.015	.046	.061	3
156s	.074	23	710	.032	.046	.078	1.4
157s	.056	23	1560	.015	.046	.061	3
158s	.089	23	710	.032	.073	.105	2.3
160	.079			0	.073	.073	r-only
65 Tb	(.055) <sup>a</sup>			.010	.073	.083	7
159s	.055	22	2280	.010	.073	.083	7
66 Dy	(0.39) <sup>a</sup>			.225	.224	.449	1
156	.0002			0	0		
158	.0004			0	0		
160s	.0089	22	430	.051	0	.051	0
161s	.074	22	940	.023	.050	.073	2.2
162s	.100	22	380	.058	.050	.108	.9
163s	.100	22	840	.026	.050	.076	1.9
164s	.11	22	330	.067	.074	.141	1.1

<u>Element Isotope</u>	<u>Abund.</u>	<u>I<sub>A</sub></u>	<u>σ<sub>A</sub></u>	<u>N<sub>s</sub></u>	<u>N<sub>r</sub></u>	<u>N<sub>r</sub> + N<sub>s</sub></u>	<u><math>\frac{N_r}{N_s}</math></u>
67 Ho	(.078) <sup>a</sup>			.010	.074	.084	7
165s	.078	22	2210	.010	.074	.084	7
68 Er	(.21) <sup>a</sup>			.127	.232	.359	2
162	.0002			0	0		
164	.0031			0	0		
166s	.069	22	500	.044	.074	.118	1.7
167s	.051	22	1000	.022	.046	.068	2.1
168s	.057	22	360	.061	.046	.107	.8
170	.029			0	.066	.066	r-only
69 Tm	(.039) <sup>a</sup>			.014	.046	.060	3
169s	.039	22	1530	.014	.046	.060	3
70 Yb	(.19) <sup>a</sup>			.174	.213	.387	1.2
168	.0003			0	0		
170s	.0058	22	2340	.009	0	.009	0
171s	.027	22	1000	.022	.066	.088	3
172s	.042	22	486	.045	.066	.111	1.5
173s	.031	22	658	.034	.027	.061	.8
174s	.059	22	344	.064	.027	.091	.4
176	.024		280	0	.027	.027	r-only
71 Lu	(.037) <sup>a</sup>			.0076	.027	.035	3.5
175s	.036	22	2900	.0076	.027	.035	3.5
176	.001			0	0		

<u>Element Isotope</u>	<u>Abund.</u>	<u>I<sub>A</sub></u>	<u>σ<sub>A</sub></u>	<u>N<sub>s</sub></u>	<u>N<sub>r</sub></u>	<u>N<sub>r</sub> + N<sub>s</sub></u>	<u><math>\frac{N_r}{N_s}</math></u>
72 Hf	(.175) <sup>c</sup>			.167	.069	.236	.4
174	.0003			0	0		
176s	.0090	22	2400	.009	0	.009	0
177s	.032	22	1000	.022	.027	.049	1.2
178s	.048	22	456	.048	.014	.062	.3
179s	.024	22	900	.025	.014	.039	.6
180s	.062	22	350	.063	.014	.077	.2
182	7.5x10 <sup>6</sup> yr.			0	(.014)		
73 Ta	(.026) <sup>c</sup>			.016	.014	.030	.9
180				0	0		
181s	.026	21	1300	.016	.014	.030	.9
74 W	(0.20) <sup>c</sup>			.128	.056	.184	.4
180	.0002			0	0		
182s	.053	21	420	.050	<u>.014</u>	.064	.3
183s	.029	21	1155	.018	.014	.032	.8
184s	.061	21	350	.060	.014	.074	.2
186	.057			0	.014	.014	r-only
75 Re	(.054) <sup>c</sup>			.008	.044	.052	5
185s	.020	21	2650	.008	.014	.022	1.8
187	.034		970	0	.030	.030	r-only

Element Isotope	Abund.	$I_A$	$\sigma_A$	$N_s$	$N_r$	$N_r + N_s$	$\frac{N_r}{N_s}$
76 Os	(.40) <sup>c</sup>			.063	.448	.511	7
184	.00008			0	0		
186s	.0064	21	3000	.007	0	.007	0
187s	.0066	21	3000	.007	0	.007	0
188s	.053	21	1500	.014	.061	.075	4
189s	.064	21	2000	.011	.056	.067	5
190s	.106	21	886	.024	.103	.127	4
192	.164			0	.228	.228	r-only
77 Ir	(.328) <sup>c</sup>			.063	.33	.39	5
191s	.126	21	1000	.021	.113	.134	6
193s	.202	21	500	.042	.22	.26	5
78 Pt	(.650) <sup>c</sup>			.209	.59	.80	3
190	.00007			0	0		
192s	.0051	21	1000	.021	0	.021	0
194s	.21	21	400	.050	.35	.40	7
195s	.22	21	700	.033	.11	.14	3.3
196s	.17	21	210	.100	.11	.21	1.1
198	.047		240	0	.022	.022	r-only
79 Au	(.058) <sup>c</sup>			.019	.11	.13	6
197s	.058	21	1100	.019	.11	.13	6

Element Isotope	Abund.	$I_A$	$\sigma_A$	$N_s$	$N_r$	$N_r + N_s$	$\frac{N_r}{N_s}$
80 Hg	(.284) <sup>b</sup>			.509	.11	.62	.2
196	.0005			0	0		
198s	.0285	20	560	.036	0	.036	0
199s	.048	20	780	.026	.022	.048	.8
200s	.066	20	340	.059	.022	.081	.4
201s	.038	20	560	.036	.022	.058	.6
202s	.084	20	57	.352	.022	.37	.06
204	.019			0	.022	.022	r-only
81 Tl	(.74) <sup>d</sup>			.70	.044	.74	.06
203s	.22	20	90	.20	.022	.22	.1
205	.52	8		<u>.50</u>	.022	.52	.04
82 Pb	(6.5) <sup>d</sup>			5.6	.90	6.5	.16
202	$3 \times 10^5$ yr.						
204s	.13	15	55	.13	0	.13	0
205s	$5 \times 10^7$ yr.		11	(.50)	0		
206s	1.2	6	2.8	.95	.30	1.25	.3
207s	1.3	4	5.5	.93	.41	1.34	.4
208s	3.7	3	1.1	3.59	.19	3.78	.06
83 Bi	(0.92) <sup>d</sup>			.54	.38	.92	.7
208	$3 \times 10^4$ yr.			0	0		
209s	0.92	1	1.8	.54	.38	.92	.7
210	$2.6 \times 10^6$ yr.						

## II. A SEARCH FOR EXCITED STATES OF $N^{14}$ PERTAINING TO THE SYNTHESIS OF $C^{13}$ IN THE CNO-CYCLE IN STARS

### A. General Nuclear and Astrophysical Considerations

#### 1. Summary of $C^{12}/C^{13}$ Abundance Evidence and the CNO-cycle

The discovery in a wide variety of stellar atmospheres of a detectable  $C^{12}/C^{13}$  abundance ratio using the techniques of molecular band spectra (33) has provided valuable information for application to stellar mechanisms. The production of  $C^{13}$  results from the reaction  $C^{12}(p, \gamma)$  when carbon is present in stellar interiors at temperatures of about  $10^7$  deg. K and higher. Under slowly changing conditions the sequence of reactions called the CNO-cycle will occur. Burbidge et al. (1) have studied this cycle in detail. It involves the stable nuclei  $C^{12}$ ,  $C^{13}$ ,  $N^{14}$ ,  $N^{15}$ ,  $O^{16}$ , and  $O^{17}$  and may be initiated by the presence of any one of these nuclei. The presence of  $C^{12}$  and  $O^{16}$  may occur in stellar interiors in first generation stars through the operation of helium burning in a hot helium core. In second or later generation stars this process may be augmented by the presence of the CNO-nuclei in the original material from mixing at the birth of the star.

Whatever the source of the catalyzing nuclei, if the hydrogen burning occurs for a time that is long compared with the time for one cycle, the net effect will be the production

of  $\text{He}^4$  from protons with the added result that the CNO-nuclei will be processed to an equilibrium abundance ratio. The equilibrium abundance of each CNO-nucleus is inversely proportional to the appropriate cross section times the relative velocity of the reacting particles for the reaction which destroys that nucleus. If the destructive reaction is non-resonant, as the CNO-cycle reactions are believed to be, there follows from Burbidge et al. (1), using their standard notation

$$(n)^{-1}_{\text{equil.}} \propto f_0 S_0 (AZ_0)^{-1} \tau^2 e^{-\tau} .$$

Hepbard and Vogl (34) have recently remeasured the cross sections for  $\text{C}^{12} (p, \gamma)$  and  $\text{C}^{13} (p, \gamma)$  and give respectively  $S_0 (\text{C}^{12}) = 1.33 \text{ kev barns}$  and  $S_0 (\text{C}^{13}) = 6.0 \text{ kev barns}$  for  $T_6 = 15$ . Using these data and the assumption that the most likely site for the CNO-cycle is the hot hydrogen shell about the helium core where  $T_6 = 35$ , there follows

$$\text{C}^{12}/\text{C}^{13} = 4.2 .$$

By extending this calculation to all the CNO-nuclei except  $\text{O}^{17}$ ,\* Fowler et al. (31) list for equilibrium

$$\text{C}^{12} : \text{C}^{13} : \text{N}^{14} : \text{N}^{15} : \text{O}^{16} = .024 : .006 : .95 : 4 \times 10^{-5} : .02 .$$

Thus when equilibrium is reached, the CNO-cycle essentially

\*The equilibrium amount of  $\text{O}^{17}$  is very small and depends on the cross section for the reaction  $\text{O}^{17} (p, \alpha) \text{N}^{14}$ .

converts  $C^{12}$  and  $O^{16}$  into  $N^{14}$  (95%) and leaves 3% among the carbon isotopes in the ratio  $C^{12}/C^{13} = 4$ .

For evidence on carbon stars, I quote McKellar (33):

Summarized, the present state of knowledge on the carbon isotopes in the atmospheres of the cool carbon stars is as follows: (1) there is a group of R-type stars for which the  $C^{12}/C^{13}$  abundance ratio is about 100 or more; (2) for the remainder of the R-type stars for which measurements can be made with some confidence, those on the 1,0 band of  $C_2$  appear to yield a fairly constant  $C^{12}/C^{13}$  ratio of about 5; (3) for the N-type stars, results by various investigators from a wider variety of bands give  $C^{12}/C^{13}$  ratios in the range from about 20 to 2.

It is clear that the observed  $C^{12}/C^{13}$  ratio is in many cases consistent with that expected in CNO equilibrium. In many other cases the amount of  $C^{13}$  is much less. In these latter cases one may suppose that the original material contains an excess of unburned  $C^{12}$  or that some mechanism exists for transporting  $C^{12}$  to the stellar atmosphere without the occurrence of extensive hydrogen burning. In such cases the amount of nitrogen relative to carbon should also be much less than that expected from the equilibrium ratios. The amount of nitrogen appears to be less than the equilibrium amount even in some cases for which  $C^{12}/C^{13}$  is near equilibrium. Such a situation is possible in the early stages of  $C^{12}$  burning. Accurate information of this last type may prove important in the stringent limitations it would impose on the amount of hydrogen burning encountered as  $C^{12}$  is brought up to the stellar atmosphere, for  $C^{13}$  approaches equilibrium with  $C^{12}$

more rapidly than does  $N^{14}$ . This possibility would also require that the amount of  $O^{16}$  relative to  $C^{12}$  in the catalytic material be small, as  $O^{16}$  cycles through  $N^{14}$  before reaching  $C^{12}$ . The single most important fact, however, is that there do exist many stars in which the amount of  $C^{13}$  is as large as that given by the CNO-cycle equilibrium abundances.

Two major additional  $C^{12}/C^{13}$  ratios of special interest are worth mentioning in this summary. It has long been known that terrestrially  $C^{12}/C^{13} = 90$ . Since the earth is presumed to have condensed from primitive solar material, it was believed until recently that the  $C^{12}/C^{13}$  ratio in the sun must have 90 as an upper bound, for subsequent hydrogen burning in the sun would increase the relative amount of  $C^{13}$ . However, Righini (35) has concluded that solar  $C^{12}/C^{13} = 10^4$  within an order of magnitude. These and other closely related facts have led Fowler et al. (31) to conclude that the terrestrial  $C^{13}$  was formed almost exclusively by spallation reactions in an early planetesimal stage of the evolution of the solar system. Those authors carry the solar implications much further. Using the solar abundance ratios of Goldberg et al. (29), who give  $C^{12} : N^{14} : O^{16} = 5.5 : 1 : 9.6$ , they are able to conclude that in primitive solar material the ratio  $O^{16}/C^{12}$  was 1.75 and of that amount only 1/15 has since been through the CNO-cycle. This argument implies that in the sun  $C^{12}/C^{13} = 10^3$ . Further measurements in this regard

will be of considerable interest.

## 2. Possibility of Stellar Resonances in $C^{13} (p, \gamma)$

It is clear that inferences upon stellar structure drawn from  $C^{12}/C^{13}$  ratios depend critically upon the extrapolated cross-section factors for the reactions  $C^{12} (p, \gamma)$  and  $C^{13} (p, \gamma)$ . For both reactions the extrapolation is made by adjusting the tail of a resonance to fit the observed cross-section factors to as low an energy as observation permits (34). This procedure will give good results if no resonances exist in the very low energy regions corresponding to stellar temperatures.

In the case of  $C^{12} (p, \gamma)$  there seems little reason to doubt the extrapolation, which is made from a strong resonance at  $E_r = 456$  kev. It is believed that all  $N^{13}$  levels in this energy region are known.

The situation is not so happy for the  $C^{13} (p, \gamma)$  reaction. This reaction has a Q-value of 7.549 Mev, and the evidence for  $N^{14}$  levels in the 7-8 Mev range of excitation is both meager and confusing. The lack of information results from the relative inaccessibility of this excitation energy to low energy charged particle reactions, the Q-values for the commonly investigated charged particle reactions leading to  $N^{14}$  lying in general too low and the Q-values of reactions for which  $N^{14}$  is the compound nucleus all lying too high.

For a state in  $N^{14}$  to contribute an important resonance for  $C^{13} + p$  at stellar temperatures, the resonance energy would have to fall near the effective stellar energy for the CNO-cycle. A tentative estimate indicates that the resonance energy would have to fall within 10 to 60 kev in  $C^{13} + p$  to be very effective. Such a resonance energy would demand a state in  $N^{14}$  in the excitation range 7.558 to 7.605 Mev. Resonance energies exceeding this range would appear too far out on the tail of the Maxwell-Boltzmann energy distribution for the protons ( $kT \sim 2$  kev), whereas the Coulomb barrier would make the laboratory proton width too small for resonance energies lower than this range to be effective.

A resonance of appropriate energy, however, would completely invalidate the extrapolation of Hebbard (34). The average  $\langle \sigma v \rangle$  for  $C^{13} (p, \gamma)$  could be increased by an order of magnitude and more even for high  $\ell$ -wave resonances. Such an eventuality would be vexing indeed for the general theory of stellar burning. If  $\langle \sigma v \rangle$  were only increased by a factor of ten, the equilibrium ratio for the CNO-cycle would be  $C^{12}/C^{13} = 40$ . Although this ratio would cause no problems for terrestrial and solar carbon, it would leave the value  $C^{12}/C^{13} = 5$  observed in the aforementioned stars as an unexplained mystery. A completely new mechanism for the stellar production of  $C^{13}$  would have to be devised and would almost certainly meet severe theoretical difficulties. Let it be emphasized for clarity at this point that large  $C^{12}/C^{13}$  ratios

are no great problem because the well-known mechanism of helium burning exists for the production of  $C^{12}$ . But the requirement of  $C^{12}$  as a parent for  $C^{13}$  places us at the mercy of the  $(p, \gamma)$  cross-section ratio in determining a theoretic lower bound on  $C^{12}/C^{13}$ .

In consideration of possible resonances in  $C^{13}(p, \gamma)$ , it is appropriate to review existing evidence on  $N^{14}$  energy levels in the range of 7-8 Mev excitation. Figure 21 shows a schematic summary of the existing evidence. The inelastic scattering of 22 Mev alpha particles was studied by Miller et al. (36). They find excitation energies in  $N^{14}$  of 6.47, 7.02, and 7.94 which must of necessity have large  $T = 0$  components. This result indicates that any other state in the 7-8 Mev range will most likely be a  $T = 1$  state.\* Burge and Prowse (37) have observed the inelastic scattering of protons and report levels below 7.7 Mev at 6.23, 6.46, 6.60 (doubtful), 7.02, 7.40, and 7.60. The last level is particularly interesting because it lies in the appropriate  $C^{13} + p$  energy range. Proton groups to 7.40 and 7.60 levels appeared only at one angle, however, whereas the other states appeared at all four angles observed. The scattered protons were observed with emulsion tracks, and only at the one forward angle did the protons with  $Q = -7.4$  and  $-7.6$  have sufficient energy

---

\*Miller et al. (36) do not observe the 6.23 level, however, which is nonetheless believed to be  $T = 0$ .

to be detected with their experimental arrangement. They ascribe these tracks to states at 7.40 and 7.60 because they could think of no other source for them. It is unfortunate that they did not search for these two proton groups at other angles for positive identification. In light of the fact that no known level exists at 7.60 Mev and that a Q of -7.60 Mev was observed only at one angle, this evidence can only be regarded as doubtful. Benenson (38) has observed neutrons from  $C^{13}$  (d,n) and reports levels at 6.23, 6.43, 7.00, 8.08, and one at 7.72 and a possible state at 7.50 Mev excitation in  $N^{14}$ . There is a temptation to identify the possible states at 7.50 and 7.72 with the ones reported at 7.40 and 7.60 by Burge and Prowse (37). Such an identification would seem rather arbitrary in the face of the relatively small error quoted by both investigators and the close agreement on Q-values to other observed states. Very little help is obtained from Bent et al. (39) who observed the gamma rays from  $C^{13}$  (d,n). They find an unassignable gamma ray of 7.30 Mev.

Hebbard and Vogl (34) accurately determined the positions of the 7.97 and 8.06 levels by observing the gamma ray yield as a function of proton energy in  $C^{13}$  (p,  $\gamma$ ). With regard to the uncertainties of other states of lower excitation, they placed limits on the strength of radiative capture down to a proton energy of 130 kev. By calculating proton widths for various possible  $l$ -wave resonances and observing that

spins up to  $J = 3$  exist below 7 Mev for possible cascades, they conclude that any resonance for which  $J \leq 5$  and for which the reduced proton width is greater than 1% of the single-particle limit would probably have been observed. For low  $l$ -wave resonances, considerably smaller reduced proton widths would have been observed. This argument would make the existence of any state in the excitation range 7.67-7.96 Mev unlikely.\*

In summary it may be stated that existing evidence on states in  $N^{14}$  in the excitation range 7-8.4 Mev demonstrates conclusively the existence of states at 7.03, 7.97, and 8.06 Mev. The evidence for possible states at 7.3, 7.4, 7.5, 7.6, and 7.7 Mev appears to be subject to valid doubt.

#### B. Excited States of $N^{14}$ from $N^{15}$ ( $He^3, \alpha$ ) $N^{14}$ \*

##### 1. Suitability of This Reaction

The previously mentioned uncertainties regarding the excited states of  $N^{14}$  and the possible important consequences on the rate of  $C^{13}(p, \gamma)$  at stellar temperatures stress the importance of studying this energy region with charged particles. For bombarding energies of 3 Mev or less, the only

---

\*Vogl informs me by private communication that he has continued the search to proton energies as low as 103 kev without detecting signs of a resonance.

suitable charged particle reaction available is  $N^{15}(\text{He}^3, \alpha)$  with a Q-value of 9.743 Mev from mass differences (40). Outgoing alpha particles leaving  $N^{14}$  with an excitation of about 8 Mev will also have energies of the order of 3 Mev. These energies are suitable for investigation in the Kellogg Radiation Laboratory.

Three possible models or mechanisms for reactions such as  $N^{15}(\text{He}^3, \alpha)$  are in common usage: (a) compound nucleus formation, (b) neutron pick-up, and (c) heavy particle stripping. In terms of compound nucleus formation,  $N^{15} + \text{He}^3$  lies at 14.16 Mev in  $F^{18}$ . The density of both  $T = 0$  and  $T = 1$  levels at compound nucleus energies near this value is probably quite high, and the reaction may proceed through several overlapping levels of unknown spins and parities. Such a situation would, in general, be favorable for emission of alpha particles to a wide variety of quantum states for the residual excited  $N^{14}$  nucleus. The pick-up mechanism could be effective to those  $N^{14}$  states that can be described in terms of the direct removal of a neutron from the  $N^{15}$  ground state configuration. That is, the configuration  $S^4_p^{10}$  could be populated in this manner. In a theoretical analysis of  $N^{14}$ , Warburton and Pinkston (41) conclude that the only likely members of this configuration below 9 Mev are the  $N^{14}$  ground state, the 2.31 Mev level, the 3.95 Mev level, and a level with  $(J^\pi, T) = (2^+, 0)$ , which they tentatively identify as the 7.03 Mev level on the basis of gamma ray evidence. (The

parity of the 7.03 level is undetermined, but its spin is believed to be 2 and  $T = 0$  is known from the inelastic alpha scattering.) It may be possible, therefore, that the 7.03 level be more strongly populated than other levels in this vicinity through the pick-up mechanism. The possibility of heavy particle stripping is even harder to evaluate. It will in general be proportional to the probabilities that the  $N^{15}$  ground state and final  $N^{14}$  excited state can be described respectively in terms of a bound ( $B^{11}, He^4$ ) cluster and a bound ( $B^{11}, He^3$ ) cluster. Owen and Madansky (42) find, for example, that the alpha particle angular distribution from  $C^{13} (He^3, \alpha) C^{12}$  can be accounted for by a rather complicated interference between the pick-up and heavy particle stripping amplitudes. No attempt will be made for the present reaction to evaluate the possibilities of these mechanisms. Suffice it to say that the chance of population of the excited levels of  $N^{14}$  would appear to be good.

A generally favorable situation is presented by charged particle penetrabilities. Although the Coulomb barrier for  $N / He$  is fairly large (3.5 Mev), the penetrability is reasonably insensitive to the angular momentum barrier. From the tables of Schiffer (43) for an alpha particle energy of only 2.4 Mev, the penetrability ratios are found to be

$$P_0 : P_1 : P_2 : P_3 = 1.0 : 0.74 : 0.35 : 0.10 \quad .$$

These ratios insure that the reaction may proceed without

great dynamic hindrance to a good variety of spins and parities.

## 2. General Experimental Arrangement

### a. Equipment

The experiment was conducted on the Kellogg Radiation Laboratory 3 Mev electrostatic accelerator. The  $\text{He}^3$  beam energy was determined by a  $90^\circ$  electrostatic analyzer, and the reaction products were momentum analyzed by a 16-inch radius double-focusing magnetic spectrometer.

Preparatory to the running of the experiment, I was privileged to take part in design modifications of the associated apparatus which were suggested and supervised by Prof. T. Lauritsen. An electrostatic deflection system was designed to compensate fluctuations in the beam position and entrance angle to the electrostatic analyzer. It was hoped that such corrections would make frequent recalibration of the electrostatic analyzer unnecessary. The deflectors consisted of two sets of parallel plates acting in the same direction as the energy-analyzing plates which could simultaneously adjust the position and entrance angle for greater orbit reproducibility and one set of plates in the orthogonal direction which would produce the same results when used in conjunction with the mass-separating magnet. Variable five-kilovolt power supplies and a remote-control panel were designed and built by John Domingo in a manner designed to maintain orthogonality between

position and angular displacements of the beam. When installed in the base of the accelerator column, the deflectors performed their function adequately but produced an unfortunate electron loading which reduced the terminal voltage by an undesirable amount. The deflectors were then removed, redesigned, and rebuilt in a more compact geometry which would locate the top of the deflector system well below the bottom grounded ring of the accelerator column. The rebuilt deflectors were not installed because a satisfactory method of adjusting the position of the energy analyzer was devised by Bardin et al. (44,45).

The position of the beam in the entrance tube is determined by a pair of slits which could be rotated remotely at a viewing station located by the deflector control panel. For viewing the beam position from the images of the slits, a periscope and lens system was designed to focus on a remotely insertable quartz located beneath the second of the two slits. The operation of this part of the system has been quite satisfactory.

A major problem was encountered in counting the reaction products after momentum analysis in the magnetic spectrometer. As the reaction products include all the isotopes of H and He, pulse height analysis was required to separate the alpha yield. The conventional apparatus used for particle detection at the spectrometer exit has been CsI crystals mounted on a photomultiplier tube. The problem arose from the fact

that alpha particles of twice the energy of deuterons make an only slightly larger pulse height in CsI. For the energetics used in the present experiment, elastically scattered deuterons were present in great abundance from the (HD) component of the singly-charged mass-three beam. Profile yields from thick target scattering indicated that  $(HD) / He^3 = 10^{-3}$  in the incident beam. This large amount of deuterium is probable evidence of a leak in the four-way valve system allowing small amounts of deuterium to leak into the ionization bottle. The elastic scattering yields of D were found to be at least an order of magnitude greater than the alpha yields from the reactions. The net effect for CsI detection was that the alpha-particle pulse height spectrum appeared as a small bump on the high-energy side of the deuterium pulse-height spectrum. This situation ruined the statistics of the alpha counting. To correct this problem a new detection system was designed for the spectrometer exit. A solid-state counter with a counting area of  $1/2 \text{ cm}^2$  was mounted in a cylindrical housing that is rapidly interchangeable with the CsI and photomultiplier tube. The counter is a p-n junction with a counting layer depth equal to the range of 4 Mev protons. The counter pulse-height resolution was found to be better than 1% for 4 Mev alpha particles. The pulses from the counter went through conventional amplification and were stored and analyzed in a 100-channel pulse-height analyzer. Since the response of the counter is accurately linear in energy, protons and

alphas make a pulse height twice as large as do deuterons after momentum selection. A  $10^{-4}$  cm nickel foil was placed in front of the counter surface to lower the alpha energy to a point intermediate to that of the deuterons and protons. Figure 22 demonstrates a typical pulse-height spectrum thus obtained.

#### b. Targets

The nitrogen targets used in this experiment were prepared by Hebbard (46). Titanium was evaporated onto a nickel backing, and the resultant layer was nitrided by induction heating to a red-heat for a short time in an atmosphere of dry ammonia. The resulting TiN compound has been found to be stable under bombardment. The ammonia for the  $N^{15}$  target was prepared from ammonium nitrate, supplied by the Eastman Kodak Company, with the ammonium radical enriched in  $N^{15}$  to 67%. The  $N^{14}$  target was prepared by the same procedure using natural ammonia.

The thickness of the TiN layer to 429 kev protons was originally measured by Hebbard by observing the yield of the 4.43 Mev gamma rays from  $N^{15} (p, \alpha \gamma) C^{12}$  near the 429 kev resonance for that reaction as a function of proton energy. The result was a 7 kev thickness for 429 kev protons. In the present experiment the thickness of each target spot used was calculated from the integrated alpha yield of  $N^{15} (p, \alpha) C^{12}$ , which measures the total number of  $N^{15}$  atoms in the target.

The known chemical composition of the target and the titanium and nitrogen stopping cross sections were then employed to calculate the thickness of the target, which agreed with Hebbard's value. The amount of  $N^{15}$  present was found to be  $1.9 \times 10^{17}$  atom  $cm^{-2}$  with variations of as much as 25% for various target spots. The amount of  $N^{14}$  in the  $N^{14}$  target surface layer was found to be  $2.0 \times 10^{17}$   $cm^{-2}$  by again using the  $N^{15}$  (p,  $\alpha$ )  $C^{12}$  yield and the natural composition of nitrogen. A belatedly discovered major difference in the two targets will be mentioned later.

### c. Calibrations and Errors

I had the advantage of performing this experiment at the conclusion of accurate Q-value measurements by Bardin et al. (44, 45), who devised a method for electrostatic analyzer alignment capable of reproducing the  $Li^7$  (p,n) threshold to better than one part in eight thousand. The analyzer has also been found to be linear over its range to better than 0.1%. At the beginning of each run the position of the 1210 kev resonance in  $N^{15}$  (p,  $\alpha$ )  $C^{12}$  was found to agree with Bardin's calibration to better than 0.1%. For these reasons the incident  $He^3$  energy was computed to be 2.763 Mev from the calibrations of Bardin et al. with a probable error of 0.1% or 3 kev.

The magnetic spectrometer is not so accurately reproducible because of a combination of hysteresis effects and jarring of the cone-bearing fluxmeter mounts as described by

Bardin (45). For this reason the spectrometer was calibrated against the incident particle energy at the beginning of each run. This calibration was made in several ways which all agreed for a given run: (a) the elastic scattering of  $\text{He}^3$  from a nickel blank, (b) the energy of the alphas from  $\text{N}^{15} (p, \alpha) \text{C}^{12}$  at the 1210 kev resonance, and (c) the energy of the protons to the 3.945 level in  $\text{N}^{14}$  from  $\text{C}^{12} (\text{He}^3, p) \text{N}^{14}$ . This last reaction was found to be the most satisfactory for the following reasons: (a)  $\text{C}^{12}$  was always present as a thin layer on the front surface of the target and as such needed no surface layer correction; (b) the protons possessed energies at both  $90^\circ$  and  $150^\circ$  that placed them in the middle of the spectrometer energy range under investigation; and (c) the Q-value of  $834 \pm 4$  kev measured in the course of the experiment for this reaction agrees exactly with the latest tabulation of Ajzenberg-Selove and Lauritsen (47), the probable error not contributing appreciably to the final probable error of the experiment. This Q-value was calculated using the calibration of the spectrometer based on a clean elastic scattering profile from a nickel blank.

It is appropriate at this point to stress the advantages of calibrating  $E_2$  against  $E_1$  as done in this experiment. The present case will serve as a fine example. Suppose that a known Q-value such as  $\text{C}^{12} (\text{He}^3, p)$  is used to calibrate the spectrometer against an incident energy  $E_1$ . If the incident energy were actually in error by an amount  $\Delta E_1$ , then  $E_2$  would

be in error by an amount  $\Delta E_2 = \left(\frac{\delta E_2}{\delta E_1}\right)_c \Delta E_1$ . If the Q-value of a second reaction is now measured at the same  $E_1$  and very near the same  $E_2$ , that Q-value will be in error by an amount

$$\Delta Q = \left(\frac{\delta Q}{\delta E_1}\right) \Delta E_1 + \left(\frac{\delta Q}{\delta E_2}\right) \Delta E_2 = \left[ \left(\frac{\delta Q}{\delta E_1}\right) + \left(\frac{\delta Q}{\delta E_2}\right) \left(\frac{\delta E_2}{\delta E_1}\right)_c \right] \Delta E_1 .$$

Consider a numerical example at  $90^\circ$ . For  $C^{12} (He^3, p)$  the quantity  $(\delta E_2/\delta E_1)_c = 0.73$ . For the reaction being studied,  $N^{15} (He^3, \alpha)$ , the quantities  $\delta Q/\delta E_1$  and  $\delta Q/\delta E_2$  are respectively  $-0.78$  and  $1.28$ . By inserting these values, one finds

$$\Delta Q = [-.78 + 1.28 (.73)] \Delta E_1 = .15 \Delta E_1 .$$

The above equation means that an estimated error of 3 kev in  $E_1$  is almost completely compensated by the calibration procedure. An exactly analogous argument applies to small uncertainties in the spectrometer angle and will not be explicitly presented here. If these were the only sources of error, the uncertainty in the measured Q-value would roughly equal the uncertainty of the Q-value against which the calibration was made.

The major uncertainty in the Q-values of this experiment comes from a different source. For the  $(He^3, \alpha)$  reactions on nitrogen, the incident particle energy must be reduced by the energy thickness of the surface carbon layer plus one-half the energy thickness of the TiN layer for the incident particle  $M_1$  of energy  $E_1$ , and the observed  $E_2$  must be increased by the

analogous quantity for particle  $M_2$  and energy  $E_2$ . The lion's share of this uncertainty comes from the surface carbon layer. Using the integrated yield of  $C^{12} (He^3, p)$  and the  $90^\circ$  differential cross section of 0.8 mb/ster. given by Bromley et al. (48) the amount of carbon on the surface was found to be commonly as high as  $8 \times 10^{17}$  atom  $cm^{-2}$ . This value changed from spot to spot and also changed continuously with running time. This amount of carbon corresponds to a 16 kev thickness for 2.8 Mev  $He^{3++}$  ions. By monitoring this yield, the author feels that he has known the thickness of the carbon surface layer to an accuracy of  $\pm 3$  kev at all times. The amount of carbon on the  $N^{14}$  target was found to be about four-tenths as much as that on the  $N^{15}$  target. This fact is no doubt a result of the much greater accumulated bombardment time to which the  $N^{15}$  target has been exposed in its history. This uncertainty in carbon thickness causes an uncertainty in  $Q$  of

$$\Delta Q = \left(\frac{\partial Q}{\partial E_1}\right) \Delta E_1 + \left(\frac{\partial Q}{\partial E_2}\right) \Delta E_2 = \pm 6 \text{ kev} .$$

By making a Gaussian fold of this uncertainty with the additional ones of calibration and target half-thickness, the author assigns a probable error of  $\pm 8$  kev to the  $(He^3, \alpha)$   $Q$ -value measurements.

### 3. Results

The yield of alpha particles as a function of their energy was measured at the laboratory angles of  $150^\circ$  and  $90^\circ$

for an incident  $\text{He}^3$  energy of 2.76 Mev. The energy range of the alphas measured in this experiment was selected at both angles to cover the range of 7 to 8 Mev excitation for the residual  $\text{N}^{14}$  nucleus in the reaction  $\text{N}^{15} (\text{He}^3, \alpha) \text{N}^{14}$ . Since the  $\text{N}^{15}$  target contained 33%  $\text{N}^{14}$  atoms, the yields were repeated with the natural nitrogen target to obtain clear evidence for that portion of the yield coming from  $\text{N}^{14} (\text{He}^3, \alpha) \text{N}^{13}$ . Measurements were taken at the two indicated angles to allow for more positive identification of the reactions involved and also to allow for the possibility that a given alpha group could have a very small yield at one of the two angles. Measurements were not taken at forward angles for several reasons: (a) for the higher energies at forward angles the resolution of the reaction groups decreases due to the decreased dispersion of particle energies versus spectrometer setting, i.e.,  $\delta E_2 / \delta V_m$  increases; (b) important parts of the reaction spectrum would be obscured by the presence of the very strong reaction  $\text{Cl}^{12} (\text{He}^3, \alpha) \text{Cl}^{11}$ ; and (c) energy loss corrections in the target and surface layers would become more uncertain due to the necessarily large angle between the reaction products and the normal to the target.

The momentum resolution of the magnetic spectrometer used in the experiment was  $p/\delta p = 231$ , which corresponded to a 1/4 inch exit slit on the spectrometer. Greater resolutions could be obtained only with a corresponding loss in transmission which would have been undesirable in the face of the

low yields. The corresponding energy resolution  $E_2/\delta E_2 = 115$  was, at any rate, smaller than the total thickness of the target layer and hence did not contribute to the total width of observed groups.

The resulting yields are plotted in figures 23-26. All the alpha yields are normalized to a 500  $\mu\text{c}$  bombardment of the target with  $\text{He}^{3+}$  ions, although in many cases as much as 2000  $\mu\text{c}$  of bombardment were employed to obtain satisfactory statistics. The yields are plotted against the voltage in millivolts developed across a precision resistor by the current passing through the fluxmeter coil. This voltage,  $V_m$ , is inversely proportional to the particle momentum. The yields are shown with statistics bars which represent  $\pm\sqrt{n}$  statistics on the total yield at each spectrometer setting.

The yield curves are marked with arrows showing the expected position of alpha groups to the excited state of the final nucleus indicated. Thus an arrow with the notation  $\text{N}^{14} (7.97)$  indicates the expected energy of alpha particles from the reaction  $\text{N}^{15} (\text{He}^3, \alpha) \text{N}^{14*}$  leaving  $\text{N}^{14}$  with 7.97 Mev excitation. Arrows are also placed to indicate where alpha groups corresponding to  $\text{N}^{14}$  excitations of 7.40 and 7.60 Mev would appear. The numbers on the arrows indicating the states  $\text{N}^{14} (7.03)$ ,  $\text{N}^{13} (7.17)$ , and  $\text{N}^{13} (7.39)$  are the actual Q-values calculated from these data. The error is  $\pm 0.008$ .

An anomaly with regard to the natural nitrogen target is immediately evident. A broad peak appears after the low

energy end of the  $N^{13}$  (7.39) alpha group. That this peak does not occur with the 67%  $N^{15}$  target immediately rules out  $N^{14}$  as its source. After many unsuccessful attempts to find a suitable contaminant in the  $N^{14}$  target to account for this peak, I returned to an examination of the nitrogen distribution in the two targets. The density of nitrogen as a function of target depth was measured by observing the low energy end of the alpha spectrum from  $N^{15}$  (p,  $\alpha$ )  $C^{12}$  with the proton energy set on the broad resonance at 1030 kev. The results as shown in figure 27 indicate clearly that the nitrogen density in the  $N^{14}$  target is not a singly-peaked function of target depth. The repeated heatings in the nitriding process apparently allowed a layer of TiN to diffuse into the nickel backing in such a way that the nitrogen density did not drop off monotonically with target depth. The comparative yields of figure 27 are normalized in such a way that the integrated area under the two curves would be equal for equal numbers of nitrogen atoms in the two targets. It can be seen that there is actually more nitrogen in the  $N^{14}$  target than in the 67%  $N^{15}$  target, although the main peak of the  $N^{14}$  target contains only two-thirds as much as does the  $N^{15}$  target. Numerically, the  $N^{15}$  target composition is  $1.9 \times 10^{17} N^{15} \text{ cm}^{-2}$  /  $.95 \times 10^{17} N^{14} \text{ cm}^{-2}$ , and the  $N^{14}$  main peak contains  $2.0 \times 10^{17} N^{14} \text{ cm}^{-2}$ . The evaluation of alpha energy of figure 27 in terms of target stopping power allows an unfolding of the  $N^{14}$  target yields into that from the main peak alone.

The results of this unfolding are shown in figures 28 and 29. The errors in this procedure are rather large, as indicated, but there is little doubt that the origin of this shadow peak is well accounted for by this procedure. It should be noted that the shadow of the  $N^{13}$  (7.17) alpha group falls under the main peak of the  $N^{13}$  (7.39) alpha group. This unfortunate distortion of the 7.39 group is much more in evidence at  $150^\circ$  than at  $90^\circ$  where the cross section to the  $N^{13}$  (7.39) state is much larger. It should also be noted that the yield from the  $N^{15}$  target to the  $N^{14}$  (7.03) state is superimposed upon the yield to the  $N^{13}$  (7.17) state from the 33%  $N^{14}$  in the  $N^{15}$  target.

There is a rather sizable continuum of alpha particle energies upon which the discrete groups are superimposed. This fact may be largely due to the reaction  $N^{14}(\text{He}^3, p)O^{16}$  with a  $Q_m = 15.2$  Mev which can populate a large number of alpha unstable states in  $O^{16}$ . The fact that the continuum from the  $N^{14}$  target is about twice as large as that from the  $N^{15}$  target would seem to substantiate this supposition. Alpha unstable states in  $O^{17}$  are also populated by the reaction  $N^{15}(\text{He}^3, p)O^{17}$ , but these states probably decay primarily by neutron rather than alpha emission.

Q-values were not computed for the alpha particles populating the  $N^{14}$  (7.97) and  $N^{14}$  (8.08) states because of poor counting statistics due to their partial overlap. The crucial point with regard to this experiment is that they are in fact

populated as suspected. Some amplification of the  $90^\circ$  yields from the  $N^{15}$  target in this regard will be illuminating. Consider first the yield from the reaction  $C^{12} (He^3, \alpha) C^{11}$  shown at  $V_m = .375$  in figure 23. The observed width at half maximum of this yield is determined by the largest of the following emergent energy spreads:\* (a) the energy resolution window of the spectrometer, (b) the total energy thickness of the target layer, and (c) the energy spread due to the finite acceptance angle of the spectrometer. Of these the last is considerably the greatest for this reaction as  $\delta E_2 / \delta \theta$  is very large for  $(He^3, \alpha)$  reactions observed at  $90^\circ$  on light nuclei. The expected spread in fluxmeter voltages will be given by

$$\Delta V_m = \left( \frac{\delta V_m}{\delta E_2} \cdot \frac{\delta E_2}{\delta \theta} \right) \Delta \theta_{spec.} = .0055 \text{ mv,}$$

which can be seen to agree exactly with the observed width. Since the total width of the 7.97 Mev level is less than 400 ev (34), the same argument may be applied to the yields to that state, giving  $\Delta V_m = .0044$  for the expected half-width. Since the observed yield reaches half-maximum near  $V_m = .3606$ , it should have fallen again to one-half near  $V_m = .3650$ . The additional fact that the alphas from  $C^{12} (He^3, \alpha) C^{11}$  have fallen to near zero for  $V_m = .370$  implies that the flat plateau in the yield from  $.364 \leq V_m \leq .370$  is caused from an alpha group near  $V_m = .368$ . The final state being populated is surely

---

\*The total laboratory width of the final state is not considered because the ground state of  $C^{11}$  is narrow.

$N^{14}$  (8.06), and the yield is roughly equal to that to the  $N^{14}$  (7.97) level. At  $150^\circ$  these two groups are clearly resolved.

The  $150^\circ$  yield to the 8.06 state of  $N^{14}$  shows a rather marked peculiarity, namely its great width. The admittedly poor statistics nonetheless indicate a width for the 8.06 state of  $\Gamma = 70 \pm 15$  kev which is at least twice as great as the laboratory proton width measured by Hebbard and Vogl (34). No explanation of this anomaly can be presented at this time. Repeated surveys of this region gave no variations from this behavior. The only other state with an observed width greater than the resolution width is the state at 7.39 Mev in  $N^{13}$  which shows  $\Gamma = 50 \pm 10$  kev.

The differential cross section for the reaction to the observed states can be estimated from the thin-target expression for integrated yields found in Brown et al. (49):

$$\frac{d\sigma}{d\Omega} = \frac{1}{n_1 n_0} \frac{R}{\Omega} \int \frac{Y(I)dI}{I}$$

where  $R$  and  $\Omega$  are the momentum resolution and solid angle of the spectrometer. Considerable uncertainty must be assigned to the cross-section estimates. This uncertainty results from target thickness variations and the difficulty in measuring the integrated yield in the face of the several subtractions performed. Table VI shows the results of these estimates.

TABLE VI

<u>Final Nucleus</u>	<u><math>E_x</math> in Final Nucleus (Mev)</u>	<u><math>(\frac{d\sigma}{d\Omega}) \mu\text{b/ster.}</math></u>	
		<u>90°</u>	<u>150°</u>
N <sup>14</sup>	8.06	45 ± 20	54 ± 20
N <sup>14</sup>	7.97	45 ± 20	21 ± 10
N <sup>14</sup>	7.034 ± .008	135 ± 40	77 ± 25
N <sup>13</sup>	7.388 ± .008	320 ± 60	70 ± 25
N <sup>13</sup>	7.166 ± .008	115 ± 30	110 ± 30

The bottom three excitation values are the averages of the measurements taken in the course of this experiment. What is actually measured is, of course, a Q-value; therefore, it should be noted for clarity that these excitations are based on the following mass Q-values: (a)  $Q_m = 9.743$  for the reaction  $N^{15} (\text{He}^3, \alpha) N^{14}$ , (b)  $Q_m = 10.024$  for the reaction  $N^{14} (\text{He}^3, \alpha) N^{13}$ . The mass Q-values are determined from the 1960 mass tables (40).

Finally it may be mentioned for completeness that alpha groups from  $N^{15} (\text{He}^3, \alpha) N^{14}$  were also observed in a quick preliminary survey to states in  $N^{14}$  with excitations of 6.23, 5.83, 5.69, and 5.10 Mev. These were the only alpha groups specifically looked for, but it seems likely that groups to the other well-known states would also be observable. Deuterons to the first four excited states of  $O^{16}$  from the reaction  $N^{15} (\text{He}^3, d) O^{16}$  were also evident.

#### 4. Comparison of $N^{13}$ and $C^{13}$ Energy Level Diagrams

Data on the  $N^{14}(\text{He}^3, \alpha)N^{13}$  reaction were taken with the natural nitrogen target primarily to determine which of the reaction groups seen from the 67%  $N^{15}$  target should be ascribed to the  $N^{14}$  target nucleus. Some clarification of uncertain  $N^{13}$  energy levels has resulted. A schematic comparison of  $N^{13}$  with its mirror nucleus,  $C^{13}$ , is given in figure 30. The data for this figure were taken from the energy level tabulations of Ajzenberg-Selove and Lauritsen (50). The first three excited states of  $N^{13}$  certainly correspond to the first three in  $C^{13}$ . It seems likely that the state at 6.38 Mev in  $N^{13}$  has as its mirror the 6.87 Mev level in  $C^{13}$ . Both states have  $J^\pi = 5/2^+$ , and they are the first states to appear above 5 Mev excitation in resonances of  $C^{12}$  plus a nucleon, possessing roughly equal reduced nucleon widths. The large reduced nucleon widths for the broad  $3/2^+$  levels at 8.08\* and 8.33 Mev in  $N^{13}$  and  $C^{13}$  respectively make a tentative matching of these states plausible. Charged particle reaction groups have indicated the existence in  $C^{13}$  of three levels in the region between 6.86 and 8.33 (at 7.47, 7.53, and 7.64). The corresponding region in  $N^{13}$  has been inconvenient to the common charged particle reactions, resonances in  $C^{12} + p$  accounting for almost the entirety of the known data. Resonances

---

\*Note that the  $N^{13}$  (8.08) level was not discernible in the present experiment.

at  $N^{13}$  excitations of 6.91 and 7.39 Mev have been long known, but a probable resonance at 7.19 Mev excitation has been only recently reported (51). In light of the fact that this last weak resonance has been missed by several observers, the confirmation of a state at 7.17 Mev excitation in the present experiment is important. The number of known excited states in this energy region of  $N^{13}$  and  $C^{13}$  is now equal, although further pairing of mirror states will not be attempted here.

### 5. Discussion

It was anticipated that the reaction  $N^{15} (\text{He}^3, \alpha) N^{14}$  would be capable of populating most if not all of the levels in  $N^{14}$  below about 9 Mev excitation. This hope was confirmed by the fact that seven well-substantiated states looked for between 5 and 8.1 Mev were all clearly visible. In particular, the excitation range 7-8.1 Mev in  $N^{14}$  was closely examined in an effort to discover the excitation of possible states lying between the known levels at 7.03 and 7.97 Mev. No evidence for such a state was found. This negative result intensifies the doubt expressed earlier with regard to the inconclusive evidence of other investigators. It is always difficult to make positive statements from a negative experiment. An upper limit of  $5 \mu\text{b/steradian}$  for the differential cross section of the reaction  $N^{15} (\text{He}^3, \alpha) N^{14}$  to any unobserved level in this range may be quoted. This upper limit is about 10% of the observed group yields. One possible yield of such a

magnitude may be pointed out at  $V_m = .414$  in figure 24. This one has been ignored due to a lack of corroborating evidence at  $90^\circ$ . It should be pointed out that the resolution employed in this experiment demands that any real particle group show a relative yield increase for at least three consecutive spectrometer settings. The experiment could have been improved somewhat by longer bombardments to improve the statistics. It would have been difficult to push the limit of observability below  $5 \mu\text{b/steradian}$ , however, since the corresponding yield is only about 20% of the continuum background of alphas.

It should be mentioned that time limitations prohibited an auxiliary investigation of the possibility of strong resonant enhancement of the observed yields through possible states in the compound  $F^{18}$  nucleus. Observing the yields of known particle groups as a function of bombarding energy could have provided this information. If the particle yields were found to be strongly dependent on the incident energy, the possibility of having overlooked states by using only one bombarding energy\* would be greater.

The question of whether this reaction proceeds strongly through compound nucleus formation is not a matter of idle curiosity. By so doing, it could populate two-particle excitation states in  $N^{14}$ . The single-particle excitation operators

---

\*The thickness of the TiN target layer gives the incident  $He^3$  beam an energy spread of about 20 kev.

believed to be dominant for inelastic scattering processes and the possible dominance of the stripping mechanism for (d,n) reactions would lead one to expect that the three reactions  $N^{14}(\alpha, \alpha')N^{14*}$ ,  $N^{14}(p, p')N^{14*}$ , and  $C^{13}(d, n)N^{14*}$  will populate preferentially single-particle excited states of  $N^{14}$ . The  $N^{14}$  states at 7.03, 7.97, and 8.06 are all largely single-particle excited states, belonging to the configurations  $s_{4p}^{10}$ ,  $s_{4p}^9d$ , and  $s_{4p}^9(2s)$  respectively. That these states are the ones well agreed upon by these reactions is therefore not surprising. The state at 6.44 Mev excitation is very strongly populated in both inelastic scatterings and is probably also a member of  $s_{4p}^9d$  (contingent upon  $J^\pi = 3^-$ ). On the other hand, the fact that the 6.23 Mev level is populated only weakly by (p, p') and not at all by ( $\alpha, \alpha'$ ) agrees with the configuration  $s_{4p}^8d(2s)$  given to it by Warburton and Pinkston (41) on the basis of gamma ray transition strengths.

These considerations place further doubt on the  $N^{14}$  level at 7.60 Mev reported by Burge and Prowse (37). The intensity of this inelastic proton group is at least twice as strong as is that from the 7.03 Mev state, implying that the 7.60 Mev state should also be a single-particle excitation. That such a state does not appear at all in inelastic alpha scattering could only be easily explained by a  $T = 1$  assignment. But the lack of any state in  $C^{14}$  below 6 Mev excitation is strong

evidence for the lack of  $T = 1$  states in  $N^{14}$  below 8 Mev\* (with the exception of the 2.31 Mev state in  $N^{14}$  which is the  $C^{14}$  ground state).

It seems more likely that the lack of any other visible states in the 7-8 Mev range for  $N^{14}$  from inelastic alpha scattering indicates the lack of any other single-particle excited states in this range. Warburton and Pinkston (41) point out the possibility of positive parity states in this excitation range belonging to  $s^4p^8$  (d,s). Such a state, although it would certainly possess a proton width much smaller than the single-particle limit, could still provide an effective resonance in  $C^{13} (p, \gamma) N^{14}$  at stellar energies.

The reaction  $N^{15} (He^3, \alpha) N^{14*}$  can populate two-particle excited states if it proceeds by compound nucleus formation. It has already been pointed out that the 7.03 Mev level is the only one that can be populated by neutron pick-up. The yields to the other excited states in  $N^{14}$  from this reaction would therefore be substantial evidence of the operation of the compound nucleus mechanism. The negative result from this reaction for states in the 7.03 to 7.97 Mev range of excitation has, therefore, a stronger meaning than the negative  $(\alpha, \alpha')$  results.

---

\*The 6.09 Mev state in  $C^{14}$  is believed to be the analog of the 8.06 Mev level in  $N^{14}$ .

It may be stated in conclusion that a possible resonance in  $C^{13} (p, \gamma) N^{14}$  at stellar energies is quite unlikely. This result means that the current calculations on the  $C^{12}/C^{13}$  abundance ratio produced in the CNO-cycle are correct.

Figure 21: Evidence for possible resonances in  $C^{13} \not\leftarrow p$  at stellar energies is shown with the energy level diagram of  $N^{14}$ . Nuclear reactions providing evidence for states in  $N^{14}$  in the 6-8 Mev range of excitation are indicated. The pertinent reactions are  $N^{14}(\alpha, \alpha')N^{14*}$ ,  $N^{14}(p, p')N^{14*}$ ,  $C^{13}(d, n)N^{14*}$ ,  $C^{13}(p, \gamma)N^{14}$ , and the present experiment,  $N^{15}(He3, \alpha)N^{14*}$ . The effective stellar energy range for  $C^{13} \not\leftarrow p$  is shown by a horizontal band.

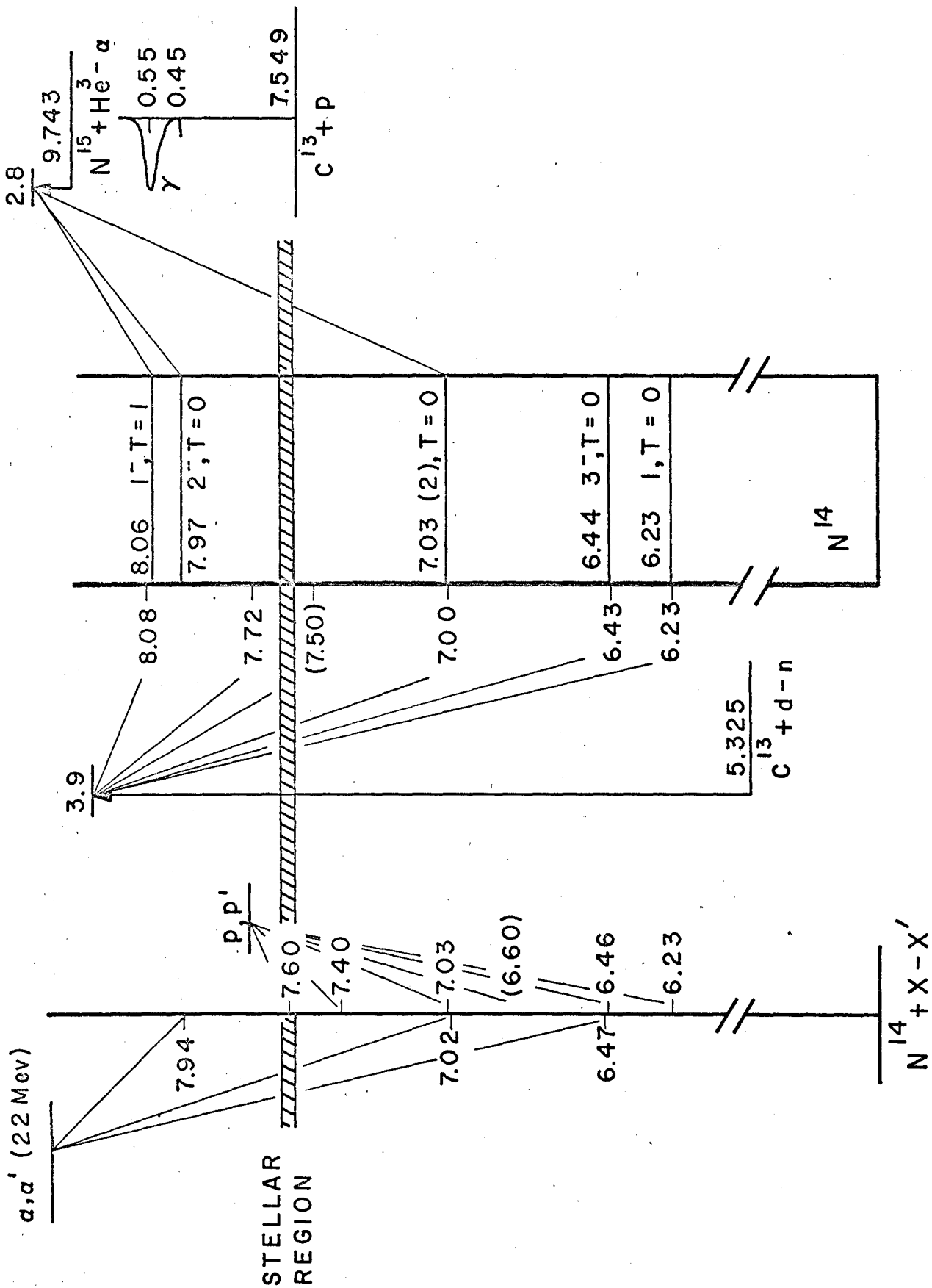


Figure 22: A typical pulse-height spectrum of the reaction products from the bombardment of the TiN target with 500  $\mu$ coul. of He<sup>3</sup> ions. After momentum analysis the particles pass through a 10<sup>-4</sup> cm. Nickel foil before detection in the solid-state particle counter. The proton energy is 3.3 Mev. The signal from the counter was stored in a 100-channel pulse-height analyzer after conventional amplification.

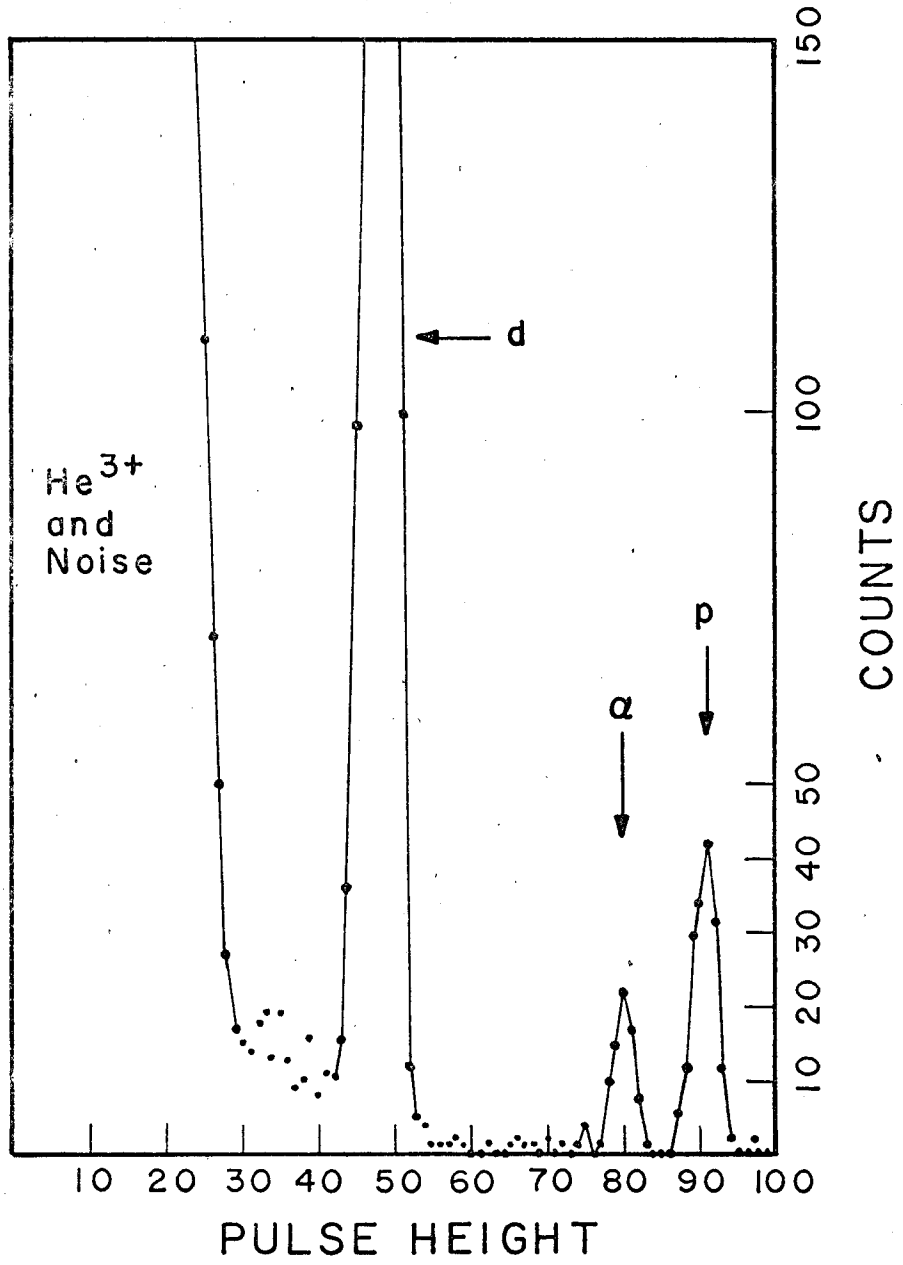


Figure 23: The yield of alpha particles from the  $\text{He}^3$  bombardment of TiN enriched to 67% in  $\text{N}^{15}$  at a laboratory angle of  $90^\circ$  versus the magnetic spectrometer setting. The yields are normalized to a  $500 \mu\text{c}$  bombardment of  $\text{He}^{3+}$  ions and are displayed with bars corresponding to  $\pm\sqrt{n}$  counting statistics. Alpha particle energies corresponding to specific excitations of the residual nucleus are indicated by arrows.

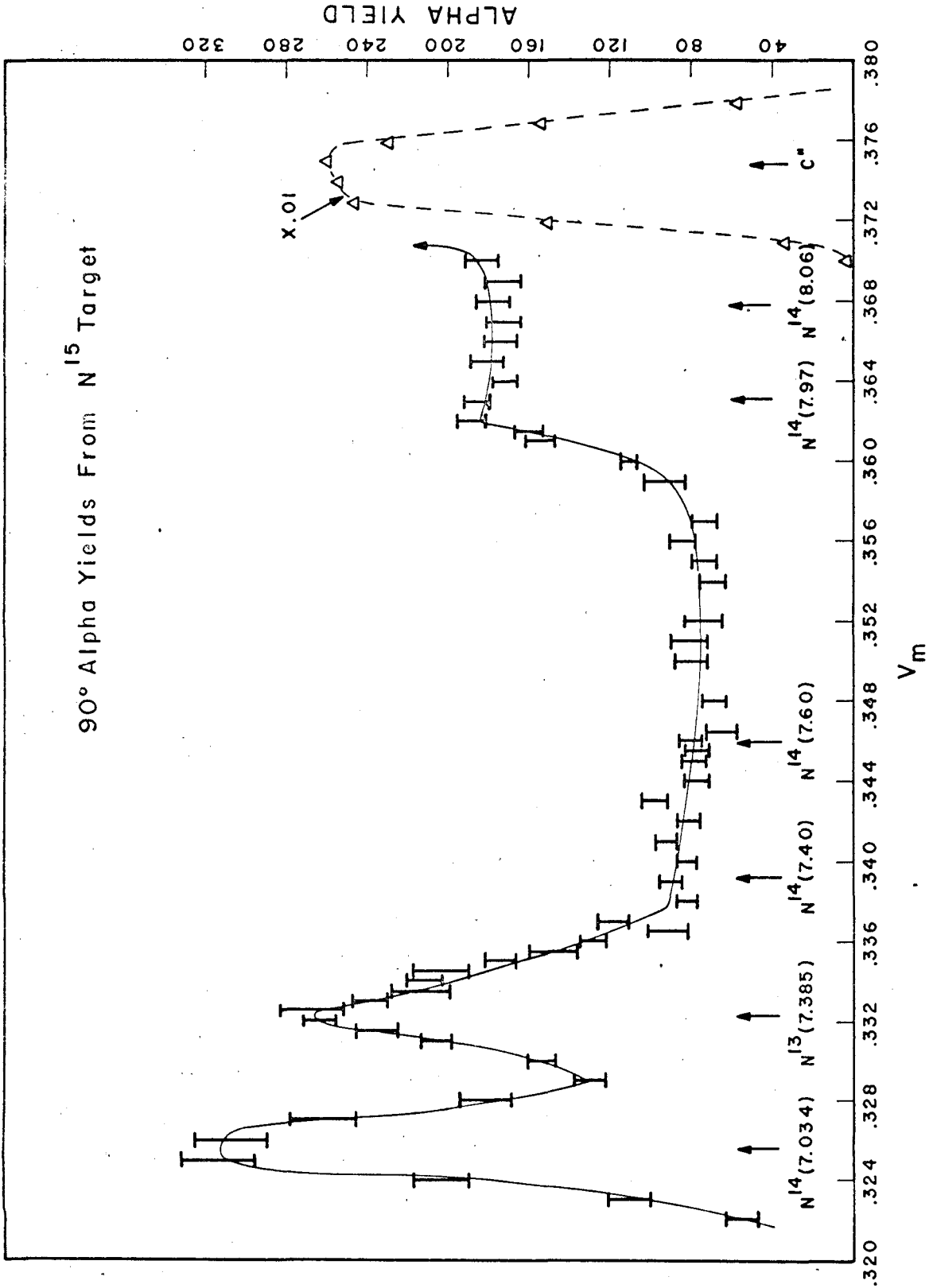


Figure 24: The yield of alpha particles from the  $\text{He}^3$  bombardment of TiN enriched to 67% in  $\text{N}^{15}$  at a laboratory angle of  $150^\circ$ .

150° Alpha Yields From N<sup>15</sup> Target

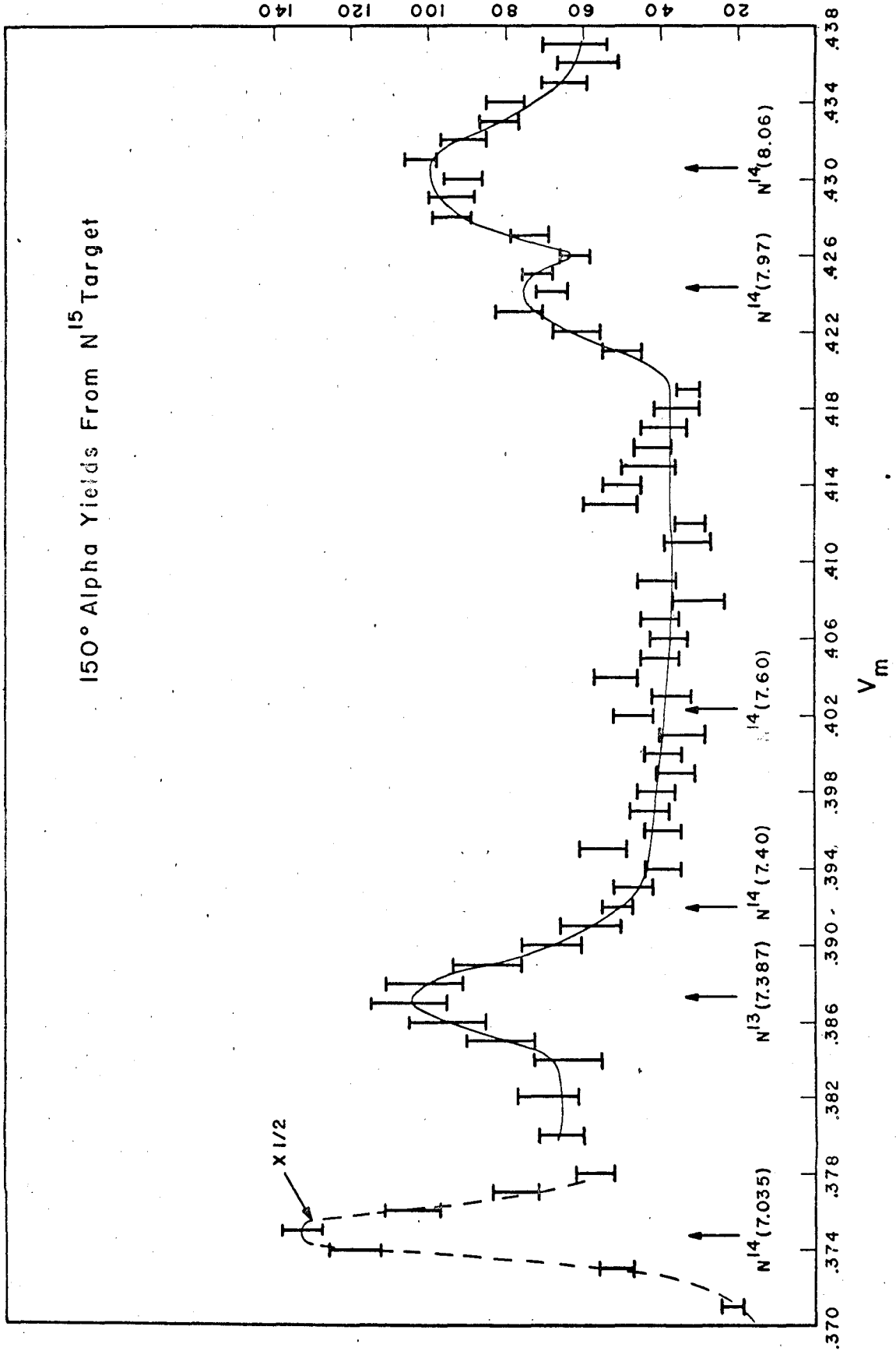


Figure 25: The yield of alpha particles from a 500  $\mu$ c bombardment of the natural TiN target at a laboratory angle of 90°.

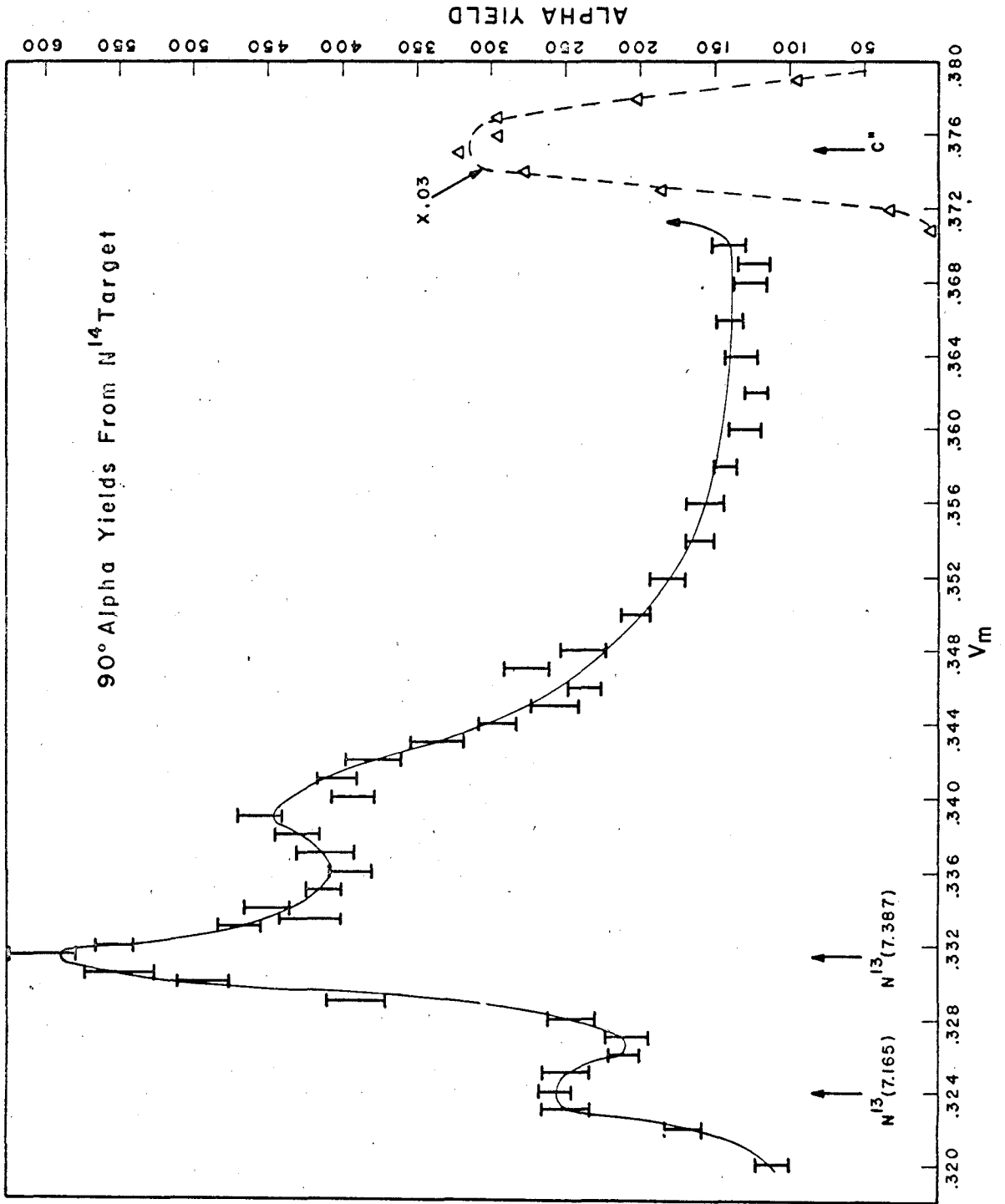


Figure 26: The yield of alpha particles from a 500  $\mu\text{c}$  bombardment of the natural TiN target at a laboratory angle of  $150^\circ$ .

ALPHA YIELD

150° Alpha Yields From N<sup>14</sup> Target

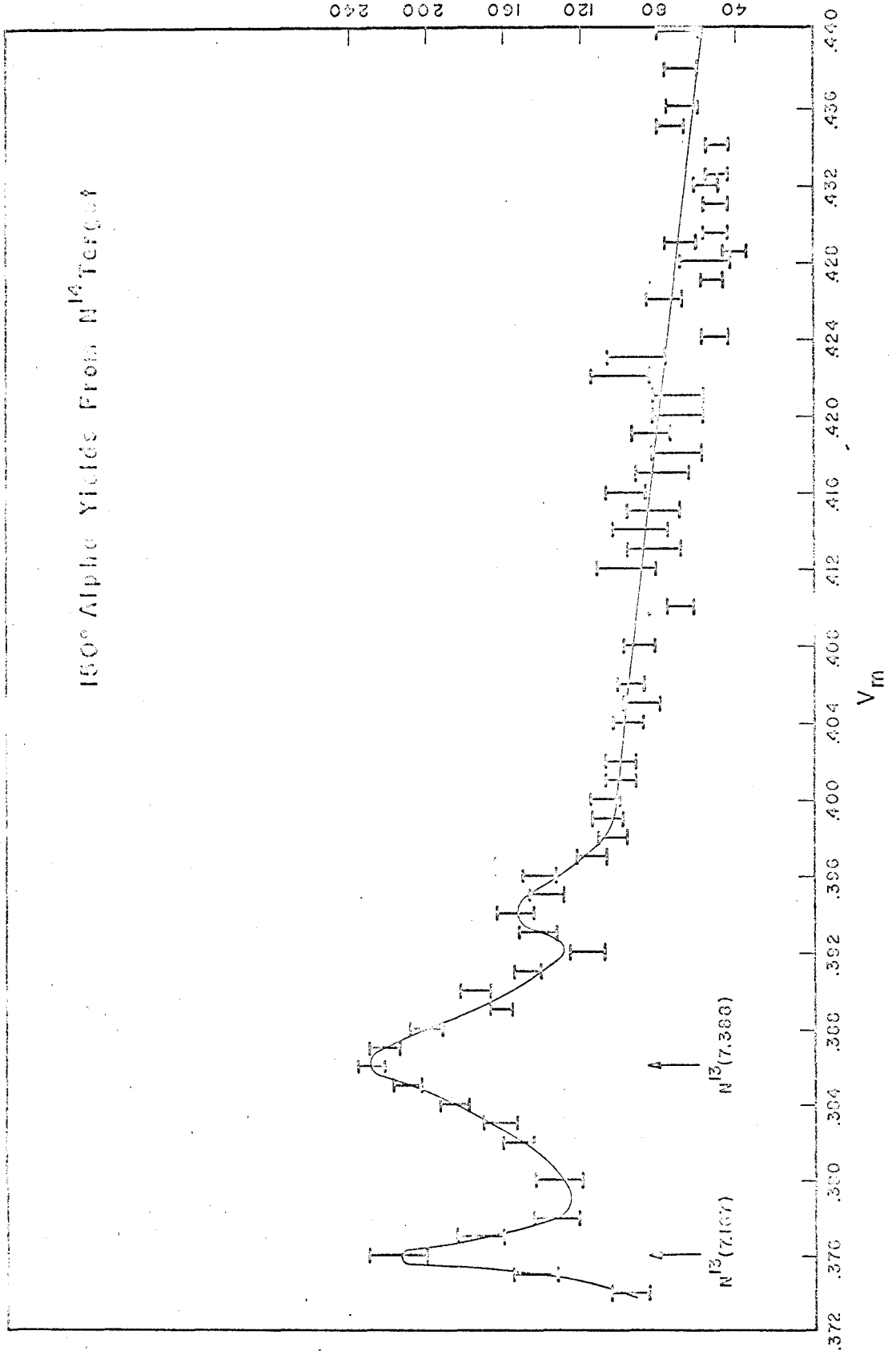


Figure 27: The yield of alpha particles at  $150^\circ$  from the reaction  $N^{15}(p,\alpha)C^{12}$  as a function of magnetic spectrometer setting. The incident proton energy is held on the broad resonance at 1030 kev, whereas the alpha energy decreases toward the right. The triangles represent yields from the 67%  $N^{15}$ -enriched TiN target, whereas the bars represent yields from the natural TiN target with  $\pm\sqrt{n}$  statistics. The two curves are normalized in such a way that the integrated area under them would have been equal for equal numbers of nitrogen atoms in the two targets. The second peak in yield from the natural target arises from a concentration of nitrogen atoms at a target depth calculable from the energy shift of the alpha particles.

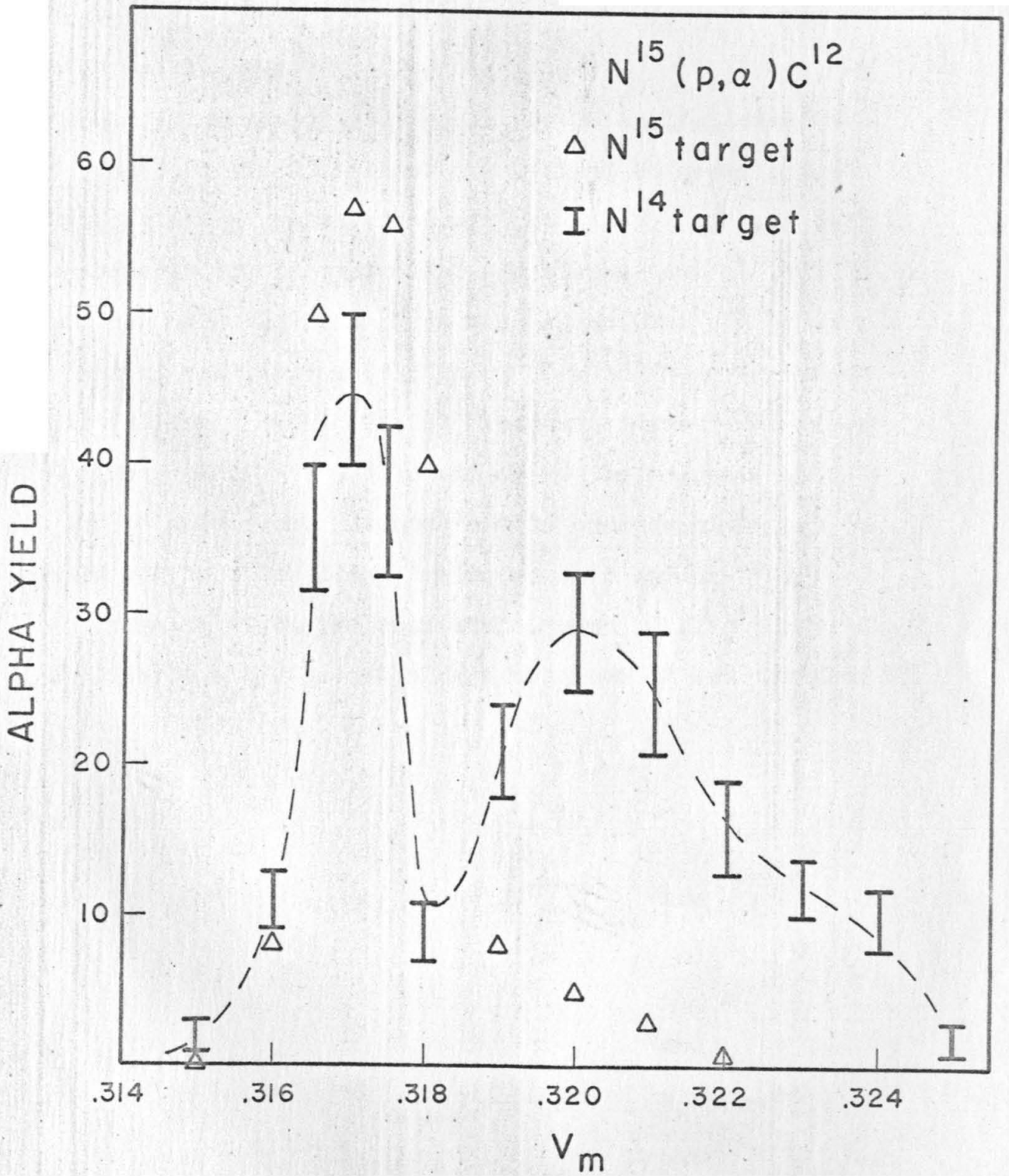


Figure 28: The corrected yield of alpha particles at  $150^\circ$  from the  $\text{He}^3$  bombardment of the natural nitrogen target. The correction was made by subtracting the contributions of the second broad peak in nitrogen density (revealed in fig. 27) from the total yield of fig. 26. The effects of this subtraction on the yields of fig. 26 are largely the following: a) the disappearance of the extraneous peak at  $V_m = .394$ , which was the shadow of the  $\text{N}^{13}(7.39)$  group; b) a reduction in the yield attributable to the  $\text{N}^{13}(7.39)$  group resulting from the subtraction of the shadow of the  $\text{N}^{13}(7.17)$  group; c) the disappearance of the peculiar broadening of the  $\text{N}^{13}(7.39)$  group; d) an apparent small shift of the energy of the  $\text{N}^{13}(7.39)$  group. This last effect is somewhat doubtful due to the poor statistics of the subtraction.

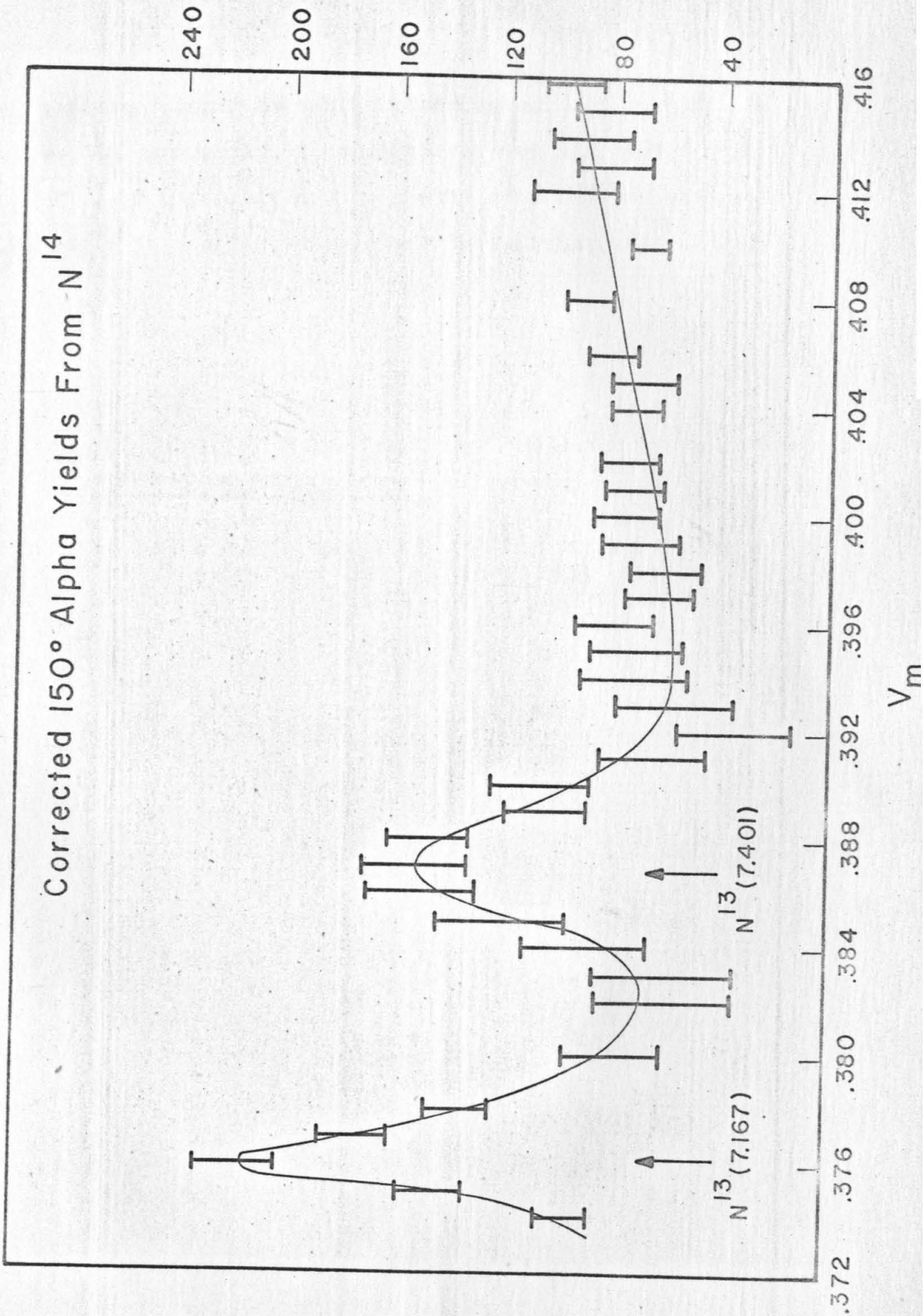


Figure 29: The corrected yield of alpha particles at  $90^\circ$  from the  $\text{He}^3$  bombardment of the natural nitrogen target. The main effect on the yields of fig. 25 is the disappearance of the extraneous peak at  $V_m = .339$ .

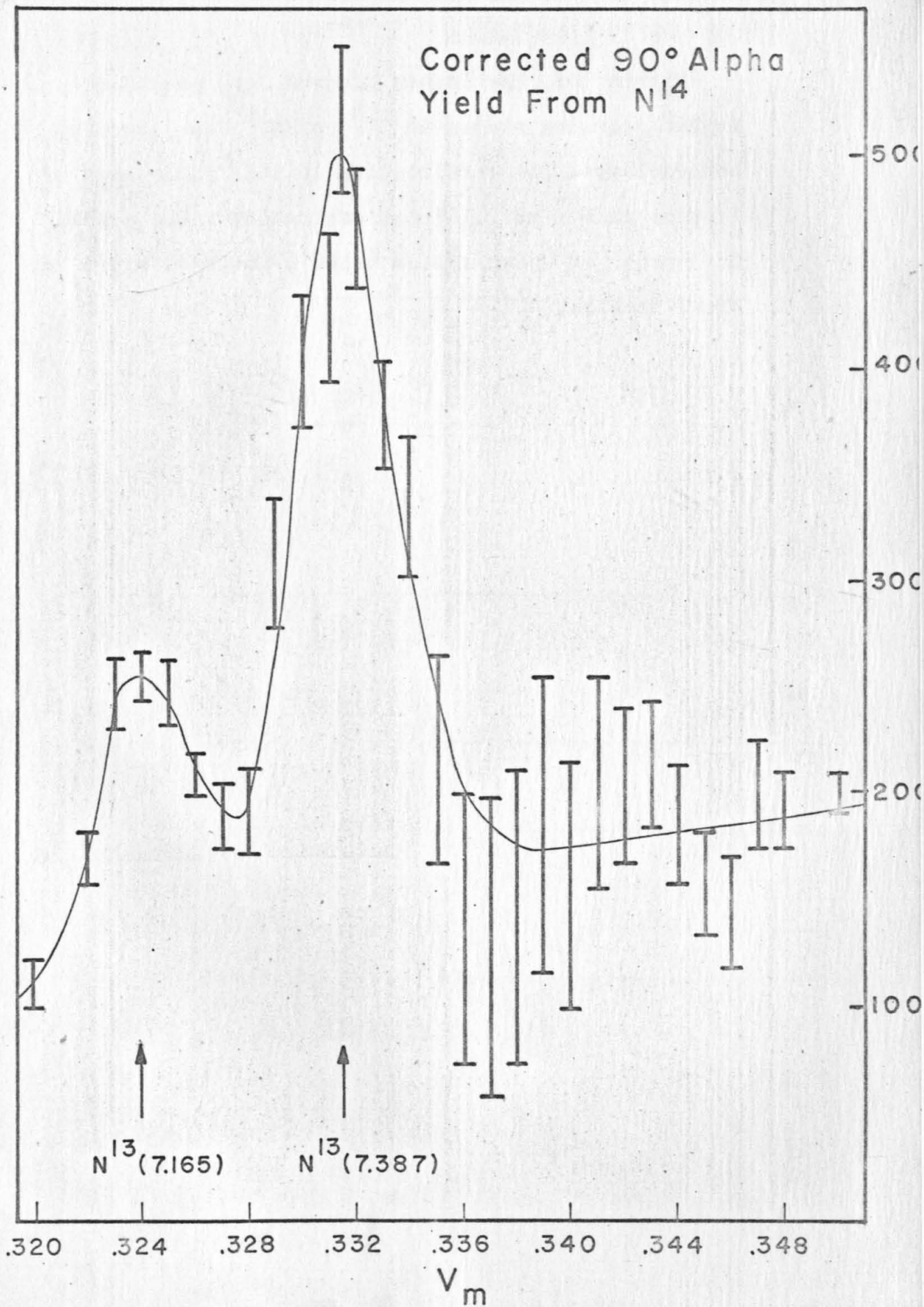
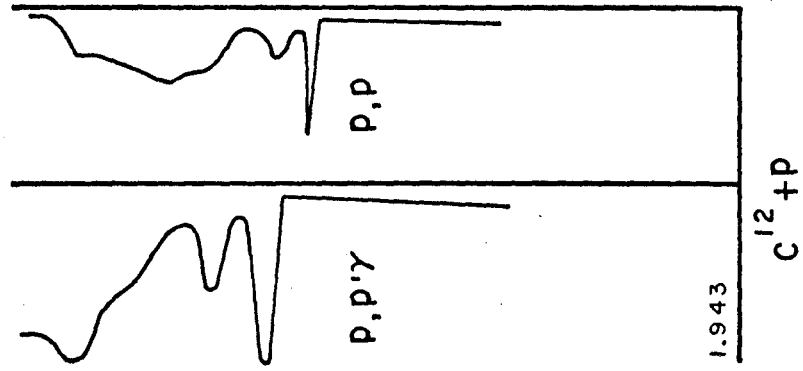
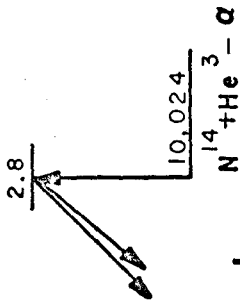
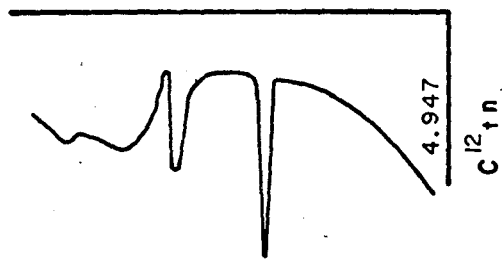


Figure 30: The isobar diagram for mass thirteen. Probable analog states in  $C^{13}$  and  $N^{13}$  are joined by dashed lines. The confirmation in this experiment of a state in  $N^{13}$  at 7.167 Mev excitation makes equal the number of known states below 8 Mev excitation in these isobars.



8.85	8.90		
8.33 3/2+	8.08 (3/2+)		
7.68 3/2+	7.39 (5/2+)		
7.50	7.17		
6.87 5/2+	6.91 3/2+		
6.10	6.38 5/2+		
5.51			
3.85 5/2+	3.56 5/2+		
3.68 3/2-	3.51 3/2-		
3.09 1/2+	2.37 1/2+		
$C^{13}$ 1/2-	$N^{13}$ 1/2-		



REFERENCES

- 1 - 28. These references are contained in the bibliography to Section I.A. of this thesis, which is a reprint of the article "Neutron Capture Chains in Heavy Element Synthesis" by D.D. Clayton, W.A. Fowler, T.E. Hull, and B.A. Zimmerman. *Annals of Physics* 12, 331 (1961).
29. L. Goldberg, E.A. Muller, and L.H. Aller, *Astrophys. J., Suppl.* 5, No. 45 (1960).
30. W.D. Ehmann, *J. Chem. Education* 38, 53 (1961). A bibliography of references to experimental determinations is included in this article.
31. W.A. Fowler, J.L. Greenstein, and F. Hoyle, *Am. J. Phys.* 29, 000 (1961).
32. S.R. Taylor, *Geochim. et Cosmochim. Acta* 19, 100 (1960).
33. A. McKellar, *Stellar Atmospheres* (Univ. of Chicago Press, Chicago); edited by J.L. Greenstein. See Chap. 16, "Isotopes in Stellar Atmospheres". References to experimental determinations of  $C^{12}/C^{13}$  are given there.
34. D.F. Hebbard and J. L. Vogl, *Nucl. Phys.* 21, 652 (1960)
35. G. Righini, *Les Molecules dans les Astres* (Liege, 1956), 265.
36. D.W. Miller, B.M. Carmichael, U.C. Gupta, V.K. Rasmussen, and M.B. Sampson, *Phys. Rev.* 101, 740 (1956).
37. E.J. Burge and D.J. Prowse, *Phil. Mag.* 1, 912 (1956).
38. R.E. Benenson, *Phys. Rev.* 90, 420 (1953).
39. R.D. Bent, T.W. Bonner, and R.F. Sippel, *Phys. Rev.* 98, 1237 (1955).
40. F. Everling, L.A. Konig, J.H.E. Mattauch, and A.H. Wapstra, *Nucl. Phys.* 18, 529 (1960).
41. E.K. Warburton and W.T. Pinkston, *Phys. Rev.* 118, 733 (1960).
42. G.E. Owen and L. Madansky, *Analysis of the Reaction  $C^{13}(He^3, \alpha)C^{12}$*  (The Johns Hopkins Univ.) NYO 2054 (1958).

43. J.P. Schiffer, " Tables of Charged Particle Penetrabilities", Argonne Nat. Lab. Report ANL-5739 (1957).
44. R.K. Bardin, C.A. Barnes, W.A. Fowler, and P.A. Seeger, Phys. Rev. Letters 5, 323 (1960).
45. R.K. Bardin, Ph. D. Thesis ( Calif. Inst. of Technology, 1961).
46. D.F. Hebbard, Nucl. Phys. 15, 289 (1960).
47. F. Ajzenberg-Selove and T. Lauritsen, Energy Levels of Light Nuclei, Technical Report ( Calif. Inst. of Technology, 1960 ).
48. D.A. Bromley, E. Almqvist, H.E. Gove, H.E. Litherland, E.B. Paul, and A.J. Ferguson, Phys. Rev. 105, 957 (1957).
49. A.B. Brown, C.W. Snyder, W.A. Fowler, and C.C. Lauritsen, Phys. Rev. 82, 159 (1951).
50. F. Ajzenberg-Selove and T. Lauritsen, Nucl. Phys. 11, 1 (1959).
51. H. Yoshiki and N. Nikolic, Bull. Am. Phys. Soc. II, 5, 46 (1960).